ABSTRACT

Li, Qiliang. **Approach towards Hybrid Silicon/Molecular Electronics for Memory Applications**. (Under the direction of **Dr. Veena Misra**.)

The focus of this research is on integrating redox-active, organic molecules into Si-based structures to first, characterize and understand the properties of molecules; second, generate a new class of hybrid silicon/molecular devices for memory applications; and third, open a new way to develop molecular-only devices. The approach of hybrid silicon/molecular electronics is to provide a smooth transition technology by integrating molecular intrinsic scalability and properties with the vast infrastructure of traditional MOS technology. This dissertation has concentrated on the fabrication, characterization and modeling of hybrid silicon-molecular devices for memory applications.

First, specific procedures have been successfully developed for attaching redox-active, tightly-bonded, well-packed, molecular self-assembled monolayers on Si and SiO_2 surfaces. The molecules can be attached on the surfaces through solution-phase or vapor-phase deposition. The molecular monolayers attached on Si and SiO_2 surfaces via covalent C-O-Si bonds exhibit stable performance during electrical characterization in a well-controlled, inert environment. Molecular multilayer films have been also deposited on Si surface with very high surface coverage.

Second, an electrolyte/molecule/Si structure has been implemented for electrical characterizations to understand the molecules and their application in memory devices. The electrical characterizations include traditional cyclic voltammetry, capacitance-voltage/conductance-voltage measurements, impedance spectroscopy, and MOSFET/DRAM

write/erase I-V measurements. A specific model based on Maxwell's equations was developed to describe and understand the kinetics of charge transport and current-voltage characteristics of the molecular capacitors. Equivalent RC circuits have been developed to understand the characterization of impedance spectroscopy and extract RC coefficients for electrolyte, molecule and Si of this structure. In addition, a possible application of electrolyte/molecule/Si capacitors in DRAM has been presented and explored.

Third, two different strategies to achieve multibit memory have been developed and optimized using the methods of attaching mixed monolayers and stacked multilayer films. Multiple redox states at well-separated, discrete gate voltages have been obtained from mixed monolayers and stacked multilayer films, which augments the advantages for memory application.

Fourth, molecular multilayer films with very high surface coverage have been achieved for application in memory devices. Metal/molecule/Si sandwich structures using molecular multilayer films were fabricated and exhibited nonvolatile electrical switching properties. A set of control experiments indicate that these switching properties are due to the interaction of metal/molecule interface instead of the redox-related processes.

In conclusion, this thesis has focused on hybrid silicon/molecular electronics and has investigated the intrinsic properties of molecules and proposed feasible ways to apply molecules in memory devices. This dissertation indicates that hybrid silicon/molecular technology may provide a smooth transition from microelectronics depending on properties of bulk materials to nanoscale electronics with molecule as the key component in circuitry.

APPROACH TOWARDS HYBRID SILICON/MOLECULAR ELECTRONICS FOR MEMORY APPLICATIONS

By

Qiliang Li

A dissertation submitted to Graduate Faculty of
North Carolina State University
in partial fulfillment of the
requirements for the Degree of
Doctor of Philosophy

ELECTRICAL ENGINEERING

Raleigh, North Carolina

October, 2004

APPROVED BY:

C. M. Osburn

J. S. Lindsey

D. W. Barlage

V. Misra
Chair of advisory committee

BIOGRAPHY

Li, Qiliang received the B.S. degree (July, 1996) in physics with an honor of Best Graduate from Wuhan University, China. He received the M.S. degree (July, 1999) in physics from Nanjing University, China, with a thesis on ferroelectric thin film for application in nonvolatile memory devices. In the fall of 1999, he went to University of Vermont as a teaching assistant in physics and studied molecular dynamics as a graduate student. After two years of study, he transferred to North Carolina State University in June 2001 and continued to study for his Ph.D. degree in Electrical Engineering. Under the guidance of Dr. Veena Misra, he has developed a greater understanding in microelectronics and molecular electronics.

Upon completion of his Ph.D. study in Raleigh, he will join the semiconductor electronics division of National Institute of Standard and Technology in Gaithersburg, Maryland, to work on CMOS devices and nanoelectronics.

ACKNOWLEDGEMENTS

First of all, I sincerely thank Dr. Veena Misra for her invaluable guidance, encouragement and support during the course of this research. It is she who built up my knowledge and confidence, and shaped my philosophy in science. I would like to express my sincere appreciation to my other committee members: Dr. Jonathan S. Lindsey, Dr. Carlton M. Osburn and Dr. Doug W. Barlage, for their discussion, suggestion and encouragement.

I would like to acknowledge the help from current and former members in Dr. Misra's group: Guru Mathur, Srivardhan Gowda, Dr. Qian Zhao, Dr. Shyam Surthi, Heather Lazar, Mais Homsi, Yanxia Lin, Yong Luo, Bei Chen, Jae-Hoon Lee, Rashmi Jha, Dr. Nivedita Biswas, Dr. Vaidyanathan Raman, Dr. Huicai Zhong, Dr. Jing Liu, Dr. You-Seok Suh and Dr. Gregory Heuss. I also appreciate the help from Dr. D. F. Bocian, Dr. Zhiming Liu, Dr. Amir Yasseri, Dr. Thomas A. Sorenson, Dr. Robert C. Tenent, Dr. Vladimir Malinovskii, Dr. Karl-Heinz Schweikart and Dr. W. G. Kuhr. And special thanks go to lab staff members: Joan O'Sullivan, Henry Taylor, Harold Morton, and Ginger Yu.

I wish to express my deepest thanks to my parents, my parents in law, and my wife Xing Ling, for their love and long-time support.

TABLE OF CONTENTS

LIST OF TABLES

LIST OF FIGURES

Chapter 1 Introduction on Challenges of CMOS Scaling and Current Status of Molecular Electronics

1.1 CMOS Scaling: Challenges and Strategies

During the second half of the 20th century, microelectronic technology has not only led to computers and the internet, but also brought us to the beginning of an exciting scientific revolution we now call nanotechnology. Nanotechnology has been defined by Albert Franks as: "that area of science and technology where dimensions and tolerances in the range of 0.1nm to 100 nm play a critical role". As Dr. R. P. Feynman noted in his famous speech in 1959: "The principles of physics, as far as I can see, do not speak against the possibility of maneuvering things atom by atom … … There is plenty of room at the bottom."

For the past thirty years, Metal Oxide Semiconductor Field Effect Transistor (MOSFET), the heart of microelectronics technology, has kept scaling down with thinner gate oxides and shorter channel lengths to accomplish the goals of high speed, low power and high density for integrated circuit. As Complementary Metal Oxide Semiconductor (CMOS) technology extends to and beyond 65-nm technology node, many challenges to MOSFET scaling are raised including (1) thin gate oxide stability, (2) channel length modulation (CLM), (3) mobility degradation, (4) drain induced barrier lowering (DIBL), (5) hot carrier effect, and (6) gate induced drain leakage (GIDL). The industrial and academic communities are aggressively searching for solutions to meet these challenges: (1) non-classical CMOS to extend the life of CMOS technology and (2) fundamentally new technologies to replace CMOS technology.

Some of the recent approaches for enabling continued MOSFET scaling include research on using high-k dielectric and electrode material for gate stack, reducing source/drain series resistance, improving carrier transport properties of the channel, and designing new transistor structure such as silicon on insulator (SOI) structure, multiple-gate FET, transport-enhanced FET with strained semiconductor, and so on.

While non-classical CMOS still depends on the properties of bulk semiconductor materials, new technologies are trying to utilize the properties of materials at the nanoscale. The approaches towards fundamentally new technologies mainly include coherent quantum computing, biological computing, single/few electron devices, spin transistor and molecular electronics for the applications in logic and memory devices. Coherent quantum computing, biological computing and spin transistor are very new concepts and technologies for constructing computational logic devices compared to current electronic/semiconductor technologies. Coherent quantum computing is based on the phase of quantum wavefunctions to store and manipulate the information. The biological computing utilizes biochemical processes based on DNA. Spin transistor relies on the spin up/down direction to manipulate the electron transport for the use in spin FET and spin-valve transistor.

Single/few electron devices (SED) rely on Coulomb blockade effect to control electron movement with integer electron precision for applications in both logic and memory where single/few electron transistor is one of the basic components. Such a transistor consists of a quantum dot connected to an electron source and a sink via tunneling barriers. The quantum dot works like a small electron island to charge/discharge only integer number of electrons which occupy certain discrete energy states controlled by the gate. The disadvantages of SED approach are (1) operation at very low temperature, (2) sensitivity to background charge and noise, and (3) fabrication of mono-disperse sizes of quantum dots.

These new approaches need detailed studies before they can be considered as the alternatives to CMOS. As shown in Figure 1.1, the 2003 ITRS Emerging Technology Sequence indicates that some new technologies may be closer to application in real-world memory devices, such as Phase Change Memory (PCM), floating-body DRAM, Nanofloating gate memory (NFGM) and Insulator Resistance Change Memory (IRCM). However, as indicated in the following discussion, these nearer-term new technologies have inherent disadvantages which may limit their implementation. The typical operation current for PCM is very high (0.1-0.2 mA/device) and prevents the scaling of the drive/access MOSFET. Floating-body DRAM and NFGM are basically dependent on the standard MOSFET structure and as such are limited by CMOS scaling. The retention time of floating-

body DRAM decreases with scaling, and NFGM approach suffers lack of reproducibility. Meanwhile, the physical mechanisms of IRCM are not fully understood and the reliability (operation cycle <1000) may be a critical limitation. [1]

1.2 Comparisons between Molecule and Other Materials

1.2.1 The Advantages and Disadvantages of Molecular Electronics

Information processing on a molecular basis by means of molecular electronics competes to a large extent with conventional microelectronics approaches based upon inorganic metal/oxide/semiconductors structures. Molecular electronics is expected to have the following advantages [2]:

(1) Inherent scalability with molecular size: molecule represents the ultimate of atomic control over a diversity of physical properties. In addition, it is much easier to handle a molecule than an atom for nanotechnology.

(2) Assembly and recognition: the intermolecular interaction can be exploited to form self-assembled structures or modify electronic behaviors.

(3) Dynamical stereochemistry: many molecules have multiple distinct stable geometric/electronic structures so molecular switches between two stable structures can be obtained. These transitions between different structure result from the addition or removal of electron (e.g. ferrocene and porphyrin molecule) or chemical reactions (e.g. DNA).

(4) Synthetic tailorability. Molecular properties can be tailored with choice of composition and geometry by chemists.

The main disadvantages of molecules are their unknown reliability under electrical/stress and the instability at high temperature or in volatile environments. The instability at high temperature makes most molecules incompatible with current CMOS processes that would be needed to integrate molecules into CMOS circuits. Fortunately, the porphyrin molecules being investigated in this work have demonstrated stability at relatively high temperature (~450^{o}C) and may be integrated with CMOS process temperature

requirements. The volatile environment (such as oxygen, water and high temperature) may break the molecule's bond to the electrode or dispose the molecule.

1.2.2 Comparison between Molecules and Nanowires/Nanotubes

A field-effect transistor built by crossing two nanowires or nanotubes, e.g. typically 5 nm in diameter, has a volume of 5×5×5 cubic nanometer at the crossing junction. At a typical doping level of 10^{18} cm^{-3}, this junction would contain approximately 0.13 dopant atoms. Consequently, field-effect transistors fabricated at these wiring densities might exhibit non-statistical and unpredictable behaviors. [2] Other concerns, such as the gate oxide thickness, power consumption due to the leakage currents, and fabrication costs, also highlight the difficulty of scaling standard electronics materials to molecular dimensions.

At device areas of a few tens of square nanometers, molecules are inherently attractive because of their inherent scalability. Molecules consist of groups of atoms with specific and predetermined stable structures, which result in diverse range of physical and electronic properties. With such physical properties, information-storage, switching, organization and recognition can be achieved at molecular level.

1.3 Status of Molecular Electronics Technology for Future Electronics Application

Two fundamentally different approaches to molecular electronics are graphically termed 'top down' and 'bottom up'. 'Top-down' refers to making nanoscale structures by machining and etching techniques, whereas 'bottom-up', or molecular nanotechnology, applies to building organic and inorganic structures atom-by-atom, or molecule-by-molecule. Top-down or bottom-up is a measure of the level of advancement of nanotechnology.

Molecular technology has not historically played a prominent role in electronic devices. However, due to their inherent scalability and intrinsic properties, molecules are being aggressively pursued for their potential impact in future nanoscale electronics devices since 1970s [3-6]. The cross-disciplinary publications in this field by chemists, physicists, engineers and other researchers have dramatically increased over the past several years. New molecular-electronic systems, analytical tools, and device architectures have been introduced

and explored. In addition, a fundamental understanding about physical properties and organization of molecules has been achieved. However, molecular electronics to date has primarily been implemented at the 'top-down' level with some emerging activities at the 'bottom-up' level. The following section discusses five demonstrated/proposed methods to integrate molecules as an active component for future devices.

1.3.1 Crossbar Molecular Circuit

In this approach, the switching element is a metal/molecule/metal sandwich junction wherein molecules are placed at the cross section of two nanoscale metal wires. This sandwich molecular device has two stable, highly-retentive and reversible states: high-resistance state and low-resistance state [7, 8]. An example of this memory was recently shown by the Hewlett Packard Research group. This example consisted of an 8×8 crossbar circuit [9]. This approach has the advantage of architectural simplicity and potential of high density via fabrication of highly dense nanowires. However, this approach has two major disadvantages including high rate of defective switching elements and the difficulty in controlling metal/molecule interface. Nevertheless, a defect-tolerant architecture using this crossbar circuit has been developed [10]. However, as shown in their recent publications [11, 12], the earlier results on electron transport phenomena in metal/molecule/metal junction may not be truly molecular but instead be dominated by electrode reactions with molecules.

1.3.2 Nanocell Molecular Circuit

Another architecture based on metal/molecule/metal sandwiched junctions named as Nanocell molecular circuit was proposed by Rice University and Yale University [13-16]. The circuit is formed by using a random distribution of metal nano particles connected to each other through molecules. Metal lines are then created around the cell to provide input and output leads. Molecules are then attached to the metal nano particles such that a random path is formed between any two input-output metal lines. The active component for this cell is metal/molecule/metal switch which has memory retention of over 16 minutes. [17-19] One path may include more than one molecular switch. By developing appropriate computation algorithms, the molecules pathways can be learnt first and then the whole cell can be programmed to perform a particular function. This nanocell approach uses similar molecular

switches as the crossbar approach but uses a vastly different circuit architecture. Both of these two approaches may face the difficulty of controlling the metal/molecule interface. Compared to the crossbar approach, the nanocell approach has the advantage of simplicity in large-scale circuit fabrication. However, the disadvantage is that this strategy heavily relies on complex programming algorithms.

1.3.3 Molecular Quantum-dot Cellular Automata

Molecular Quantum-dot Cellular Automata (QCA) is a very different approach in molecular electronics for application in computational logic devices [20-24]. A molecular QCA element may typically consist of four quantum dots or molecular redox centers positioned in a square geometry and two movable electrons. These two electrons always occupy opposite corners such that they form two stable states: state "0" and state "1". Changing the position of electrons on one side via voltage will result in changing the output on the other side. Molecular QCA element can be aligned together to make small logic structures based on domino effect caused by the interaction of multiple cells together. The interaction between cells is columbic and no current flows between the cells so QCA approach has negligible power issues. This approach is highly sophisticated and can lead to very advanced logic circuits. The main obstacle is the intense difficulty in the precise placement of molecular quantum dots at the nanoscale. Columbic interaction depends on the distance between two molecules so the precise placement of molecules is required for this memory application. In addition, columbic interaction needs to overcome the effect of background charge and thermal noise, and therefore this approach requires very low operation temperatures.

1.3.4 Molecular FET

This approach has been carried out by Bell Labs and some other groups, and has been implemented with a standard MOSFET structure. [25-28] Here, the silicon channel is replaced by self-assembled monolayers (SAMs) of organic molecules and a back-gate is used for current modulation. Molecular FET has similar device structures as carbon nanotube FET (CNFET). However, the validity of the observed results is still under question and molecular-based FET still requires tremendous research effort. If successful, the advantages of using

organic molecule as the channel materials are low cost, simple fabrication and molecule's inherent properties.

1.3.5 Hybrid CMOS/Molecular Memory

This approach, proposed by our group (University of California, Riverside, North Carolina State University and Zettacore, Inc.), is focused on hybrid CMOS/molecular devices wherein redox-active charge-storage molecules are incorporated into silicon structures to generate a new class of nanoscale electronic devices. [29-32] These redox-active molecules, which can be designed to self-assemble on surfaces as monolayers, exhibit charge-storage states at discrete voltages. Application of an oxidizing voltage causes the redox-active monolayers to lose electrons, resulting in a positively charged monolayer (write state). When a reducing voltage is applied, electrons are transferred back to the molecules and the molecules go back to the neutral state (erase state). This approach can provide a smooth transition from CMOS technology to molecular-only electronics technology by integrating the vast infrastructure of developed CMOS technology with inherent molecular properties.

This approach is concentrating on developing hybrid molecular DRAM and FLASH devices containing redox molecule as the active component for charge-storage medium. This approach has superior features to conventional semiconductors due to (1) discrete redox states for charge storage, (2) the storage of multiple bits in a given memory storage location, (3) charge-retention times in the minutes >1,000 times that of semiconductors (measure by University of California, Riverside), (4) low power consumption and low operating voltage, and (5) scalability to molecular dimensions.

1.4 Overview of Dissertation

The focus of this dissertation is on the fabrication, characterization and modeling of hybrid silicon-molecular electronics for application in memory devices. The challenges in CMOS scaling and the need for developing fundamentally new concepts/approaches for next-generation technology have been presented. A series of new approaches for future electronic applications including the research trends in molecular electronics have been also discussed. Following the introductory chapter, Chapter 2 provides the structure and

properties of the molecules under investigation, and the attachment methodologies for different molecules on different surfaces. Chapter 3 presents the electrical characterization, modeling, and stability of molecules in silicon-based structures, and the application of silicon-molecular capacitor in DRAM cells. Chapter 4 explores the strategies to obtain multiple redox states for information storage. Chapter 5 describes the methods to obtain multilayer films of molecules and their application in metal/molecule/silicon sandwiched structure. Finally, a summary of this dissertation and a discussion on possible future research is presented in Chapter 6.

1.5 References:

[1] International Technology Roadmap for Semiconductors, 2003Edition, *Emerging technology sequence*, available on the Web at http://public.itrs.net.

[2] J. Heath and M. Ratner, "*Molecular electronics*," PHYSICS TODAY, vol. 56, pp. 43-49, 2003.

[3] H. Kuhn and D. Mobius, "*Systems of monomolecular layers - assembling and physico-chemical behavior*," ANGEWANDTE CHEMIE-INTERNATIONAL EDITION, vol. 10, pp. 620-&, 1971.

[4] B. Mann and H. Kuhn, "*Tunneling through fatty acid salt monolayers*," JOURNAL OF APPLIED PHYSICS, vol. 42, pp. 4398-&, 1971.

[5] A. Aviram and M. Ratner, "*Molecular rectifiers*," CHEMICAL PHYSICS LETTERS, vol. 29, pp. 277-283, 1974.

[6] M. Ratner and A. Aviram, "*Molecular rectifiers - model calculations*," BULLETIN OF THE AMERICAN PHYSICAL SOCIETY, vol. 19, pp. 341-341, 1974.

[7] Y. Chen, D. Ohlberg, X. Li, D. Stewart, R. Williams, J. Jeppesen, K. Nielsen, J. Stoddart, D. Olynick, and E. Anderson, "*Nanoscale molecular-switch devices fabricated by imprint lithography*," APPLIED PHYSICS LETTERS, vol. 82, pp. 1610-1612, 2003.

[8] C. Collier, E. Wong, M. Belohradsky, F. Raymo, J. Stoddart, P. Kuekes, R. Williams, and J. Heath, "*Electronically configurable molecular-based logic gates*," SCIENCE, vol. 285, pp. 391-394, 1999.

[9] Y. Chen, G. Jung, D. Ohlberg, X. Li, D. Stewart, J. Jeppesen, K. Nielsen, J. Stoddart, and R. Williams, "*Nanoscale molecular-switch crossbar circuits*," NANOTECHNOLOGY, vol. 14, pp. 462-468, 2003.

[10] J. Heath, P. Kuekes, G. Snider, and R. Williams, "*A defect-tolerant computer architecture: Opportunities for nanotechnology*," SCIENCE, vol. 280, pp. 1716-1721, 1998.

[11] D. Stewart, D. Ohlberg, P. Beck, Y. Chen, R. Williams, J. Jeppesen, K. Nielsen, and J. Stoddart, "*Molecule-independent electrical switching in pt/organic monolayer/ti devices*," NANO LETTERS, vol. 4, pp. 133-136, 2004.

[12] J. Heath, J. Stoddart, and R. Williams, "*More on molecular electronics*," SCIENCE, vol. 303, pp. 1136-1137, 2004.

[13] M. Reed, C. Zhou, M. Deshpande, C. Muller, T. Burgin, L. Jones, and J. Tour, "*The electrical measurement of molecular junctions*," MOLECULAR ELECTRONICS: SCIENCE AND TECHNOLOGY, vol. 852, pp. 133-144, 1998.

[14] C. Zhou, M. Deshpande, M. Reed, L. Jonesll, and J. Tour, "*Nanoscale metal self-assembled monolayer metal heterostructures (vol 71, pg 611, 1997)*," APPLIED PHYSICS LETTERS, vol. 71, pp. 2857-2857, 1997.

[15] C. Zhou, M. Deshpande, M. Reed, L. Jones, and J. Tour, "*Nanoscale metal self-assembled monolayer metal heterostructures*," APPLIED PHYSICS LETTERS, vol. 71, pp. 611-613, 1997.

[16] M. Reed, C. Zhou, C. Muller, T. Burgin, and J. Tour, "*Conductance of a molecular junction*," SCIENCE, vol. 278, pp. 252-254, 1997.

[17] J. Chen, M. Reed, A. Rawlett, and J. Tour, "*Large on-off ratios and negative differential resistance in a molecular electronic device*," SCIENCE, vol. 286, pp. 1550-1552, 1999.

[18] J. Chen, M. Reed, C. Asplund, A. Cassell, M. Myrick, A. Rawlett, J. Tour, and P. Van Patten, "*Placement of conjugated oligomers in an alkanethiol matrix by scanned probe microscope lithography*," APPLIED PHYSICS LETTERS, vol. 75, pp. 624-626, 1999.

[19] J. Tour, W. Reinerth, L. Jones, T. Burgin, C. Zhou, C. Muller, M. Deshpande, and M. Reed, "*Recent advances in molecular scale electronics*," MOLECULAR ELECTRONICS: SCIENCE AND TECHNOLOGY, vol. 852, pp. 197-204, 1998.

[20] C. Lent, B. Isaksen, and M. Lieberman, "*Molecular quantum-dot cellular automata*," JOURNAL OF THE AMERICAN CHEMICAL SOCIETY, vol. 125, pp. 1056-1063, 2003.

[21] M. Lieberman, X. Wang, W. Hu, R. Rajagopal, M. Jiang, G. Snider, and G. Bernstein, "*Formation, characterization, and sub-50 nm patterning of organosilane monolayers with embedded disulfide bonds.*," ABSTRACTS OF PAPERS OF THE AMERICAN CHEMICAL SOCIETY, vol. 224, pp. U399-U400, 2002.

[22] M. Lieberman, S. Chellamma, Y. Wang, Q. Hang, G. Bernstein, and C. Lent, "*Molecules and supramolecular arrays for quantum-dot cellular automata.*," ABSTRACTS OF PAPERS OF THE AMERICAN CHEMICAL SOCIETY, vol. 224, pp. U474-U474, 2002.

[23] X. Wang, W. Hu, R. Ramasubramaniam, G. Bernstein, G. Snider, and M. Lieberman, "*Formation, characterization, and sub-50-nm patterning of organosilane monolayers with embedded disulfide bonds: An engineered self-assembled monolayer resist for electron-beam lithography*," LANGMUIR, vol. 19, pp. 9748-9758, 2003.

[24] M. Manimaran, G. Snider, C. Lent, V. Sarveswaran, M. Lieberman, Z. Li, and T. Fehlner, "*Scanning tunneling microscopy and spectroscopy investigations of qca molecules*," ULTRAMICROSCOPY, vol. 97, pp. 55-63, 2003.

[25] C. Miramond and D. Vuillaume, "*1-octadecene monolayers on si(111) hydrogen-terminated surfaces: Effect of substrate doping*," JOURNAL OF APPLIED PHYSICS, vol. 96, pp. 1529-1536, 2004.

[26] J. Collett and D. Vuillaume, "*Nano-field effect transistor with an organic self-assembled monolayer as gate insulator*," APPLIED PHYSICS LETTERS, vol. 73, pp. 2681-2683, 1998.

[27] Z. Bao, H. Schon, H. Meng, J. Zheng, and J. Slusky, "*Molecular-scale organic transistors and nanopatterning using self-assembled monolayers.*," ABSTRACTS OF PAPERS OF THE AMERICAN CHEMICAL SOCIETY, vol. 223, pp. C42-C42, 2002.

[28] X. Chen, Z. Bao, J. Schon, A. Lovinger, Y. Lin, B. Crone, A. Dodabalapur, and B. Batlogg, "*Ion-modulated ambipolar electrical conduction in thin-film transistors based on amorphous conjugated polymers*," APPLIED PHYSICS LETTERS, vol. 78, pp. 228-230, 2001.

[29] Z. Liu, A. Yasseri, J. Lindsey, and D. Bocian, "*Molecular memories that survive silicon device processing and real-world operation*," SCIENCE, vol. 302, pp. 1543-1545, 2003.

[30] Q. Li, G. Mathur, M. Homsi, S. Surthi, V. Misra, V. Malinovskii, K. Schweikart, L. Yu, J. Lindsey, Z. Liu, R. Dabke, A. Yasseri, D. Bocian, and W. Kuhr, "*Capacitance and conductance characterization of ferrocene-containing self-assembled monolayers*

on silicon surfaces for memory applications," APPLIED PHYSICS LETTERS, vol. 81, pp. 1494-1496, 2002.

[31] K. Schweikart, V. Malinovskii, J. Diers, A. Yasseri, D. Bocian, W. Kuhr, and J. Lindsey, "*Design, synthesis, and characterization of prototypical multistate counters in three distinct architectures*," JOURNAL OF MATERIALS CHEMISTRY, vol. 12, pp. 808-828, 2002.

[32] K. Roth, N. Dontha, R. Dabke, D. Gryko, C. Clausen, J. Lindsey, D. Bocian, and W. Kuhr, "*Molecular approach toward information storage based on the redox properties of porphyrins in self-assembled monolayers*," JOURNAL OF VACUUM SCIENCE & TECHNOLOGY B, vol. 18, pp. 2359-2364, 2000.

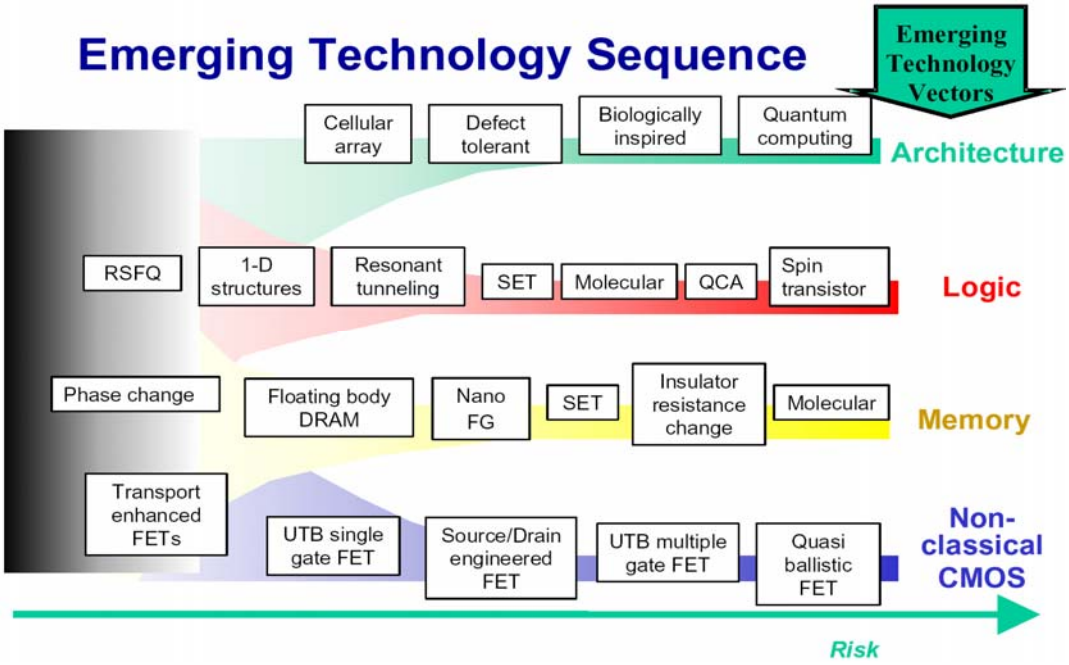

Figure 1.1 ITRS, Emerging technology Sequence, 2003

Chapter 2 Molecular Materials, Attachment Methods and Characterization Techniques

2.1 Introduction

Our project is focused on constructing a new class of hybrid silicon-molecular devices that utilize the redox-active, organic molecules to store information. In the first step, our study has been focused on developing a collection of redox-active molecules which are able to attach on specific electroactive surfaces and form self-assembled monolayers. During this study, a library of molecules has been synthesized. [1-10] Then specific procedures have been developed to attach molecule to Si-based structures. Various electrical measurement techniques have been applied to characterize the Si/molecular devices.

2.2 Molecular Materials and Properties

Typical molecules consist of a group of atoms in a stable structure. As devices scale down to the nanometer regime, the inherent scalability and intrinsic properties of molecules are very attractive because molecules represent the ultimate, atomic control over diverse physical properties. The materials used in our project are organic, redox-active, nanoscale molecules.

The generic structure of a redox-active molecule used in this work consists of redox-active components, linkage components and surface attachment groups. As shown in Figure 2.1, the redox-active components span several classes including (A) ferrocenes, (B) monomeric porphyrins, (C) ferrocene-porphyrin conjugates, (D) triple-deckers of lanthanide porphyrins and phthalocyanines, (E) covalently linked dyads of triple deckers (F) weakly coupled multimeric porphyrins, and (G) tightly coupled multimeric porphyrins. The primary goal for designing more complex redox-active components is to increase the number of available redox states, thereby increasing the storage density. The linkage components can be engineered to tune the charge retention properties. The surface attachment groups are synthetically designed for the molecule to attach on specific surfaces via covalent bonds. Several surface attachment groups have been designed and are shown in Figure 2.2. They

include: (1) a thiol group for the attachment of molecule on Au surface, and (2) an alcoholic linker for the attachment of molecule on Si surface. Figure 2.3 shows molecules with phosphonic surface groups for the attachment of molecule on SiO_2 surface. As shown in Figure 2.4, four molecules 4-ferrocenylbenzyl alcohol (**Fc-BzOH**), 5-(4-hydroxymethylphenyl)-10,15,20-trimesitylporphinatozinc(II) (**Por-BzOH**), dihydroxyphosphorylmethylferrocene (**P-Fc**), and 5-(4-dihydroxyphosphorylphenyl)-10,15,20-trimesitylporphinatozinc(II) (**P-Por**) were investigated in this thesis for application in hybrid CMOS/molecular electronics. The characteristics of devices with these four molecules should be applied to devices with other redox-active molecules. The properties and attachment details for these four molecules are provided in Table 2.1.

Physically, a redox-active molecule contains a charge-storage center surrounded by insulators/barriers. The redox-active component acts as the charge-storage center with both the linkage and the surface group acting as the insulator. Figure 2.5 shows the schematic of an electrolyte/porphyrin/Si structure (top diagram) with a porphyrin molecule covalently attached to a Si atom, and the schematic of the energy/barrier of this electrolyte/molecule/semiconductor (EMS) structure (bottom diagram). The porphyrin molecular component including a single Zn atom is the charge-storage medium which can be in neutral state and mono- or di- positively charged states through losing one or two electrons, respectively. The molecular components surrounding the center act as the barriers against charge loss. The electrons tunnel through the barrier during the oxidation and reduction processes. This energy/barrier diagram is in some degree similar to a electron donor-bridge-electron acceptor (DBA) structure in a metal/molecule/metal junction [11]. The double layer of the electrolyte/molecule interface acts as another barrier between the molecule and gate electrode. The electrolyte solution itself is ion-conductive and electron-limited in this case. Once the molecule has been oxidized, wherein an electron tunnels out of the molecule to substrate, no electrons are available in the electrolyte to tunnel into the molecule and reduce this charge. This results in a positive charge on the molecule. The positive charges in the molecule layer can be reduced at a lower gate potential wherein an electron tunnels back to molecule from the Si substrate.

Generally, these redox-active molecules have multiple stable states. The switching between the states is dynamically reversible through losing or storing a charge. In a well-

controlled and inert environment, the switching properties of molecules can endure up to 10^{10} cycles [12], which also indicate that the molecules are intrinsically stable during the redox processes.

2.3 Attachment Methods

The attachment of well-ordered, tightly-packed, stable layers of molecules on active surfaces is very important for the application of molecule in electronic devices. The attachment of molecule into Si-based structures in this project is via the formation of self-assembled monolayers (SAMs). The SAMs, different from Langmuir-Blodgett molecular films, are attached on active surfaces via a covalent bond to the atoms on the surface. Specific tether groups can be designed such that they only attach to specific surfaces. The technique of self-assembly is potentially advantageous for large-scale fabrication of molecule-based circuitry. [11]

The attachment of SAMs on Au, Si or SiO_2 surface is via the use of chemical solution deposition. The attachment of thiol-terminated molecules on Au surface was developed by several groups [10, 13, 14]. The attachment of molecules on Si or SiO_2 is of interest due to silicon's prevalence in current microelectronic devices. Robust attachments to silicon can provide ways to integrate molecule in hybrid CMOS/molecular electronic applications [15-17]. The process flow including photolithography, surface processing and attachment procedures for attachment on Si and SiO_2 is shown in Figure 2.6. Details of the process steps are also listed below:

(1) 450-nm field oxide was grown thermally by wet oxidation

(2) Photolithography (MA-6 aligner) and oxide etch (BOE etch) steps were used to define active areas ranging from 5 to 200-μm squares.

(3) A 10-nm oxide was grown thermally on the active area. Next:

(a) The oxide was etched on the active areas by 1% HF to obtain a hydrogen passivated Si surface for the attachment of alcoholic tether terminated molecules.

(b) For attachment to SiO_2, the oxide was etched for various times to obtain thin oxides of varying thicknesses. Thin oxides were also obtained through rapid

temperature oxidation (RTO) at varying thermal budget conditions. Once the Si or SiO_2 surface was prepared, the samples will be kept in an inert atmosphere consisting of Ar or N_2.

(4) Solutions containing molecules were made by dissolving 1-mg ferrocene or 2-mg porphyrin into a 400-μL solvent. The available solvents include: benzonitrile (BN) (Aldrich, 99.8%) for **Fc-BzOH** and **Por-BzOH** and tetrahydrofuran (THF) (Aldrich, 99.8%) for **P-Fc** and **P-Por**.

(5) The molecular solutions were then deposited on the active surfaces by placing droplets on the active areas with each drop being placed for 5 minutes. A saturated SAM of molecules was formed after 40 minutes (or 8 drops of molecular solution). During the attachment, samples are continuously kept in an inert environment under either argon or nitrogen. The attachment temperatures for each molecule are shown in Table 2-1.

(6) After the SAMs are formed, the samples are cleaned by sonication in dichloromethane (DC) (Aldrich, 99.8%) thrice for 3 minutes each. Then the samples are dried by flowing Ar or N_2. Again, during the cleaning process, the samples are kept in an inert atmosphere.

As shown in Figure 2.7 (a), the surface coverage of **Fc-BzOH** SAM increases as the deposition time increases. It takes 5 minutes for one droplet of molecule solution to dry on the wafer. Each droplet consists of about 3 μL of molecular solution. The surface coverage of molecular SAMs saturates to 1.25×10^{14} molecules/cm^2 after 30 minutes or 6 drops. Most experiments performed in this work use 40 minutes or 8 drops to ensure that completely saturated SAMs are formed. As shown in Figure 2.7 (b), the attachment density can also be tuned by increasing the attachment time. As shown, if only one drop of **Fc-BzOH** solution is used with attachment times varying from 5 s to 15 minutes, the surface coverage of SAM increases and saturates to 1.05×10^{14} molecules/cm^2. This result indicates that the self-assembly covalent bond formation of molecules with the substrate takes a certain amount of time. The attachment behavior of other molecular SAMs is similar to the **Fc-BzOH** SAMs.

The attachment of multilayer film of **P-Fc** is similar to the steps described above except that the attachment temperature is higher (from 170 to 210^{o}C) and the surface

coverage of multilayer film increases as temperature or deposition time increases. The surface coverage of **P-Fc** in multilayer films can be up to 40 times of that in the monolayer. Detail will be discussed in CHAPTER 5.

2.4 Characterization Techniques

After the molecules are attached, a solution of 1.0-M tetrabutyl ammonium hexafluorophosphate (TBAH) in propylene carbonate (PC) was used as the conducting gate electrolyte. Figure 2.8 shows the schematic diagram of the setup for electrical characterization. The samples are measured in a standard probe station for device characterization. Backside contact to the samples is made via the chuck of the probe station. Polypropylene micropipette tip containing the silver counter electrode and 5-μL electrolyte is positioned and controlled by a XYZ-500-TIS test positioner. The end of the micropipette tip is then lowered until the surface is wetted by the electrolyte. The surface tension of the tip and the highly viscous TBAH+PC electrolyte allowed for only a small amount of electrolyte to spread across the active area. The surrounding thick field oxide further reduced the parasitic capacitance of overlap field-oxide region covered by electrolyte. The cyclic voltammetry (CyV), a current-voltage measurement at various voltage scan rates, is obtained using a CHI600A electrochemical analyzer. Capacitance-voltage (C-V), conductance-voltage (G-V) characteristics and impedance spectroscopy (IS) are obtained by a HP 4284A LCR meter. The write/erase current-voltage characteristics of molecular DRAM are measured using a HP 4155B semiconductor parameter analyzer.

2.5 References

[1] A. Balakumar, A. Lysenko, C. Carcel, V. Malinovskii, D. Gryko, K. Schweikart, R. Loewe, A. Yasseri, Z. Liu, D. Bocian, and J. Lindsey, "*Diverse redox-active molecules bearing o-, s-, or se-terminated tethers for attachment to silicon in studies of molecular information storage*," JOURNAL OF ORGANIC CHEMISTRY, vol. 69, pp. 1435-1443, 2004.

[2] R. Loewe, A. Ambroise, K. Muthukumaran, K. Padmaja, A. Lysenko, G. Mathur, Q. Li, D. Bocian, V. Misra, and J. Lindsey, "*Porphyrins bearing mono or tripodal benzylphosphonic acid tethers for attachment to oxide surfaces*," JOURNAL OF ORGANIC CHEMISTRY, vol. 69, pp. 1453-1460, 2004.

[3] K. Muthukumaran, R. Loewe, A. Ambroise, S. Tamaru, Q. Li, G. Mathur, D. Bocian, V. Misra, and J. Lindsey, "*Porphyrins bearing arylphosphonic acid tethers for attachment to oxide surfaces*," JOURNAL OF ORGANIC CHEMISTRY, vol. 69, pp. 1444-1452, 2004.

[4] K. Schweikart, V. Malinovskii, J. Diers, A. Yasseri, D. Bocian, W. Kuhr, and J. Lindsey, "*Design, synthesis, and characterization of prototypical multistate counters in three distinct architectures*," JOURNAL OF MATERIALS CHEMISTRY, vol. 12, pp. 808-828, 2002.

[5] D. Gryko, J. Li, J. Diers, K. Roth, D. Bocian, W. Kuhr, and J. Lindsey, "*Studies related to the design and synthesis of a molecular octal counter*," JOURNAL OF MATERIALS CHEMISTRY, vol. 11, pp. 1162-1180, 2001.

[6] D. Gryko, C. Clausen, K. Roth, N. Dontha, D. Bocian, W. Kuhr, and J. Lindsey, "*Synthesis of "porphyrin-linker-thiol" molecules with diverse linkers for studies of molecular-based information storage*," JOURNAL OF ORGANIC CHEMISTRY, vol. 65, pp. 7345-7355, 2000.

[7] D. Gryko, F. Zhao, A. Yasseri, K. Roth, D. Bocian, W. Kuhr, and J. Lindsey, "*Synthesis of thiol-derivatized ferrocene-porphyrins for studies of multibit information storage*," JOURNAL OF ORGANIC CHEMISTRY, vol. 65, pp. 7356-7362, 2000.

[8] C. Clausen, D. Gryko, R. Dabke, N. Dontha, D. Bocian, W. Kuhr, and J. Lindsey, "*Synthesis of thiol-derivatized porphyrin dimers and trimers for studies of architectural effects on multibit information storage*," JOURNAL OF ORGANIC CHEMISTRY, vol. 65, pp. 7363-7370, 2000.

[9] C. Clausen, D. Gryko, A. Yasseri, J. Diers, D. Bocian, W. Kuhr, and J. Lindsey, "*Investigation of tightly coupled porphyrin arrays comprised of identical monomers for multibit information storage*," JOURNAL OF ORGANIC CHEMISTRY, vol. 65, pp. 7371-7378, 2000.

[10] J. Li, D. Gryko, R. Dabke, J. Diers, D. Bocian, W. Kuhr, and J. Lindsey, "*Synthesis of thiol-derivatized europium porphyrinic triple-decker sandwich complexes for multibit molecular information storage*," JOURNAL OF ORGANIC CHEMISTRY, vol. 65, pp. 7379-7390, 2000.

[11] J. Heath and M. Ratner, "*Molecular electronics*," PHYSICS TODAY, vol. 56, pp. 43-49, 2003.

[12] Z. Liu, A. Yasseri, J. Lindsey, and D. Bocian, "*Molecular memories that survive silicon device processing and real-world operation*," SCIENCE, vol. 302, pp. 1543-1545, 2003.

[13] K. Roth, N. Dontha, R. Dabke, D. Gryko, C. Clausen, J. Lindsey, D. Bocian, and W. Kuhr, "*Molecular approach toward information storage based on the redox properties of porphyrins in self-assembled monolayers*," JOURNAL OF VACUUM SCIENCE & TECHNOLOGY B, vol. 18, pp. 2359-2364, 2000.

[14] J. Chen, M. Reed, C. Asplund, A. Cassell, M. Myrick, A. Rawlett, J. Tour, and P. Van Patten, "*Placement of conjugated oligomers in an alkanethiol matrix by scanned probe microscope lithography*," APPLIED PHYSICS LETTERS, vol. 75, pp. 624-626, 1999.

[15] Q. Li, S. Surthi, G. Mathur, S. Gowda, V. Misra, T. Sorenson, R. Tenent, W. Kuhr, S. Tamaru, J. Lindsey, Z. Liu, and D. Bocian, "*Electrical characterization of redox-active molecular monolayers on sio2 for memory applications*," APPLIED PHYSICS LETTERS, vol. 83, pp. 198-200, 2003.

[16] K. Roth, A. Yasseri, Z. Liu, R. Dabke, V. Malinovskii, K. Schweikart, L. Yu, H. Tiznado, F. Zaera, J. Lindsey, W. Kuhr, and D. Bocian, "*Measurements of electron-*

transfer rates of charge-storage molecular monolayers on si(100). Toward hybrid molecular/semiconductor information storage devices," JOURNAL OF THE AMERICAN CHEMICAL SOCIETY, vol. 125, pp. 505-517, 2003.

[17] Q. Li, G. Mathur, M. Homsi, S. Surthi, V. Misra, V. Malinovskii, K. Schweikart, L. Yu, J. Lindsey, Z. Liu, R. Dabke, A. Yasseri, D. Bocian, and W. Kuhr, "*Capacitance and conductance characterization of ferrocene-containing self-assembled monolayers on silicon surfaces for memory applications*," APPLIED PHYSICS LETTERS, vol. 81, pp. 1494-1496, 2002.

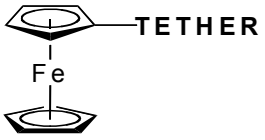

A

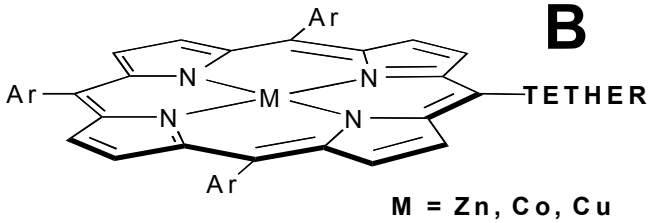

B

M = Zn, Co, Cu

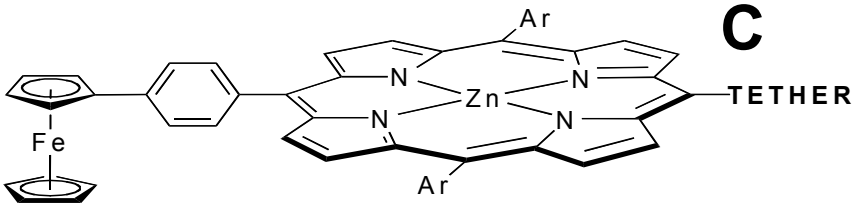

C

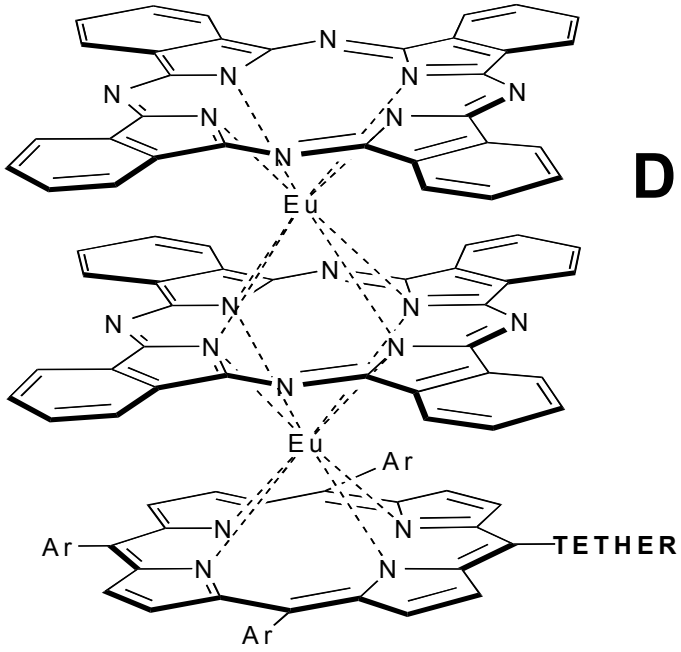

D

(See reference **1-10**)

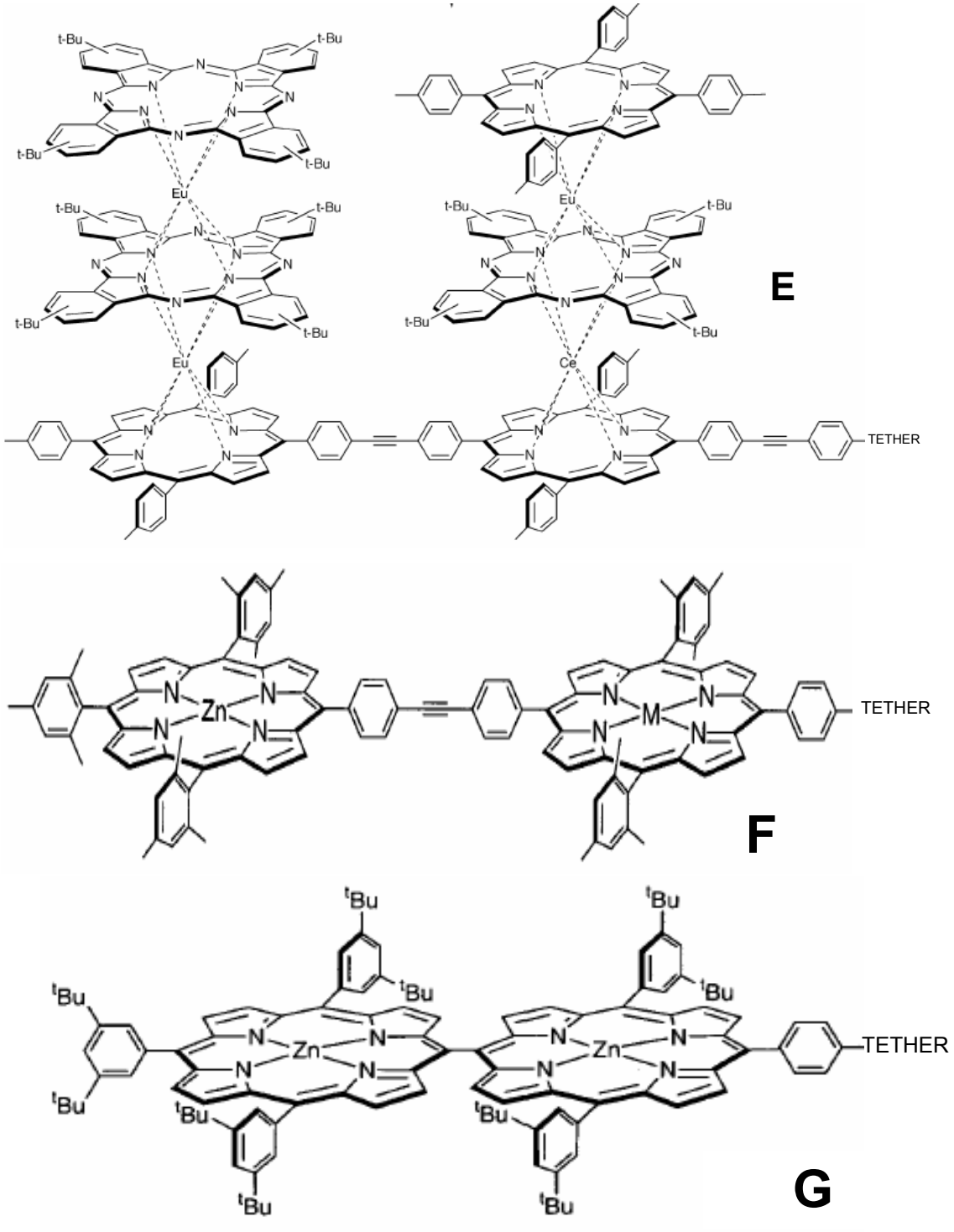

Figure 2.1 Schematics of molecules. From the top to bottom: Ferrocene (A), porphyrin (B), ferrocene-porphyrin conjugate (C), triple-decker porphyrin (D), dyad of triple deckers (E), weakly coupled multimeric porphyrin (F), and tightly coupled multimeric porphyrin (G). (See reference **1-10**)

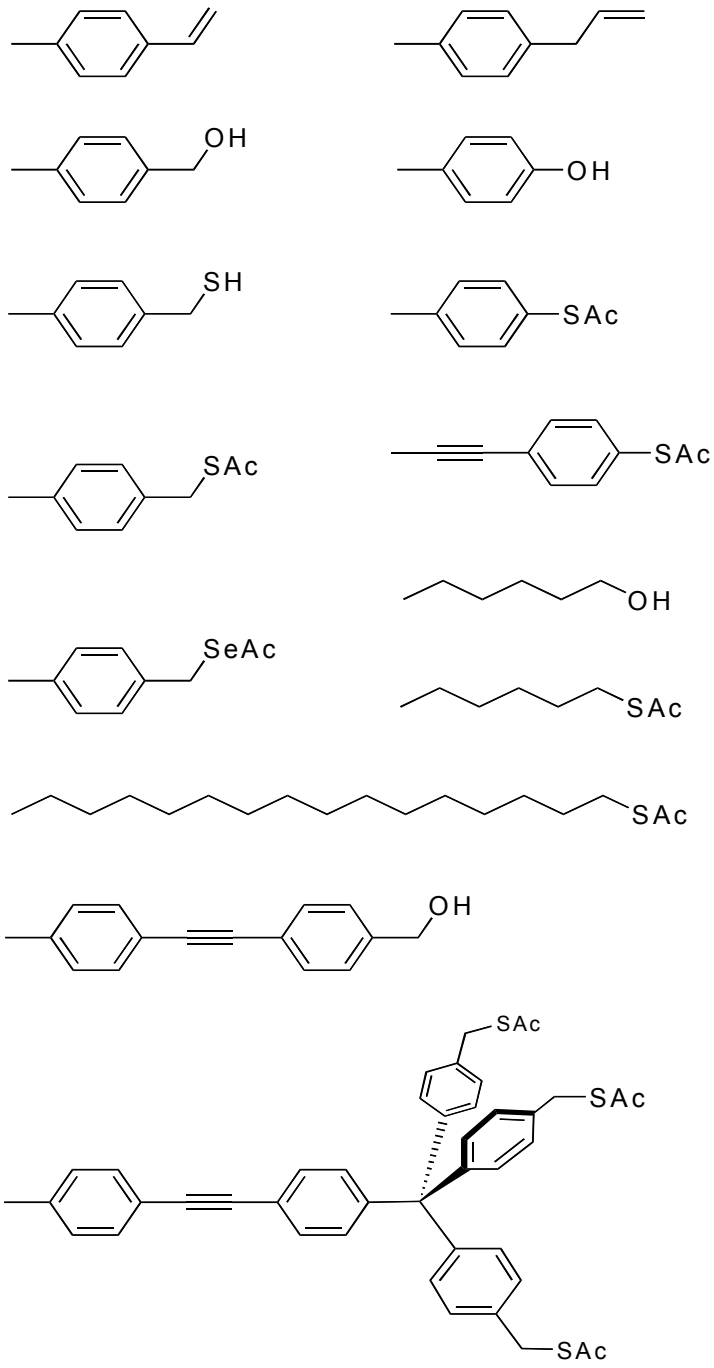

Figure 2.2 Specific tethers on the one end of molecule for attachment on specific surfaces via covalent bonds.

(See reference **1-10**)

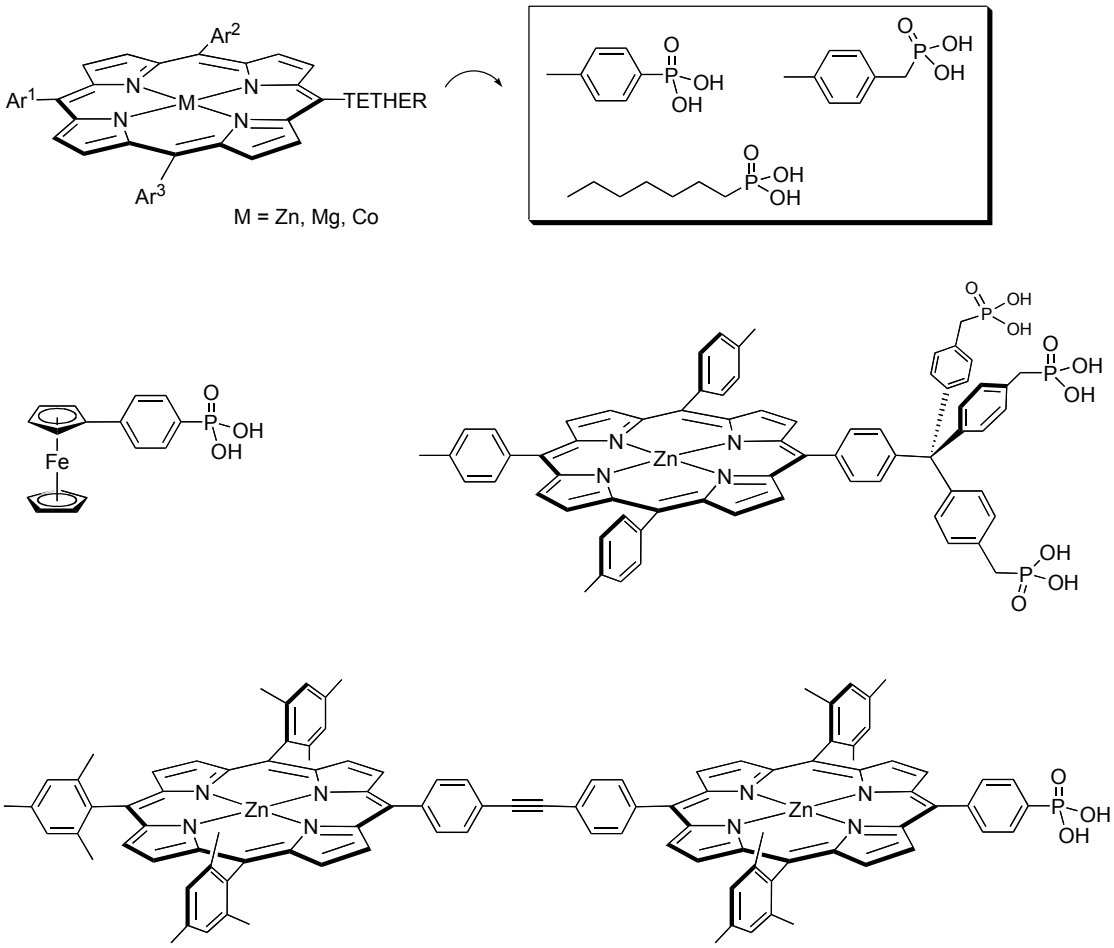

Figure 2.3 Various molecules with phosphonic tether specific for attachment on SiO_2

(See reference **1-10**)

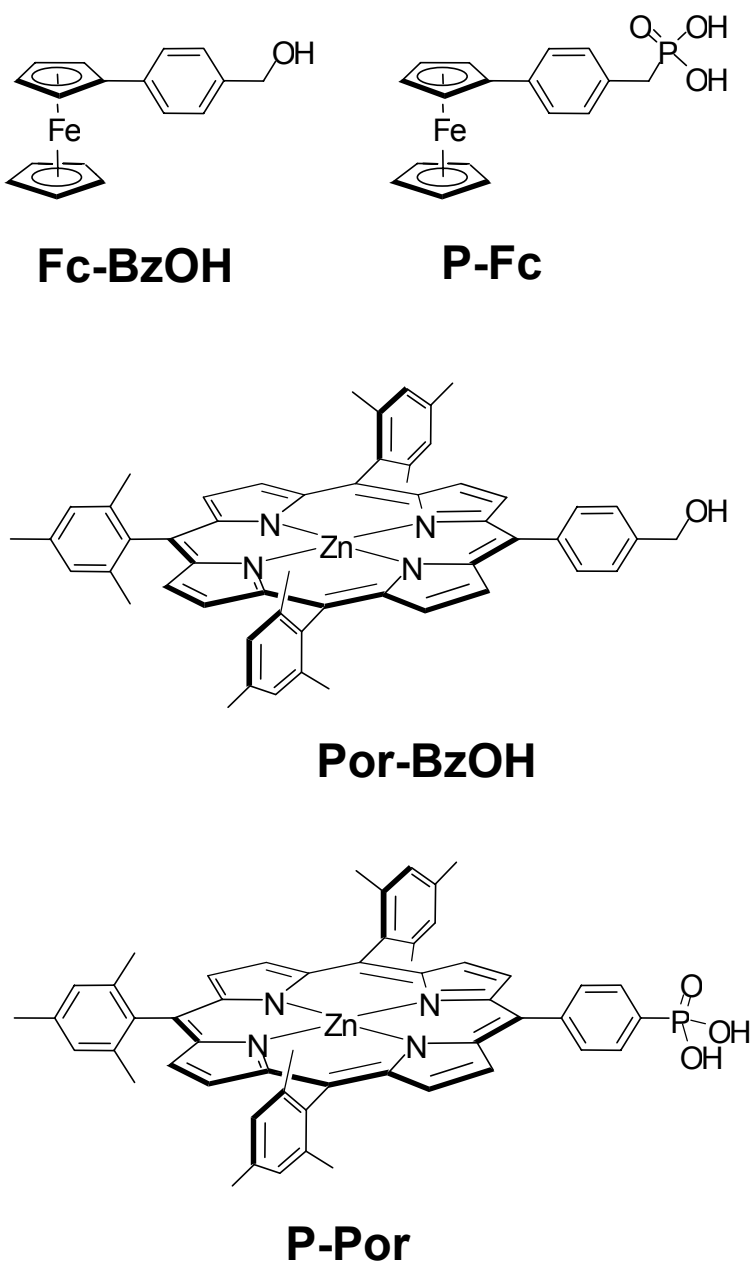

Figure 2.4 Schematics of molecular structures of four generally-used molecules in this thesis (See reference 3, 16)

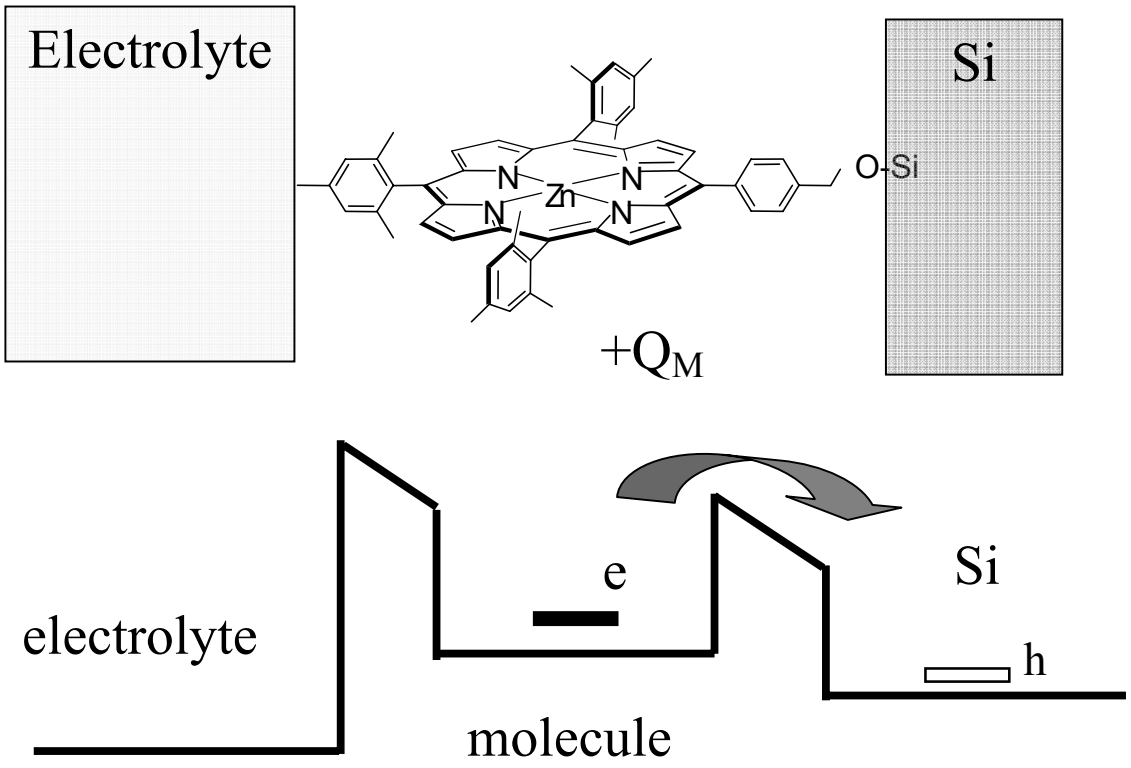

Figure 2.5 (Top) schematics of EMS structure with molecule attaching on Si surface via covalent bond and electrolyte as the gate electrode for molecules; (Bottom) energy band diagram of EMS structure.

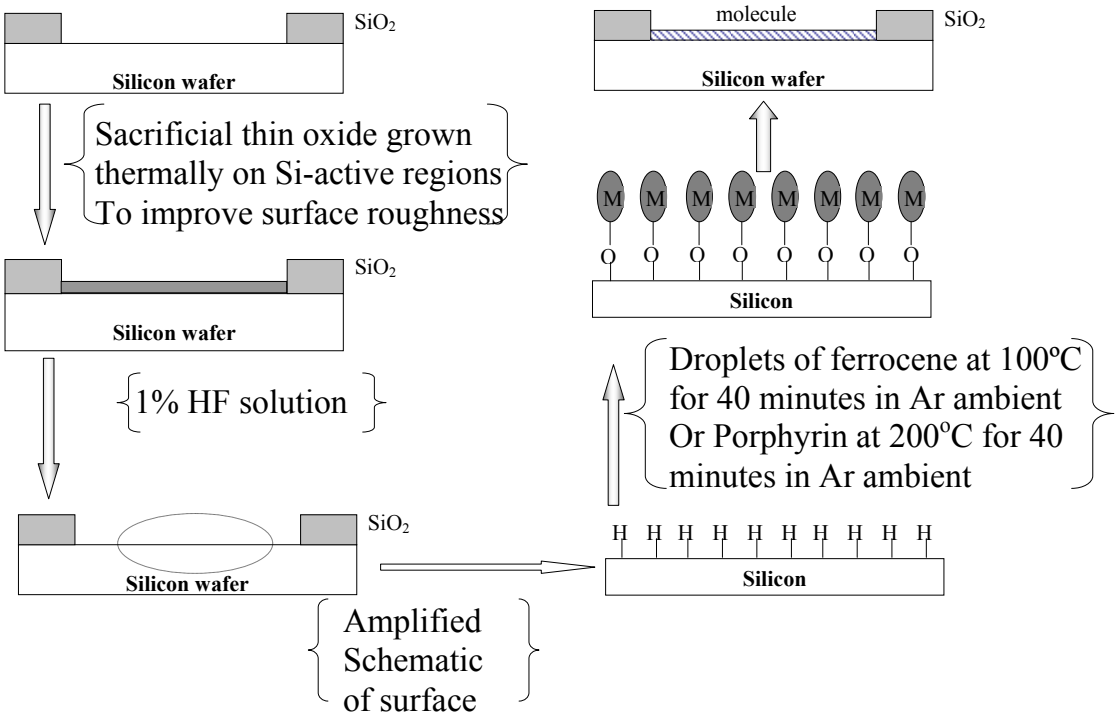

Figure 2.6 Surface processing and reaction for the attachment of molecules

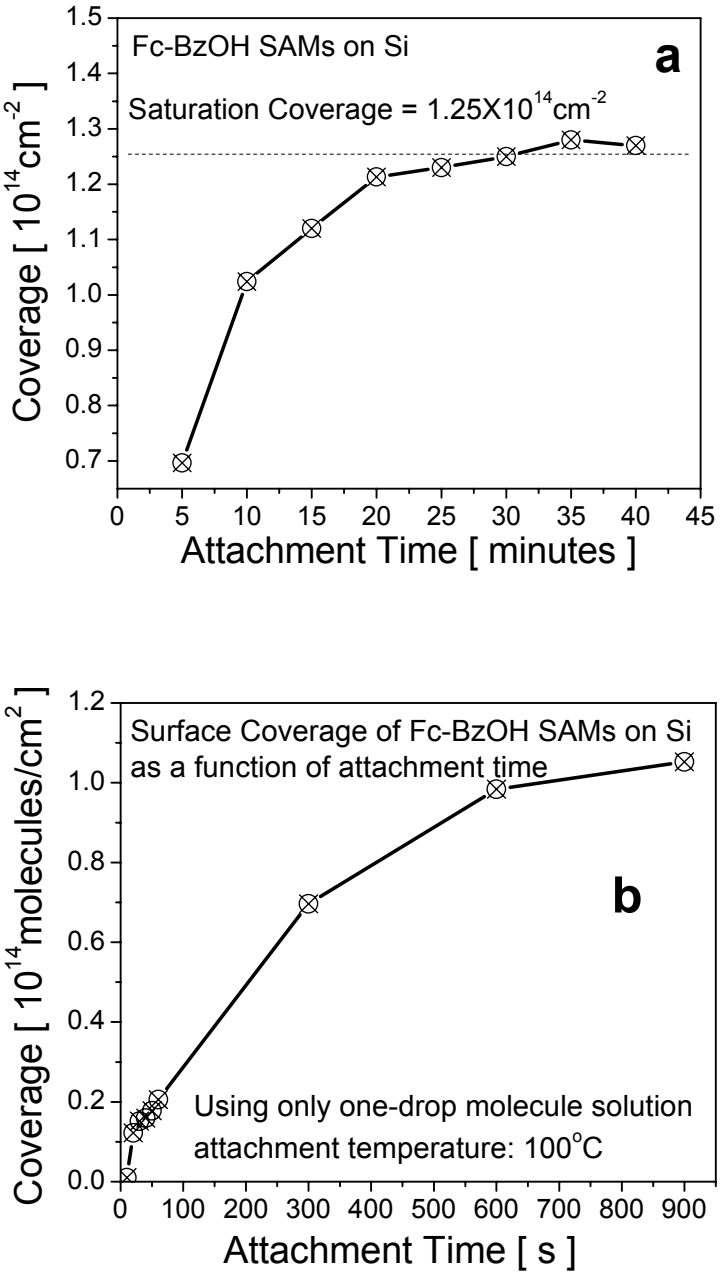

Figure 2.7 (a) Surface coverage of **Fc-BzOH** SAM increases as deposition time increases for 5 minutes per drop. (b) For deposition of only one drop of molecule solution, surface coverage of **Fc-BzOH** SAM increases as attachment time increase.

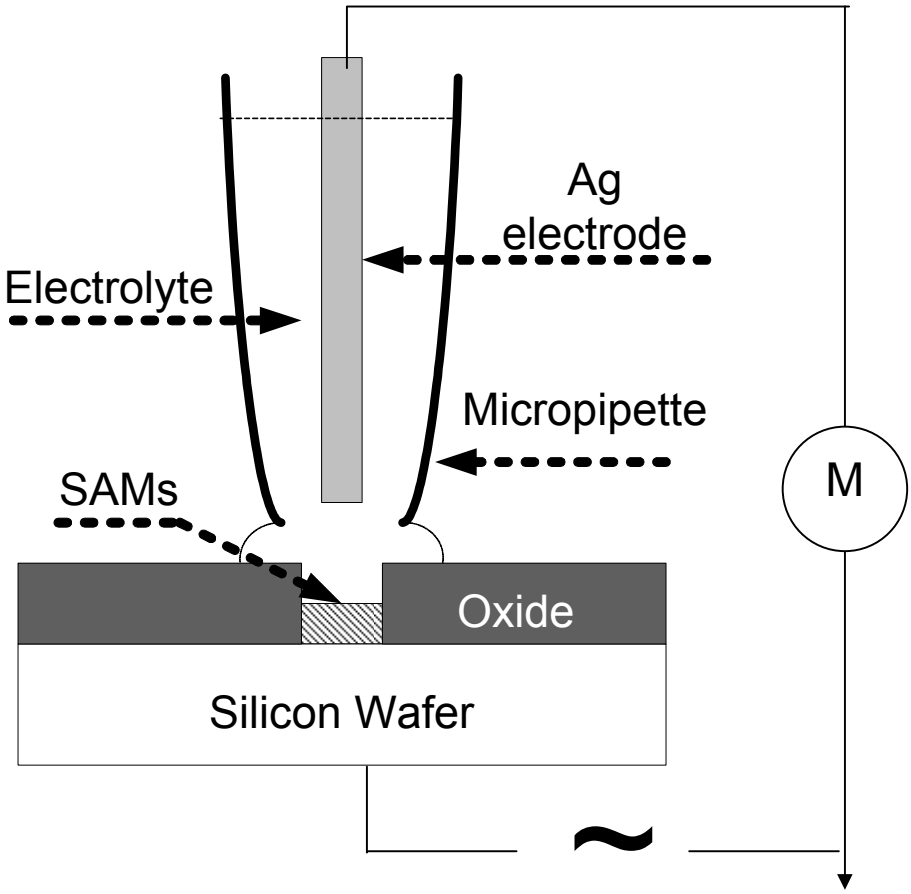

Figure 2.8 Schematic of characterization setup for cyclic voltammetry (current-voltage) and impedance measurements. "~" represents the voltage source for measurement and M is an electrometer.

Tables:

Table 2.1 Attachment solutions, attachment temperatures, saturated surface coverage and attaching surfaces for the four molecules shown in Figure 2.4.

Molecule	Molecule solution	Attachment temperature	Max surface coverage	Attaching surface
Fc-BzOH	1 mg molecule in 400-μL BN	100°C	1.25×10^{14} molecule/cm^2	Si
Por-BzOH	2 mg molecule in 400-μL BN	200°C	0.4×10^{14} molecule/cm^2	Si
P-Fc	1 mg molecule in 400-μL DMF	100°C	1.25×10^{14} molecule/cm^2	SiO_2
P-Por	2 mg molecule in 400-μL DMF	200°C	0.4×10^{14} molecule/cm^2	SiO_2

Chapter 3 Electrolyte/Molecule/Si Capacitor for Memory Applications

3.1 Introduction

As Complementary Metal Oxide Semiconductor (CMOS) technology extends to and beyond the 90-nm technology node, many challenges are continuously being raised, such as thin oxide instability, gate/drain leakage, channel length modulation and so on. The industrial and academic communities are aggressively searching for solutions to meet these challenges: (1) non-classical CMOS to extend the life of CMOS technology and (2) fundamentally new technologies to replace CMOS technology. [1] Molecular electronics, one of the emerging nanoscale technologies to extend or replace silicon technology, has been gaining more attention in the past few years owing to the intrinsic scalability of molecular properties and the ability to tune the electronic properties over a broad range through molecular design and chemical synthesis. [2] Their specific role depends on the method in which they are incorporated. [3-7]

The long-term objective of molecular electronics is to learn to construct circuitry using individual molecules as the active component in a bottom-up approach. A more near-term strategy entails the development of hybrid CMOS/molecular devices where redox-active molecules are used to augment the features of traditional, silicon-based, photolithographically constructed circuitry. Compared to other strategies of molecular electronics, our approach has the following advantages: (1) it is a smoother transition technology, which integrates molecule's properties with the vast infrastructure of traditional CMOS technology; (2) intrinsic discrete charge-storage states at very low operating voltage; (3) multiple redox states in a given information storage location [8]; and (4) charge-retention time in the minutes, which is 1,000 times longer than that of DRAM devices. [9]

In this chapter, we have: (1) explored characterization of redox-active molecules attached to Si surfaces and developed theoretical models to explain the electrical characteristics [10, 11], and (2) explored attachment and characterization of molecules on SiO_2 [12] (see **Appendix A** and **B**). Cyclic voltammetry (CyV) (a current-voltage measurement at various voltage scan rate), capacitance-voltage (C-V) and conductance-

voltage (G-V) techniques, and impedance spectroscopy (IS) have been used to characterize the capacitor with redox-active molecular monolayers. Although CyV has been widely used to characterize redox properties of molecules and IS has also been used to characterize non-redox-active monolayers and thin films, [13-15] this study typically involved C-V/G-V and IS of redox-active molecular monolayer on Si and the theoretical models for these hybrid capacitors. In addition, the application of electrolyte/molecule/silicon (EMS) capacitor in DRAM devices has been discussed and examined. This type of analysis is very important for understanding the behavior of any new hybrid electronic device.

3.2 Experimental Details

Hybrid silicon/molecular capacitor consists of an electrolyte/molecule/Si (EMS) structure with molecules attached to Si surfaces followed by the placement of electrolyte as the conducting gate electrode. Figure 3.1 shows the chemical structure of the redox-active compounds: (a) 4-ferrocenylbenzyl alcohol (**Fc-BzOH**) and (b) alcohol derivatized Zn trimesitylporphyrin (**Por-BzOH**). The molecules are synthesized with benzyl alcohol linkers, which enable the attachment of a well-packed self-assembled monolayer (SAM) on Si surfaces via the formation of a covalent Si-O bond. [11, 16] **Fc-BzOH** molecule exhibits two stable states: neutral and mono-positive state while **Por-BzOH** molecule exhibits three stable states: neutral and two redox states (mono- and di-positive states). Multiple redox states are of special interest for memory applications since higher density can be obtained in a single memory location. In addition, multiple state memories can also be enabled by such molecules.

A schematic of the EMS structure is shown in Figure 3.1 (c). The substrates used were (100) p-Si (B, $5x10^{18}/cm^3$) wafers. Active areas of $1x10^{-4}$ and $4x10^{-4}$ cm^2 were defined through a 450 nm field oxide using photolithography. A 10 nm sacrificial oxide was grown in the active areas and then removed slowly prior to attachment using 1% HF to obtain a hydrogenated Si surface. As shown in Table 3.1, the solutions for deposition are prepared by dissolving the redox-active molecules in organic solvents. During the attachments, the temperature of silicon substrate was maintained at 100^oC and 200^oC for the attachments of **Fc-BzOH** and **Por-BzOH**, respectively. It is important to note that the attachment temperature and time are critical factors in achieving a dense and stable monolayer. As

shown in Figure 3.2, the coverage of **Fc-BzOH** SAMs on Si surface saturates at 1.25×10^{14}molecules/cm^2 as the attachment time increases, while the coverage of **Por-BzOH** SAMs saturates at a lower value (0.4×10^{14}molecules/cm^2) due to the bigger size of porphyrin molecules compared to that of ferrocene molecules. The surface coverage of molecules is extracted from the current-voltage curves and will be discussed later. Since the density of Si atoms on (100) surface is ~6.8×10^{14}atoms/cm^2, about 82% (for **Fc-BzOH**) and 94% (for **Por-BzOH**) of Si atoms on the surface are not bonded to the molecules, and remain passivated with hydrogen atoms. A high-temperature, vapor-phase deposition technique has also been recently developed for porphyrin attachment to Si. This is expected to enable large-scale production in the industry and prevent ambient exposure after molecular attachment. [17]

After the molecules are attached, a solution of 1.0 M tetrabutyl ammonium hexafluorophosphate (TBAH) in propylene carbonate (PC) was used as the conducting gate electrolyte for electrical characterization. The interface between electrolyte and molecules acts as an ion-balancing and electron-limiting double layer. Figure 3.1 (c) shows the schematic diagram of the setup for electrical characterization. The samples were measured in a standard probe station for device characterization. Backside contact to the samples is made via the chuck of probe station. Polypropylene micropipette tip containing the silver counter electrode and approximately 5-μL of electrolyte was positioned and controlled by a XYZ-500-TIS testing positioner. Micropipette tip was then lowered until the surface was wetted by the electrolyte. The surface tension of the tip and the highly viscous TBAH+PC electrolyte allowed only a small amount of electrolyte to spread across the active area. The surrounding thick field oxide was further reducing the parasitic capacitance of the overlap region that was covered by the electrolyte. The current-voltage CyV curves is obtained using a CHI600A electrochemical analyzer. C-V, G-V characteristics and IS are obtained by an HP 4284A LCR meter. The write/erase current-voltage characteristics are measured using an HP 4155B semiconductor parameter analyzer.

3.3 Results, Modeling and Discussion

3.3.1 Current-Voltage Characteristics

The current-voltage CyV characteristics of EMS capacitor with **Fc-BzOH** and **Por-BzOH** SAMs at various voltage scan rates are shown in Figure 3.3 (a) and (b), respectively. The **Fc-BzOH** capacitor exhibits one redox state: mono-positively charged while **Por-BzOH** capacitor exhibits two stable redox states: mono- and di-positively charged states. The lower curves in the CyV (negative current) represent the oxidation processes, whereas the upper curves (positive currents) represent reduction processes. During oxidation, positive charges are stored by removing electrons from the molecules, leaving behind holes in the molecular SAM. The redox waves observed at different potentials are associated with the discrete redox states of the molecules. At a given scan rate, the amplitude of the oxidation and reduction waves for each charge-storage state were equal to each other (with respect to the background current). This equivalence indicates that the same amount of charges is being transferred in and out of the SAMs during the oxidation and reduction processes, respectively. The area under the current peaks, normalized by the product of voltage scan rate and the electron charge, provides a measure of the coverage of the molecules on Si surface. The coverage and redox potentials for both the molecules are shown in Table 3.1.

3.3.2 Specific Charge-Current Models

The simple EMS structure and its energy band diagram are shown in the top and bottom panels of Figure 3.4, respectively. Since conduction in the electrolyte is due to the movement of ions, electrons can only pass between the molecule and Si substrate via tunneling induced by the potential across the system. Since the tunneling barrier between the redox center of molecule and Si substrate is very short (<1 nm), we can assume the kinetics of electron tunneling in the system is so fast that the electron either stay in the redox centers or Si, and external electrical signal is much slower than this kinetic. (The limitation of this assumption will be discussed shortly.) So the redox centers in the SAMs form a sheet of surface charge centers and these charge centers can be neutral or positively charged by losing one electron (**Fc-BzOH**) or up two electrons (**Por-BzOH**). With this assumption, we applied Maxwell's equation to describe the system:

$\nabla \times H = J + \frac{\partial}{\partial t} D$,

$\nabla \bullet \nabla \times H = \nabla \bullet J + \frac{\partial}{\partial t}(\nabla \bullet D)$, where H is magnetic field strength, J is current density, and D is electric displacement.

For a system without magnetic field ($H = 0$), we have

$0 = \nabla \bullet J + \frac{\partial}{\partial t} \rho$

$0 = \frac{\partial}{\partial z} J + \frac{\partial}{\partial t} \rho$, where ρ is charge density.

Since the potential is only across in the z direction, the surface charge density of the SAMs is given by $\sigma = \int \rho \cdot dz$. We have

$$J + \frac{\partial}{\partial t} \sigma = 0 \qquad (1).$$

Physically, this equation describes that the current across the system is induced by the rate of changing surface charge density. Accordingly, this current is transient.

For the redox process, i.e. $Fc \Leftrightarrow Fc^+ + e^-$, Nernst's equation can be used to describe the relationship between the oxidizing and reducing charge centers density Γ_O and Γ_R:

$\frac{\Gamma_O(t)}{\Gamma_R(t)} = \exp(\beta \cdot u)$,

$\Gamma_R(t) = \frac{\Gamma}{1 + \exp(\beta \cdot u)}$, where ideally $\beta = q/kT$, $u = V - V_o$ (V_0 is redox potential) and $\Gamma = \Gamma_O + \Gamma_R$ is the surface coverage of the molecules.

Using $\sigma(t) = q\Gamma_R(t)$ and equation (1), we have current-voltage equation:

$$J = \beta q \Gamma \upsilon \frac{e^{\beta(V - V0)}}{\left[1 + e^{\beta(V - V0)}\right]^2} \qquad (2),$$

where υ is the potential scan rate. It should be noted that equation (2) has also been developed by electrochemical methods [18]. As stated by equation (2), current peak J_P occurs at redox potential (V_0) and is linear with scan rate $J_P = \beta q \Gamma \upsilon / 4$. Integrating the peak area under the waves of J-V curve, surface coverage can be calculated $\Gamma = \int JdV / q\upsilon$. All these deductions stated above are in close agreement with experimental data except that the

peak width of measurement is significantly larger than predicted by equation (2), and is due to the combination of non-ideal effects of the molecular monolayer [19, 20] and the series resistance of the electrolyte and Si substrate. This non-ideal effect consumes a fraction of voltage across the EMS structure. Approximately, this non-ideal effect can be incorporated by modifying β, such that

$$\beta = aq/kT \qquad (3),$$

where ***a*** is the non-ideal factor small than 1.

The experimental data and simulations based on equations (2)-(3) of *J-V* curves for **Fc-BzOH** and **Por-BzOH** capacitors are shown in Figure 3.5 (a) and (b), respectively. The corresponding coefficients for the simulation are also shown in the figure. The non-ideal factors "***a***" were 0.62 and 0.59 for **Fc-BzOH** and **Por-BzOH** SAMs on Si, respectively. The oxidation and reduction voltages of the same redox state were separated slightly because the overall kinetics of the EMS system may not be fast enough to be detected by the electrical analyzer. This redox potential separation clearly indicates the limitation of the assumption we have drawn above. Faster voltage scan rates or a larger barrier between molecular redox center and Si substrate will induce larger separation [12]. It is reported that the kinetics decreases exponentially with increasing barrier length and frequency [16, 21-23]. Therefore, the current and current peak equations combining kinetics component should be more appropriately expressed as:

$$J = \beta q \Gamma \upsilon \frac{e^{\beta(V-V0)}}{\left[1+e^{\beta(V-V0)}\right]^2} e^{-\upsilon/\upsilon 0} \qquad (4),$$

$$J_P = (\beta q \Gamma / 4) \upsilon e^{-\upsilon/\upsilon 0} \qquad (5),$$

where $\upsilon 0$ is the kinetic-related coefficient for a particular EMS system. J_P is still closely linear with scan rate υ when it is much smaller than $\upsilon 0$. While υ is getting close to $\upsilon 0$ the exponential term begins to dominate the total current. And larger coefficients $\upsilon 0$ indicates faster kinetic rate. The J_P-υ curves and fits are shown in Figure 3.6 (a) and (b) for **Fc-BzOH** and **Por-BzOH** EMS capacitors, respectively. As shown in the figures, the addition of kinetics in equation (5) results in a better fit than just a linear fit. The peak current densities of both molecules are taken from their mono-positive state. From equation (5) and the fits, the surface coverage can be obtained as 1.25 and 0.4×10^{14} molecules/cm^2 for **Fc-BzOH** and **Por-BzOH** molecules, respectively. The kinetic-related coefficients $\upsilon 0$ for **Fc-BzOH** and

Por-BzOH molecules are 991 and 901 V/s, respectively. This indicates that the kinetic rate of the mono-positive state of **Fc-BzOH** molecule is slightly faster than that of **Por-BzOH** molecule.

The kinetic rate can be also depicted by the peak separation between oxidation and reduction waves of the same redox state in current-voltage CyV curves. Larger peak separation for the same scan rate also indicates slower kinetic rate. [12] As shown in Figure 3.6 (c), the mono-positive state of **Por-BzOH** molecule has a slightly larger peak separation than that of **Fc-BzOH** molecule, and for the **Por-BzOH** molecule, the di-positive state has larger peak separation than the mono-positive state. These results indicate the kinetic rate of **Fc-BzOH** is slightly faster than that of **Por-BzOH**, which is in agreement with the fitting results of equation (5). In addition, these results also indicate that for **Por-BzOH** molecule, the kinetic rate of mono-positive state is faster than that of di-positive state, which is also in agreement with the reported data. [24]

3.3.3 C-V and G-V Characterization

The *C-V&G-V* characteristics of **Fc-BzOH** and **Por-BzOH** SAMs were examined using an LCR meter with parallel mode at 100 Hz, as shown in Figure 3.7 (a) and (b), respectively. Even at low frequency, the capacitance and conductance are such that the quality factor of the whole system is large enough to provide reasonable accuracy in the measurements. Capacitance and conductance peaks related to the oxidation and reduction processes are clearly observed at the voltages corresponding to current-voltage CyV measurements, however the redox potential observed in *C-V&G-V* curves are slightly different from the CyV measurements due to difference in the measurement system. The *C-V&G-V* curves can be divided into three regions: depletion, accumulation, and redox regions. The depletion and accumulation phenomena are associated with the silicon substrate, which resemble those of a metal-oxide-Si capacitor. The C-V&G-V waves in the redox regions are due to charging-discharging of the molecules, similar to current-voltage CyV waves. The total capacitance, C, consists of the background, parallel-plate capacitance, C_0, and the faradic redox-charging capacitance, C_f, :

$$C = \frac{\partial Q}{\partial V} = \frac{\partial Q_0}{\partial V} + \frac{\partial Q_f}{\partial V} = C_0 + C_f,$$

where Q_0 is the background, parallel-plate charge and Q_f corresponds to the faradic charges associated with the redox processes.

Faradic redox-charging capacitance, C_f, dominates the total capacitance in redox region, and is derived as:

$C_f = q \cdot \frac{\partial}{\partial V}\Gamma_R(V)$, using $Q_f = q\Gamma_R(V)$. So the faradic capacitance is simply expressed as:

$$C_f = q\beta \cdot \Gamma \frac{e^{\beta\cdot(V-V0)}}{[1+e^{\beta\cdot(V-V0)}]^2} \qquad (6).$$

Equation (6) is in agreement with the experimental measurements. Although capacitance does not increase with scan rate, the conductance, like the current, does increase with scan rate. This result indicates that the *C-V&G-V* characterization is similar to current-voltage measurement. Capacitance peaks and conductance peaks were still observed at frequencies up to 5 kHz, however the capacitance peaks were lower. Lower capacitance peaks at higher frequency are attributed to a lower effective capacitance of the electrolyte in series. The higher conductance peaks is due to a higher frequency. At frequencies higher than 5 kHz, the resistance and ion movement in electrolyte decreases dramatically and dominate the total capacitance of the measurement. Thereby, no capacitance peaks were observed.

3.3.4 Impedance Characterization and Equivalent RC Models

The impedance characteristics were obtained for a broad range of frequencies at various gate voltages. Different gate voltages: 1.0, 0.5, 0.2 and -0.4V drives the capacitor into different operating regions: depletion-1, depletion-2, accumulation and redox, respectively. The equivalent RC model for EMS capacitor operated in the depletion-1, depletion-2, and accumulation regions are shown in Figure 3.8 (top), where R_S is the series resistance of electrolyte and the Si-wafer; R_{Si} and C_{Si} in parallel are the effective impedance of Si-substrate under molecular SAMs. C_i is the combined capacitance of the double-layer (C_{dl}) and the parallel-plate capacitance (C_m) of molecular SAMs without redox processes. Since C_{dl} is very large compared to C_m, C_i is approximately equal to C_m. Figure 3.8 (bottom) shows the equivalent RC model of EMS capacitor operated in the redox region with the faradic capacitance of redox charging designated as C_f and the charge-transfer resistance

designated as R_{ct}. These coefficients were extracted using a nonlinear-square fitting method to fit the measurements of impedance spectroscopy.

The measured data and fitting results of impedance spectroscopy for **Fc-BzOH** EMS capacitor operated in four regions are shown in Figure 3.9 (a) and (b) for the real part and imaginary part of admittance, respectively, using the coefficients shown in Table 3.2. The capacitance of **Fc-BzOH** SAMs is about 0.26 nF per 10^{-4} cm^2. As shown in Figure 3.9, good fits are observed in the frequency range of 100Hz ~ 30 kHz. The impedance at lower frequencies (<100 Hz) were not selected for fitting because the measurement was affected by noise in that range. In addition, the impedance at higher frequencies (>30 kHz) were not selected for fitting because of two reasons: (1) the quality factor ($Q = 2\pi fC/G$) of the EMS capacitor is low (< 5) that the measurement may not be significantly precise when frequency is higher than 30 kHz; (2) the electrolyte has limited ion-conductivity and prevents accurate measurements. [25, 26]

The measured data and fitting results of impedance spectroscopy for **Por-BzOH** EMS capacitor operated in the four regions are shown in Figure 3.10 (a) and (b), with the fitting coefficients shown in Table 3.3. The capacitance of **Por-BzOH** SAMs is about 0.15 nF per 10^{-4} cm^2. The four regions: depletion-1, depletion-2, accumulation and redox region operate at gate voltages: 1.0, 0.5, 0.2, and -0.7 V, respectively. The mono-positive state was selected for impedance characterization because the repeated electrical stress at high voltage of the small signal DC characterization can severely degrade the redox active monolayer as will be discussed in section 3.6.

3.3.5 Dielectric Constant of SAMs

From the impedance characterization and simulation results shown in Table 3.2 and 3.3, the capacitance of the molecular SAM is about 2.6 and 1.5 μF/cm^2 for **Fc-BzOH** and **Por-BzOH**, respectively. By applying the equation: $C = \varepsilon_0 \varepsilon_m / d_m$, where ε_0 and ε_m are dielectric constants of vacuum and relative dielectric constant of molecular SAM, respectively, and d_m is the thickness of molecular SAM, ε_m/d_m is 2.94 and 1.69 nm^{-1}. Therefore, by knowing the thickness of molecular SAMs (**Fc-BzOH**: 0.8 nm, **Por-BzOH**: 1.5 nm), the relative dielectric constants are 2.4 and 2.5 for **Fc-BzOH** and **Por-BzOH** SAMs, respectively.

The flat-band voltage of EMS capacitor can be calculated using the properties of silicon substrate. In the depletion region of Si substrate, the value of total capacitance (C) varies with applied potential because the semiconductor capacitance, C_{Si}, depends on gate voltage, V_g, and the flat-band voltage, V_{fb} [27, 28]. Using the equivalent circuit shown in Figure 3.8 (a), $\frac{1}{C} = \frac{1}{C_{Si}} + \frac{1}{C_i}$, it can be shown that

$$(C_i/C)^2 - 1 = (2C_i^2/eN_D\varepsilon_0\varepsilon_s)(V_g - V_{fb}) \qquad (7),$$

Where N_D is the doping concentration of Si substrate and ε_s is the relative dielectric constant of Si. By using linear square fitting for equation (7), as shown in Figure 3.11, the flat-band voltage of this EMS system is about 0.52 V, which is the intercept of the gate voltage axis. The slope from the linear fit is about 20 V^{-1}. While the slope expressed as $2C_i^2/eN_D\varepsilon_0\varepsilon_s$ from equation (7) can be also calculated as 16 V^{-1} using N_D of $5x10^{18}/cm^3$ and C_i of 2.6 μF/cm^2, the two numbers are close and within the experimental precision when both the values of N_D and C_i are included within deviation. In addition, the similarity of the calculated number and fitted value indicated the validity of the linear fits of equation (7).

3.3.6 Molecular SAMs on n-type Si

Redox-active molecular SAMs have been also attached to n-type silicon substrates. Since the redox process of molecules occurs in the region of gate voltage where n-Si substrate is in depletion, the high resistance from Si can dominate the redox-induced conductance peaks. As shown in Figure 3.12, the CyV curve in dark does not show any current peak while the curve in strong light show current peaks similar to that of SAMs on p-type Si. In weak light condition, only a small peak is observed. It is believed that the light induces inversion of Si substrate which increases the total number of carriers available for redox processes. In addition, redox potentials also shift to the right (more positive gate voltages) as compared to SAMs on p-Si. This is due to the different surface potentials induced by different Fermi level between the substrate of n and p types and will be discussed in detail by another member of this research group.

3.3.7 Effect of Characterization Temperature

Theoretically, due to factor β in equation (4), current-voltage curves have broader widths and lower peak currents at higher temperature. The theoretical simulations of CyV curves of **Fc-BzOH** SAM on p-Si at different temperatures (room temperature ~20^{o}C and 80^{o}C) using equation (4) are shown in Figure 3.13 (a). In experimental results, the EMS capacitors with **Fc-BzOH** SAM on p-Si have been characterized in two different temperatures room temperature ~20^{o}C and 80^{o}C using a Cascade probe station with a temperature controller from Temptronic, Inc. The measured CyV curves in Figure 3.13 (b) show results that are similar to the simulations but with slight differences. The differences may be due to the fact that the EMS capacitor can not reach the same temperature as the chuck of probe station (80^{o}C) due to continuous evaporation of the electrolyte which can result in net cooling of the samples. The fits of the CyV curve measured at 80^{o}C suggests that the temperature of the EMS capacitor is about 60^{o}C when the chuck of probe station is set to 80^{o}C. However, detail studies are needed in the future to understand the high temperature behavior.

3.3.8 Control Experiments and Stability Characterization

A series of control experiments have been performed to conclusively attribute the findings of the experimental results to the redox states of the **Fc-BzOH** and **Por-BzOH** molecules. The findings from these control experiments are: (1) EMS structure with nonredox-active molecules doesn't show any redox-related peak in current-voltage and impedance measurements [11]; (2) an electrolyte-SiO_2-Si (EOS) structure with various thicknesses of thin oxide does not show any redox-related peak in current-voltage and impedance measurements [12]; (3) an electrolyte-Si (ES) structure shows similar behavior to an EOS structure. In summary, all the control experiments indicated the characteristics of EMS capacitor with **Fc-BzOH** and **Por-BzOH** are distinct and very different from similar structures that did not contain any redox-active molecules.

Stability of molecule is another key issue in molecular electronics [1, 2]. The issue of stability includes reliability, temperature stability, environmental stability and endurance under stress. In a controlled and inert environment, **Fc-BzOH** and **Por-BzOH** can be very reliable and stable. Detail studies via electrical characterization have revealed that molecular

charging properties were unchanged after cycling for more than 10^{11} electrical write/erase square wave cycles. [29] When the inert environment is replaced with ambient environment (air with a certain humidity), or the electrical pulse is replaced with full voltage-range cycle, the molecular SAMs was found to degrade much faster. As shown in Figure 3.14, there are about 80% of **Por-BzOH** molecules remaining active on the Si surface after 200 cycles of current-voltage CyV measurements in an open, ambient environment. It is believed that oxygen and water drift to Si surface, and react with Si, and replace the molecule. These mechanisms can be further accelerated by the electrical stress and thereby, the molecular SAMs are degraded faster. Experiments have also indicated that impedance characterization with small signal DC electrical stress, such as impedance spectroscopy, degrades the molecular SAMs faster than AC Cyclic voltammetry. Therefore, methodology to protect the molecules as they are integrated into devices and tune write/read signals will be crucial for obtaining real-world operation. Finally, the **Por-BzOH** molecule shows good temperature stability up to 450^{o}C which further favors this molecule for hybrid CMOS/molecular electronics.

3.4 Applications and Conclusions

As discussed in Section III, EMS capacitors can be engineered to provide distinct, discrete, multiple redox states. In addition, the two molecules studied here have also been shown to have long charge-retention using an OCPA method. [9] These properties make EMS capacitor attractive for memory applications. One of the applications is a molecular DRAM cell where the EMS capacitor replaces the capacitor in a 1T-1C structure. Figure 3.15 (a) shows the schematic of a molecular DRAM cell consisting of a regular NMOSFET and a hybrid EMS capacitor. The body and source of the regular NMOSFET are both connected to Si substrate of the EMS capacitor. The Ag/electrolyte gate of EMS capacitor is connected to the ground. The channel width, length and threshold voltage (V_{Th}) of the NMOSFET are 50μm, 50μm and 0.25 V, respectively. The write/erase operations of the DRAM cell are conducted through the characterization of drain current-drain voltage (I_D-V_D) curves with a turn-on gate voltage (0.5 V). As shown in Figure 3.15 (b), discrete current peaks at potentials corresponding to those of current-voltage CyV and C-V&G-V curves have been obtained on the I_D-V_D curves for both two DRAM devices with **Fc-BzOH** and

Por-BzOH molecules. No such peaks were observed when the gate voltage was lower than the V_{Th}. These I_D-V_D characteristics indicate that the write/erase of molecular SAMs as the charge-storage medium can be controlled by the word line (gate voltage) and the bit line (drain voltage) of the DRAM cell. It should be noted that the properties of these molecular DRAM can be optimized through the choice of molecules, and MOSFET designs. In addition, EMS structures are also of specific interest in other memory devices including FLASH due to their low write/erase voltages and the molecular properties at the nanoscale.

In summary, we have reported the current-voltage *CyV*, *C-V&G-V*, and impedance spectroscopy measurement on redox-active EMS capacitor. These results indicate that **Fc-BzOH** and **Por-BzOH** molecule are well suited for applications in hybrid memory devices. In this work, the physics and mechanism of redox-charged induced current and capacitance have been discussed. Appropriate current model and impedance RC model have been developed to describe EMS structure quantitatively with a series of physical RC coefficients and kinetic rates of the molecules. We have also demonstrated useful methodologies to characterize molecules via the use of EMS structures.

3.5 References

[1] International Technology Roadmap for Semiconductors, 2003Edition, *Emerging technology sequence*, available on the Web at http://public.itrs.net.

[2] J. Heath and M. Ratner, "*Molecular electronics*," PHYSICS TODAY, vol. 56, pp. 43-49, 2003.

[3] Y. Chen, G. Jung, D. Ohlberg, X. Li, D. Stewart, J. Jeppesen, K. Nielsen, J. Stoddart, and R. Williams, "*Nanoscale molecular-switch crossbar circuits*," NANOTECHNOLOGY, vol. 14, pp. 462-468, 2003.

[4] M. Reed, J. Chen, A. Rawlett, D. Price, and J. Tour, "*Molecular random access memory cell*," APPLIED PHYSICS LETTERS, vol. 78, pp. 3735-3737, 2001.

[5] M. Lieberman, S. Chellamma, Y. Wang, Q. Hang, G. Bernstein, and C. Lent, "*Molecules and supramolecular arrays for quantum-dot cellular automata.*," ABSTRACTS OF PAPERS OF THE AMERICAN CHEMICAL SOCIETY, vol. 224, pp. U474-U474, 2002.

[6] K. Roth, N. Dontha, R. Dabke, D. Gryko, C. Clausen, J. Lindsey, D. Bocian, and W. Kuhr, "*Molecular approach toward information storage based on the redox properties of porphyrins in self-assembled monolayers*," JOURNAL OF VACUUM SCIENCE & TECHNOLOGY B, vol. 18, pp. 2359-2364, 2000.

[7] J. Collett and D. Vuillaume, "*Nano-field effect transistor with an organic self-assembled monolayer as gate insulator*," APPLIED PHYSICS LETTERS, vol. 73, pp. 2681-2683, 1998.

[8] K. Roth, J. Lindsey, D. Bocian, and W. Kuhr, "*Characterization of charge storage in redox-active self-assembled monolayers*," LANGMUIR, vol. 18, pp. 4030-4040, 2002.

[9] K. Roth, Z. Liu, D. Gryko, C. Clausen, J. Lindsey, D. Bocian, and W. Kuhr, "*Charge-retention characteristics of self-assembled monolayers of molecular-wire-linked porphyrins on gold*," MOLECULES AS COMPONENTS OF ELECTRONIC DEVICES, vol. 844, pp. 51-61, 2003.

[10] Q. Li, G. Mathur, S. Gowda, S. Surthi, Q. Zhao, L. Yu, J. Lindsey, D. Bocian, and V. Misra, "*Multibit memory using self-assembly of mixed ferrocene/porphyrin monolayers on silicon*," ADVANCED MATERIALS, vol. 16, pp. 133-+, 2004.

[11] Q. Li, G. Mathur, M. Homsi, S. Surthi, V. Misra, V. Malinovskii, K. Schweikart, L. Yu, J. Lindsey, Z. Liu, R. Dabke, A. Yasseri, D. Bocian, and W. Kuhr, "*Capacitance and conductance characterization of ferrocene-containing self-assembled monolayers on silicon surfaces for memory applications*," APPLIED PHYSICS LETTERS, vol. 81, pp. 1494-1496, 2002.

[12] Q. Li, S. Surthi, G. Mathur, S. Gowda, V. Misra, T. Sorenson, R. Tenent, W. Kuhr, S. Tamaru, J. Lindsey, Z. Liu, and D. Bocian, "*Electrical characterization of redox-active molecular monolayers on sio2 for memory applications*," APPLIED PHYSICS LETTERS, vol. 83, pp. 198-200, 2003.

[13] S. Kar, C. Miramond, and D. Vuillaume, "*Properties of electronic traps at silicon/1-octadecene interfaces*," APPLIED PHYSICS LETTERS, vol. 78, pp. 1288-1290, 2001.

[14] Z. Jin, D. Vezenov, Y. Lee, J. Zull, C. Sukenik, and R. Savinell, "*Alternating-current impedance characterization of the structure of alkylsiloxane self-assembled monolayers on silicon*," Langmuir, vol. 10, pp. 2662-2671, 1994.

[15] V. Howarth and M. Petty, "*Admittance spectroscopy of langmuir-blodgett films on metal electrodes in aqueous solutions*," JOURNAL OF PHYSICS D-APPLIED PHYSICS, vol. 29, pp. 179-184, 1996.

[16] K. Roth, A. Yasseri, Z. Liu, R. Dabke, V. Malinovskii, K. Schweikart, L. Yu, H. Tiznado, F. Zaera, J. Lindsey, W. Kuhr, and D. Bocian, "*Measurements of electron-transfer rates of charge-storage molecular monolayers on si(100). Toward hybrid molecular/semiconductor information storage devices*," JOURNAL OF THE AMERICAN CHEMICAL SOCIETY, vol. 125, pp. 505-517, 2003.

[17] Q. Li, Q. Zhao, S. Surthi, Z. Liu, A. Yasseri, R. Loewe, D. Bocian, J. Lindsey, and V. Misra, "High temperature attachment of organic molecules on substrates," vol. patent in application: The Regent of the University of California and North Carolina State University, 2004.

[18] A. J. Bard and L. R. Faulkner, *Electrochemical methods: Fundamentals and applications*: John Wiley & Sons, New York 1980.

[19] A. Brown and F. Anson, "*Electron-transfer kinetics with both reactant and product attached to electrode surface*," JOURNAL OF ELECTROANALYTICAL CHEMISTRY, vol. 92, pp. 133-145, 1978.

[20] A. Brown and F. Anson, "*Cyclic and differential pulse voltammetric behavior of reactants confined to electrode surface*," ANALYTICAL CHEMISTRY, vol. 49, pp. 1589-1595, 1977.

[21] S. Creager and J. Sumner, "*Electron-transfer kinetics for buried redox molecules at electrode-solution interfaces.*," ABSTRACTS OF PAPERS OF THE AMERICAN CHEMICAL SOCIETY, vol. 222, pp. U315-U315, 2001.

[22] S. Creager and T. Wooster, "*A new way of using ac voltammetry to study redox kinetics in electroactive monolayers*," ANALYTICAL CHEMISTRY, vol. 70, pp. 4257-4263, 1998.

[23] J. Sumner and S. Creager, "*Redox kinetics in monolayers on electrodes: Electron transfer is sluggish for ferrocene groups buried within the monolayer interior*," JOURNAL OF PHYSICAL CHEMISTRY B, vol. 105, pp. 8739-8745, 2001.

[24] K. Roth, D. Gryko, C. Clausen, J. Li, J. Lindsey, W. Kuhr, and D. Bocian, "*Comparison of electron-transfer and charge-retention characteristics of porphyrin-containing self-assembled monolayers designed for molecular information storage*," JOURNAL OF PHYSICAL CHEMISTRY B, vol. 106, pp. 8639-8648, 2002.

[25] A. Chandra and B. Bagchi, "*Frequency dependence of ionic conductivity of electrolyte solutions*," JOURNAL OF CHEMICAL PHYSICS, vol. 112, pp. 1876-1886, 2000.

[26] A. Chandra and B. Bagchi, "*Ionic contribution to the viscosity of dilute electrolyte solutions: Towards a microscopic theory*," JOURNAL OF CHEMICAL PHYSICS, vol. 113, pp. 3226-3232, 2000.

[27] J. Diot, J. Joseph, J. Martin, and P. Clechet, "*Ph-dependence of the si/sio2 interface state density for eos systems - quasi-static and ac conductance methods*," JOURNAL OF ELECTROANALYTICAL CHEMISTRY, vol. 193, pp. 75-88, 1985.

[28] S. M. Sze, *Physics of semiconductor devices*, 2nd ed. New York: Wiley, 1981.

[29] Z. Liu, A. Yasseri, J. Lindsey, and D. Bocian, "*Molecular memories that survive silicon device processing and real-world operation*," SCIENCE, vol. 302, pp. 1543-1545, 2003.

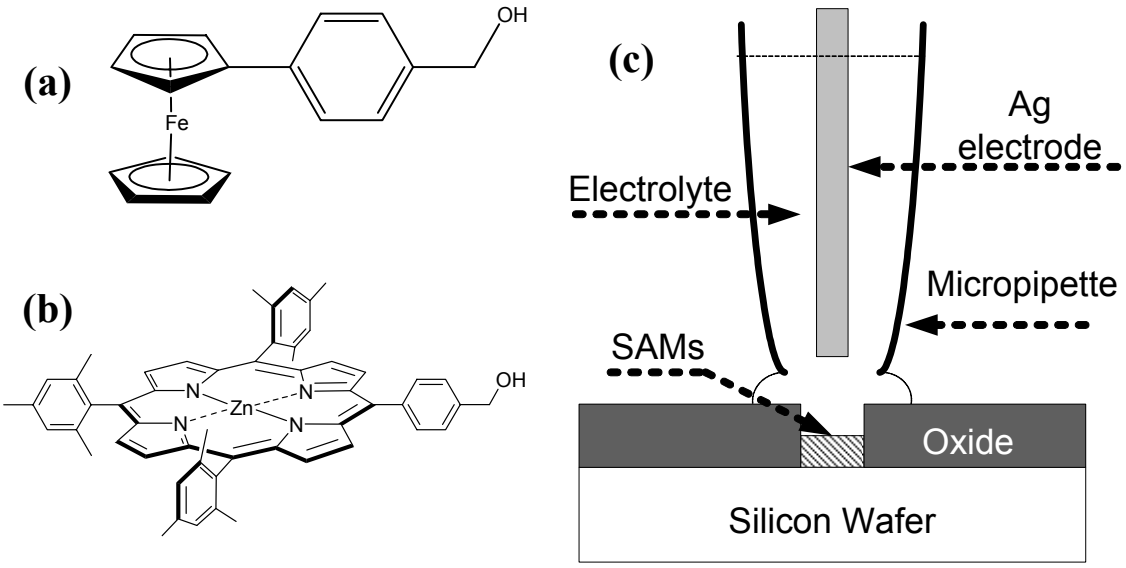

Figure 3.1 The schematics of **Fc-BzOH** (a) and **Por-BzOH** (b) molecules and the schematic diagram of EMS structure and measurement setup for electrical characterization(c). The micropipette is used to hold electrolyte.

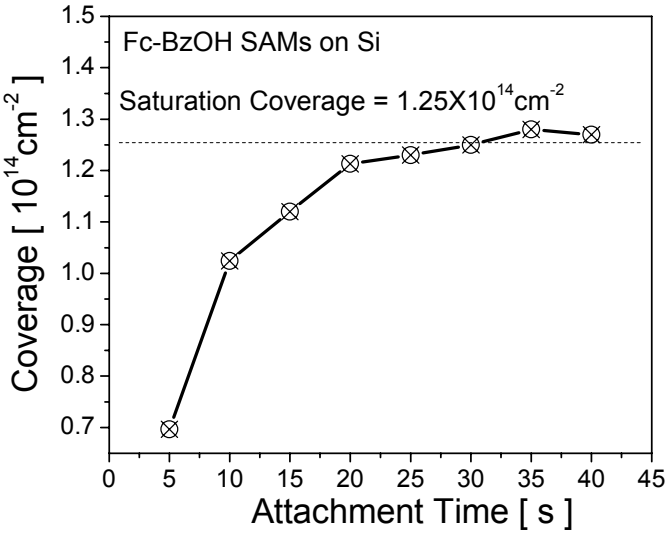

Figure 3.2 Surface coverage of molecular SAMs on Si saturates as attachment time increases.

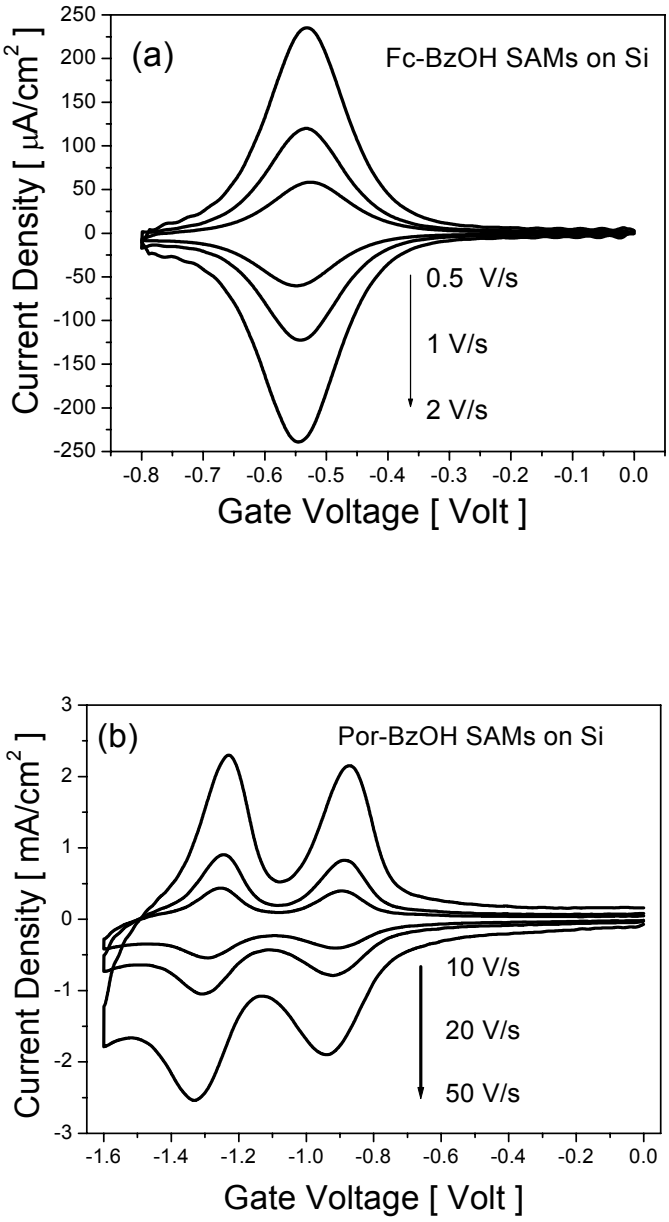

Figure 3.3 The cyclic voltammetry of **Fc-BzOH** (a) and **Por-BzOH** SAMs on Si at various potential scan rates.

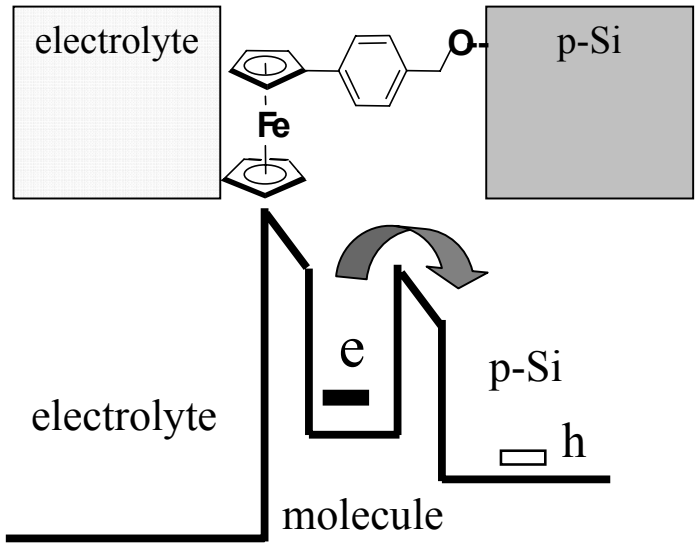

Figure 3.4 The schematic diagram of electrolyte-molecule-Si structure (top) where molecule is covalently bonding to Si surface via O-Si bond, and its band diagram (bottom) where the two barriers are due to molecular linker components and double layer of electrolyte/molecule interface, respectively.

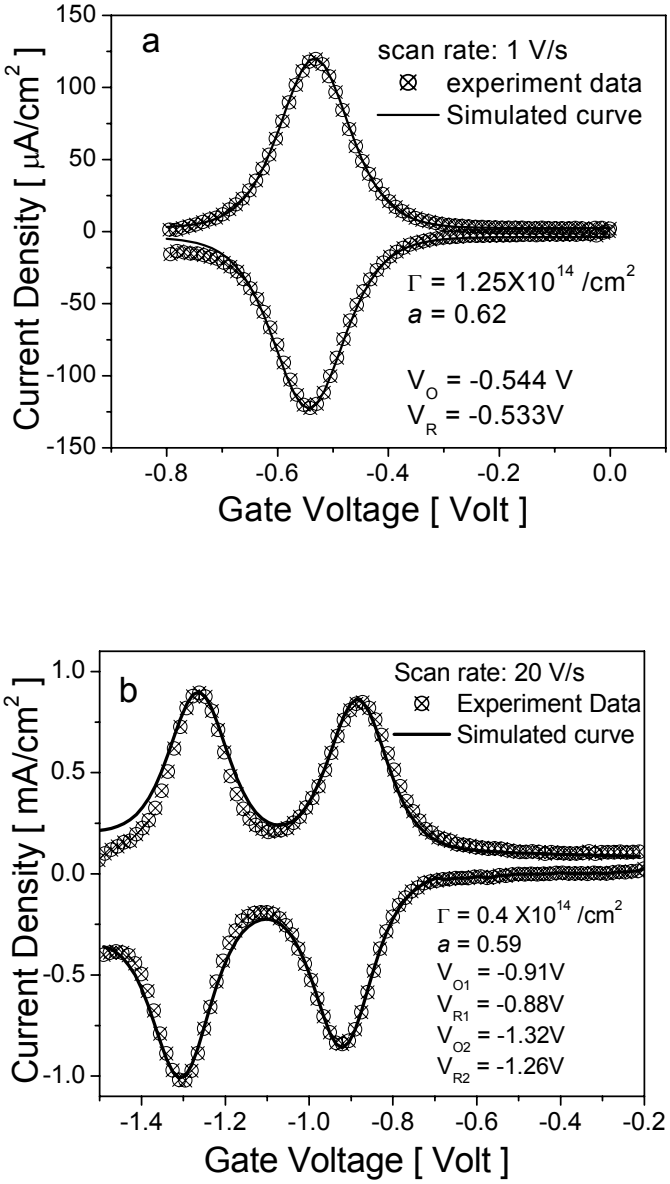

Figure 3.5 The experimental data and simulation results based on equation (2)-(3) for **Fc-BzOH** (a) and **Por-BzOH** (b) EMS capacitors.

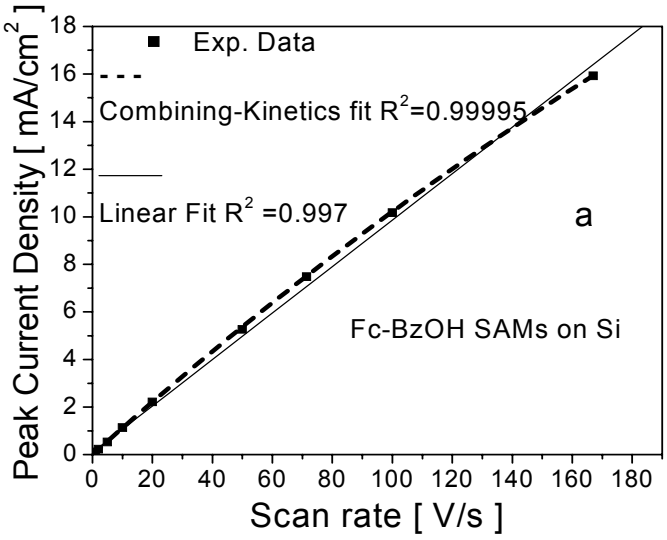
Exp. Data
Combining-Kinetics fit R2=0.99995
Linear Fit R2 =0.997
a
Fc-BzOH SAMs on Si
Peak Current Density [mA/cm2]
Scan rate [V/s]
0
2
4
6
8
10
12
14
16
18
0
20
40
60
80
100
120
140
160
180

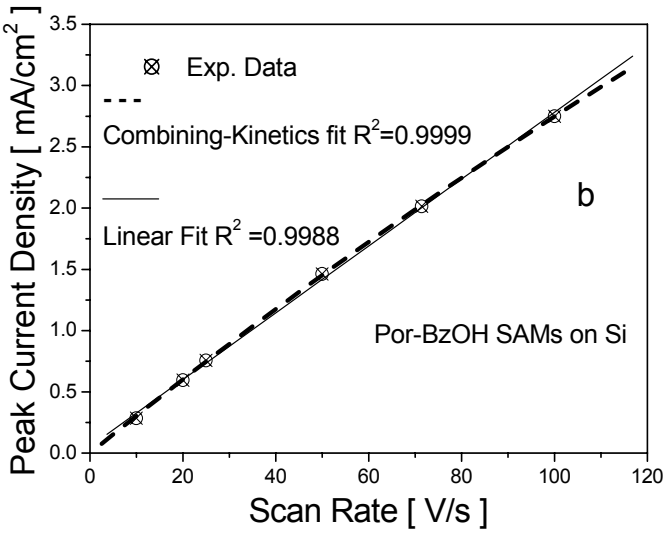
Exp. Data
Combining-Kinetics fit R2=0.9999
Linear Fit R2 =0.9988
b
Por-BzOH SAMs on Si
Peak Current Density [mA/cm2]
Scan Rate [V/s]
0.0
0.5
1.0
1.5
2.0
2.5
3.0
3.5
0
20
40
60
80
100
120

Figure 3.6

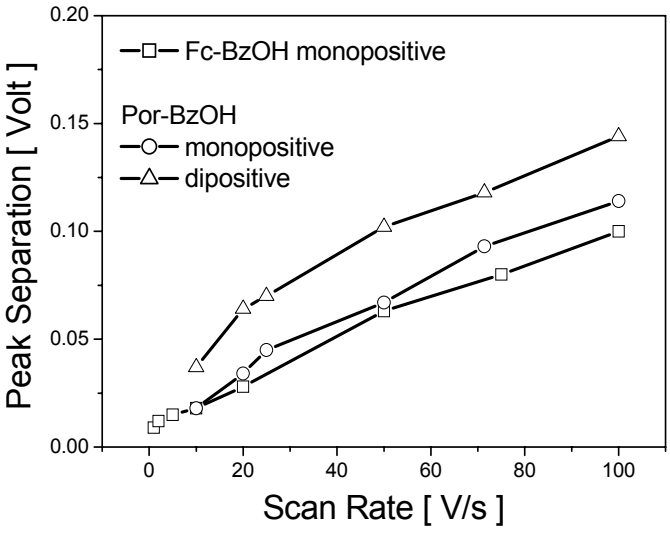

Figure 3.6 The experimental data, linear fit, and combining-kinetics fit based on equation (5) for **Fc-BzOH** (a) and **Por-BzOH** (b) SAMs on Si. Combining-kinetics fit showed a better fitting than linear fit and provided kinetics-related coefficients for both molecules. The kinetic rates can be also shown in the separation of redox peaks over a range of scan rates (c).

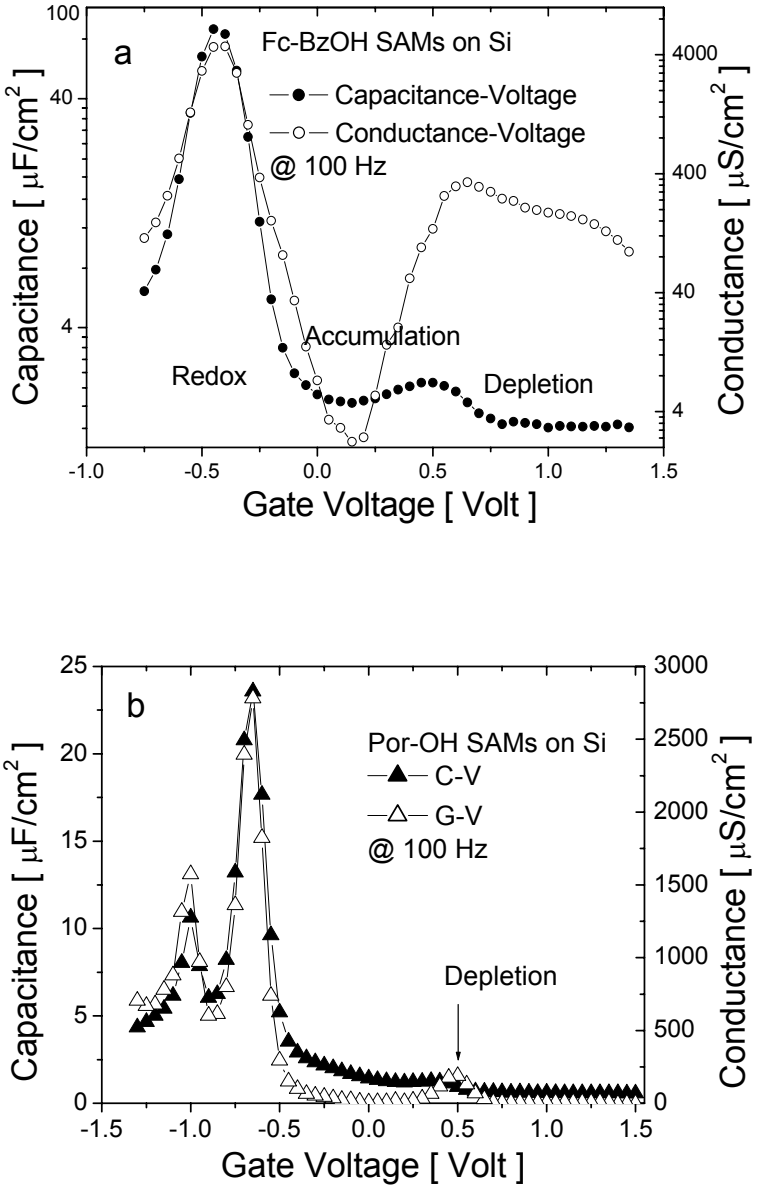

Figure 3.7 C-V&G-V curves of **Fc-BzOH** (a) and **Por-BzOH** (b) EMS capacitors at 100 Hz.

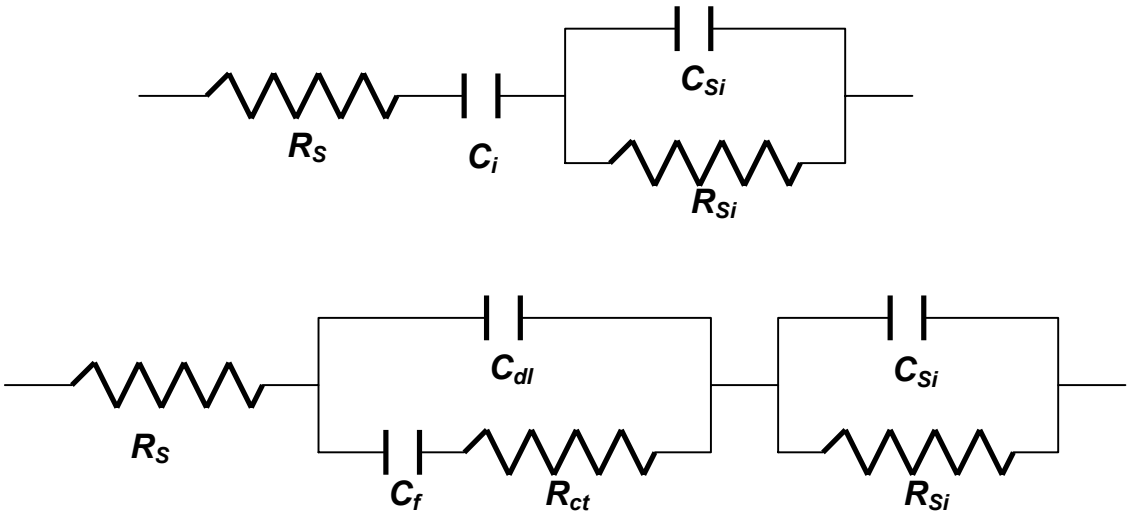

Figure 3.8 The simple RC equivalent circuit (top) for accumulation and depletion regions, and Randle's equivalent circuit (bottom) for redox region of EMS capacitor.

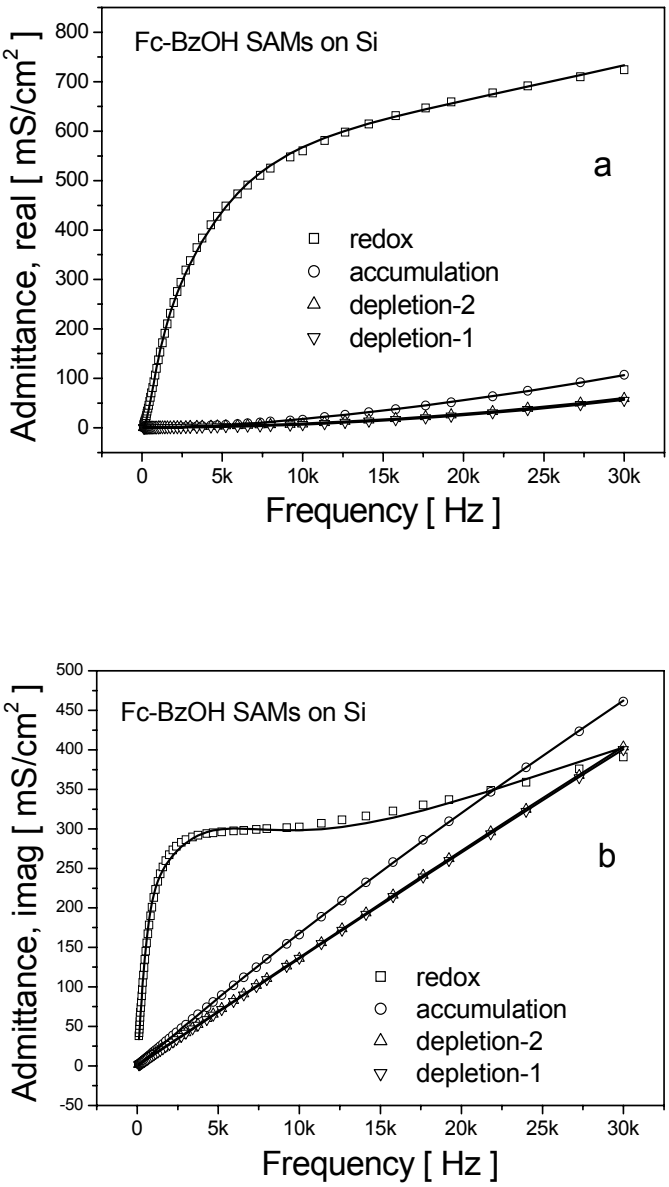

Figure 3.9 The measured impedance spectroscopy (with symbol) and simulated results (line) for various regions of **Fc-BzOH** EMS capacitor: redox (-0.4 V), accumulation (0.2 V), depletion-2 (0.5 V) and depletion-1 (1.0 V). The real part of admittance results is shown in (a), and the imagine part is shown in (b).

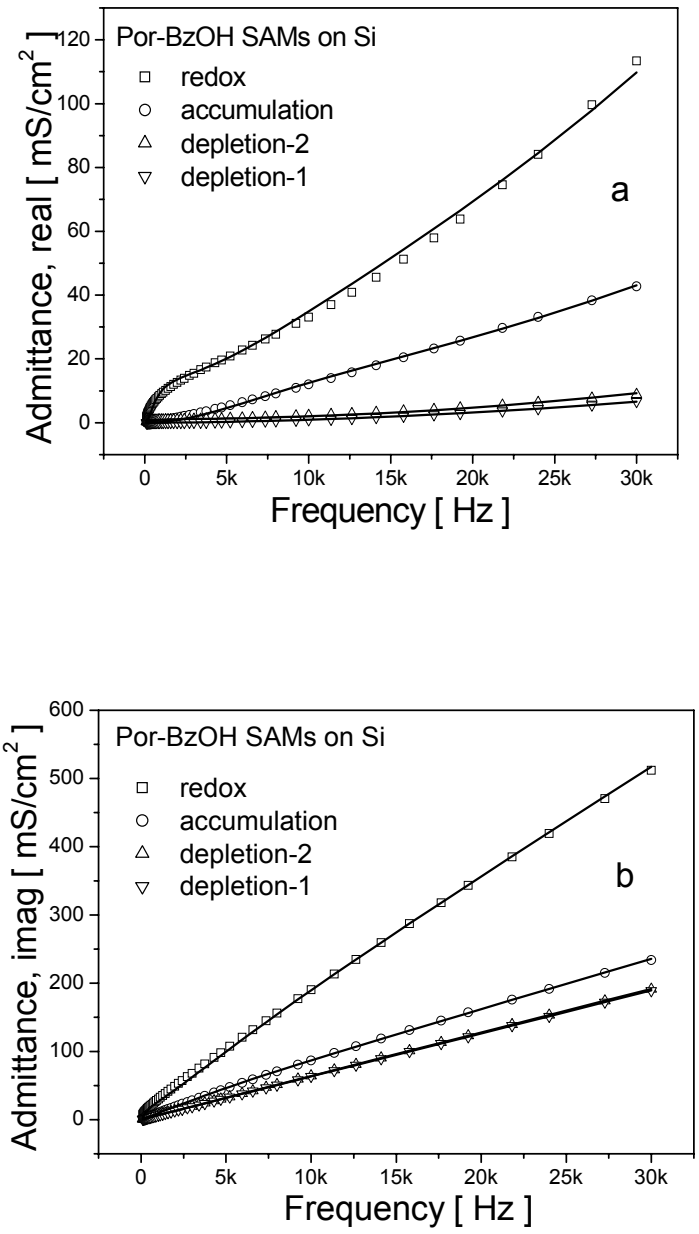

Figure 3.10 The measured impedance spectroscopy (with symbol) and simulated results (line) for various regions of **Por-BzOH** EMS capacitor: redox (-0.7 V), accumulation (0.2 V), depletion-2 (0.5 V) and depletion-1 (1.0 V). The real part of admittance results is shown in (a), and the imagine part is shown in (b).

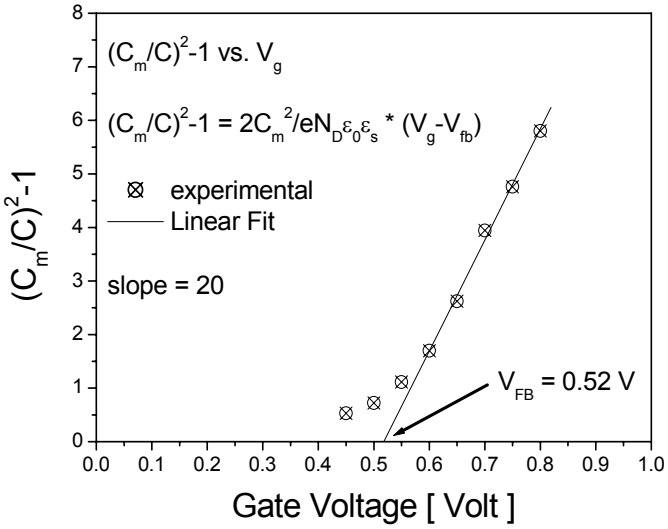

Figure 3.11 The experimental data and linear fitting result of $(C_m/C)^2$-1 vs. gate voltage to extract flat-band voltage of EMS structure.

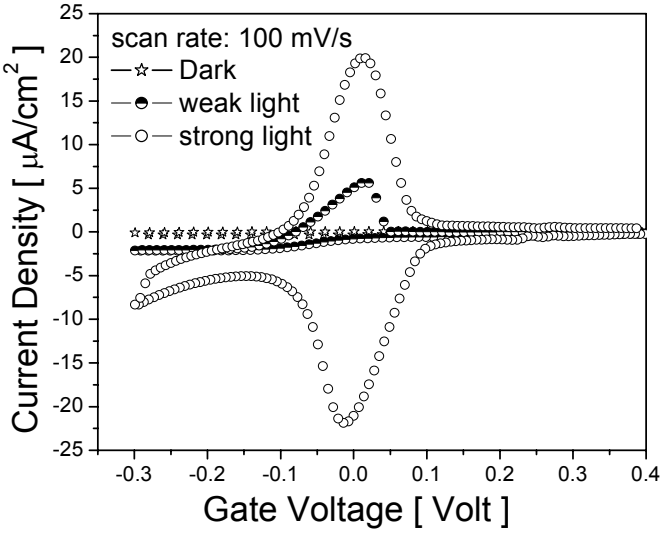

Figure 3.12 Cyclic voltammetric curves of Fc-BzOH SAMs on n-type Si

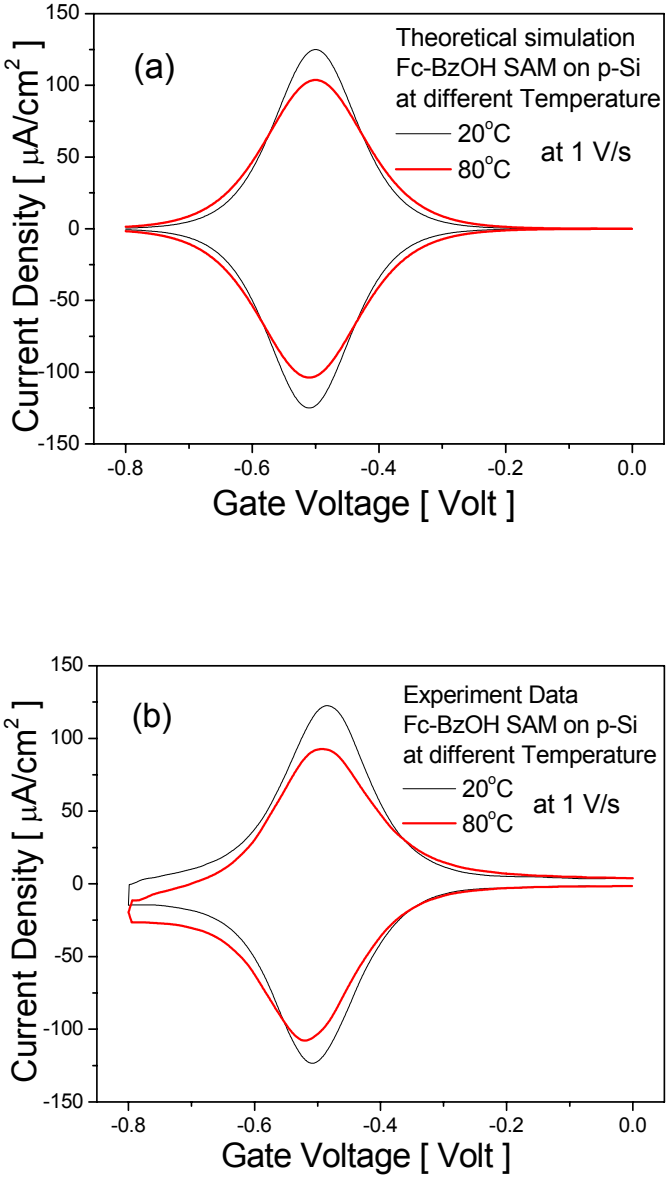

Figure 3.13 (a) Theoretical simulation of CyV of **Fc-BzOH** SAM on p-Si; (b) experimental measurement of CyV of **Fc-BzOH** SAM on p-Si at different temperature.

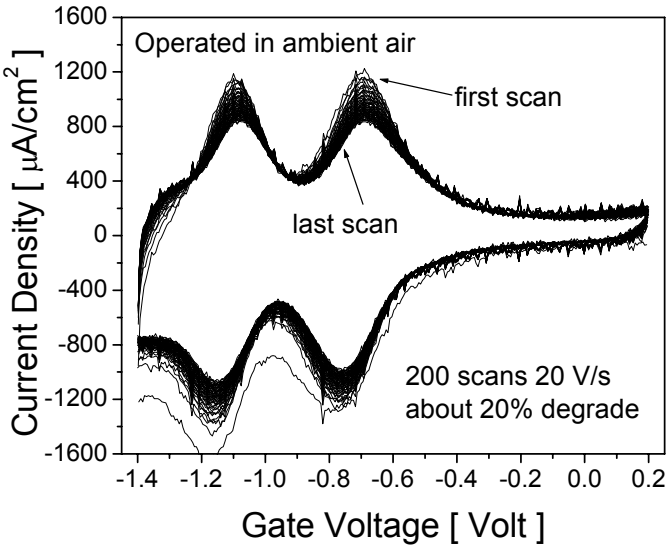

Figure 3.14 Stability characterization. The sample was measured with full-scan cyclic voltammetry in ambient air. About 20% of molecules have been degraded.

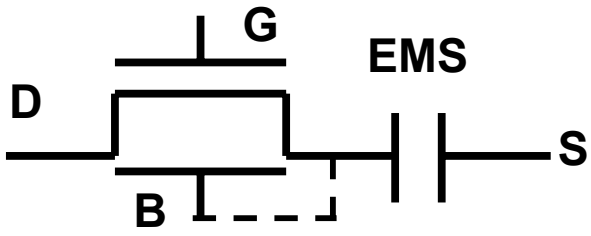

Figure 3.15 The schematic diagram of a molecular DRAM.

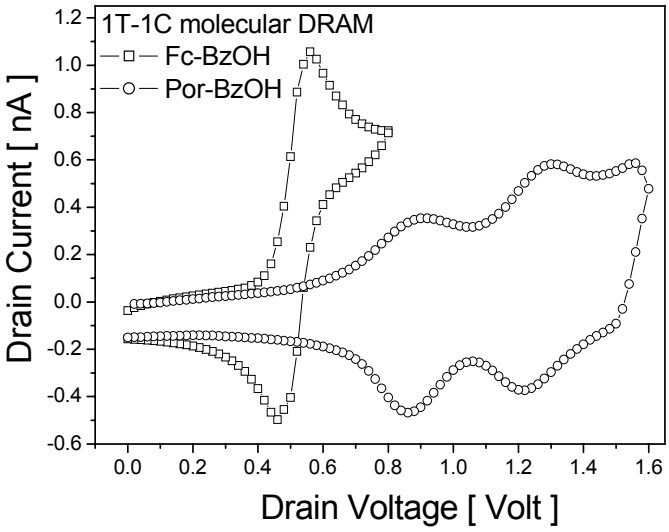

Figure 3.16 The I_D-V_D characteristics of molecular DRAM devices with **Fc-BzOH** and **Por-BzOH** molecules.

Table 3.1 The molecular solution, attachment temperature, and molecule's coverage and redox potentials of both **Fc-BzOH** and **Por-BzOH** molecules

Molecule	Molecule solution	Attachment temperature	Surface coverage	Redox potential	
				Mono-	di-positive
Fc-BzOH	1mg molecule in 400 μL BN	100°C	1.25×10^{14} molecule/cm^2	-0.53 V	NA
Por-BzOH	2mg molecule in 400 μL BN	200°C	0.4×10^{14} molecule/cm^2	-0.88 V	1.26 V

Table 3.2 The RC coefficients of **Fc-BzOH** SAMs on Si used in the models shown in Fig. 3.8 and nonlinear square fits shown in Fig. 3.9

	R_S (kΩ)	R_{Si} (kΩ)	C_{Si} (nF)	C_i / C_f (nF)	R_{ct} (kΩ)	C_{dl} (nF)
Depletion-1 Vg=1.0V	3.42	494	1.63	0.25	NA	NA
Depletion-2 Vg=0.5	3.47	141	1.28	0.26	NA	NA
Accumulation	3.99	3.06	3.05	0.27	NA	NA
Redox	5.76	8.16	7.14	4.73	9.94	0.51

Table 3.3 The RC coefficients of **Por-BzOH** SAMs on Si used in the models shown in Fig. 3.8 and nonlinear square fits shown in Fig. 3.10.

	R_S (kΩ)	R_{Si} (kΩ)	C_{Si} (nF)	C_i / C_f (nF)	R_{ct} (kΩ)	C_{dl} (nF)
Depletion-1 Vg=1.0V	1.89	1377	0.359	0.141	NA	NA
Depletion-2 Vg=0.5	2.21	834	0.33	0.147	NA	NA
Accumulation	4.84	19.0	0.69	0.154	NA	NA
Redox	1.89	138	0.677	0.164	58.7	0.441

Chapter 4 Approaches towards Multibit Memory in One Cell

4.1 Introduction

During the past few decades there has been intense interest in developing molecular-based devices for applications in electronics, including memory [1-7]. For example, monolayers consisting of a small number (~1100) of rotaxane molecules have been used as active components for switches integrated into 64-bit random access memories [8]. Among the various approaches towards building devices that incorporate molecules, the hybrid silicon/molecular approach is attractive as a transition technology because it leverages certain advantages afforded by a molecule-based active medium with the vast infrastructure of traditional MOS technology. Recently, we demonstrated that self-assembled monolayers (SAMs) of redox-active molecules on silicon are excellent candidates for hybrid memory devices. The SAMs were prepared using either a benzyl alcohol-tethered ferrocene (**Fc-BzOH**) or a benzyl alcohol-tethered porphyrin (**Por-BzOH**). In addition to the neutral state, the **Fc-BzOH** provides one state (monopositive) while the **Por-BzOH** provides two states (monopositive, dipositive). The availability of charged states at distinct voltages is highly advantageous for applications in charge-storage memory devices such as DRAM and FLASH. In addition, the molecular-based devices exhibit very low write and erase voltages [9, 10] and long charge-retention times [11, 12].

One strategy to increase memory density entails a multibit approach wherein the charge-storage element contains molecules with multiple redox states. There are several ways to obtain multiple redox states: (1) chemical synthesis, (2) semiconductor substrate engineering, (3) mixed monolayer of various redox-active molecules, and (4) stacked multilayer of various redox-active molecules. The schematic diagrams of mixed monolayer and stacked multilayer have been shown in Figure 4.1 (a) and (b), respectively, where A and B is different redox-active molecules.

Obtaining multiple bit memory via chemical synthesis using a variety of porphyrinic molecules, including a ferrocene–porphyrin conjugate bearing a single tether [13-15], strongly/weakly bonded porphyrin [16, 17], triple deckers of porphyrin [18], and dyad of

triple deckers [19] has been demonstrated. This approach is limited only by the requirements for synthesis of the covalently linked multi-redox molecule. We have also reported on multibit memory through semiconductor substrate engineering in the IEEE IEDM 2003 conference. In that work, we attached ferrocene molecules on a Si substrate with arrays of n-type and p-type area. Since the redox potentials of molecule on n and p type substrate are different and well separated, we are able to obtain multiple redox states. This chapter will focus on obtaining multiple bit memory via attachment engineering.

4.2 Multibit Memory Using Self-assembly of Mixed Ferrocene/Porphyrin Monolayers on Silicon

4.2.1 Introduction

An alternative and perhaps simpler strategy for achieving multibit functionality is afforded by mixing different redox-active molecules whose potentials are well separated. In this paper, we demonstrate this approach using mixed SAMs of **Fc-BzOH** and **Por-BzOH** on silicon surfaces to achieve a four-state (2-bit) memory element. The four states include the neutral state and three distinct cationic states obtained upon oxidation of the **Fc-BzOH** (monopositive) and the **Por-BzOH** (monopositive, dipositive) molecules. Although mixed SAMs have been previously investigated, these studies typically involved mixtures of redox-active and non-redox active molecules[20-24]. In our study, cyclic voltammetry (CyV) has been used to measure the coverage and redox potentials of the mixed SAMs. Since each redox state represents the transfer of a single electron per molecule, the total measured charge per unit area can be directly converted to molecules per unit area. Conventional capacitance and conductance (C-V and G-V) methods have been used to further characterize the mixed monolayer.

4.2.2 Experimental Details

The redox-active molecules used in this study were 4-ferrocenylbenzyl alcohol (**Fc-BzOH**) and 5-(4-hydroxymethylphenyl)-10,15,20-trimesitylporphinatozinc(II) (**Por-BzOH**). In each case, the benzyl alcohol tether affords attachment to the silicon surface via the formation of a Si-O bond [9]. The substrates were (100) p-Si (B, $5x10^{18}/cm^3$) wafers. Active

areas ranging from 25 x 10^{-8} cm^2 to 4 x 10^{-4} cm^2 were defined through a 450 nm field oxide using photolithography. A 10-nm sacrificial oxide was grown thermally and then subjected to 1% HF solution to obtain a high-quality silicon surface. The attachment of molecules to the Si surface was achieved by derivatization of the surface with the alcohol tethers. The attachment solution was prepared by dissolving a mixture of **Fc-BzOH** and **Por-BzOH** compounds in 500 μL of benzonitrile. The molar ratios (**Fc-BzOH**:**Por-BzOH**) were chosen as 1:0 (pure **Fc-BzOH**), 1:0.35, 1:1.4, 1:3.5 and 0:1 (pure **Por-BzOH**). Attachment was achieved by placing a sample of the solution on the heated Si platform (100 °C) for 80 minutes. After attachment, the samples were cleaned by sonication (three times) in dichloromethane. The samples were kept under an argon atmosphere during the entire process. For electrical characterization, a solution of 1.0 M tetrabutylammonium hexafluorophosphate in propylene carbonate was used as the conducting gate electrolyte and a silver wire served as the counter/reference electrode. In an effort to reduce the amount of overlap capacitance between the electrolyte and the substrate on the field oxide, the electrolyte area was further defined by a polydimethylsiloxane well. The capacitance-voltage (C-V) and conductance-voltage (G-V) characteristics were measured using a HP 4284A LCR meter. Traditional cyclic voltammetry (CyV) measurements were obtained using a CHI600A electrochemical analyzer.

4.2.3 Electrical Characterization and Discussion

The CyV of the SAMs of pure **Fc-BzOH**, pure **Por-BzOH**, and three mixtures of these molecules with varying ratios are shown in Figure 4.2. The bottom curves represent oxidation processes and the top curves represent reduction processes. Application of an oxidizing potential causes transfer of electrons from the molecular SAM into the silicon substrate, resulting in storage of positive charges in the SAM. Application of a reducing potential causes transfer of electrons back into the molecular layer, thereby erasing the stored charge. Each of the mixed SAMs shows three redox-current peaks at discrete applied potentials corresponding to the **Fc-BzOH** peak, designated F (at –0.35 V), and the two **Por-BzOH** peaks, termed P1 (at –0.70 V) and P2 (at –1.05 V). (Note that the sign of the potentials is negative because the voltage is applied to the gate rather than the working electrode; accordingly, the potential at the working electrode (which is at virtual ground) is

positive relative to the gate electrode.) The **Por-BzOH** redox peaks in mixed SAMs appear at approximately the same potential as that for the pure **Por-BzOH** SAM on silicon. In contrast, in the mixed SAMs the peak stemming from **Fc-BzOH** shifts to a slightly less negative potential (by 0.15 V) compared to that in SAMs of pure **Fc-BzOH** on silicon.

As the percentage of **Fc-BzOH** molecules in the mixture decreases, the F peak height decreases substantially while the P1 and P2 peak heights increase slightly. These changes are directly related to the surface coverage densities of the two types of molecules on silicon (see Table 4.1), which are related to the molar ratio of **Fc-BzOH** and **Por-BzOH** in the deposition solution. (The surface coverage of the ferrocene or porphyrin molecules is obtained by integrating the area under the respective CyV peak.) As expected, the **Fc-BzOH** current peak is higher than the **Por-BzOH** peaks at a higher concentration of **Fc-BzOH**. The peaks for the two types of molecules become comparable as the molar ratio in the deposition solution decreases to **Fc-BzOH**:**Por-BzOH** = 1 : 3.5, implying similar coverage of the ferrocene and porphyrin molecules in the mixed monolayer (in agreement with the data in Table 4.1). The coverage of **Fc-BzOH** was higher than that of **Por-BzOH**, even at a molar ratio of 1:1. The higher coverage is attributed to the smaller size of **Fc-BzOH** compared to **Por-BzOH**. The higher mobility of the smaller molecule enables faster attachment of **Fc-BzOH** on the available silicon sites. As the molar ratio of **Fc-BzOH** and **Por-BzOH** in solution is decreased to 1:3.5, the ferrocene and porphyrin molecules have about the same coverage: 1.6×10^{13} molecules/cm^2. This result indicates that altering the ratio of the two redox-active species in the deposition solution allows tuning the coverage of different molecules in the mixed monolayer. In another series of experiments, the molecules were deposited sequentially. This procedure also resulted in a mixed monolayer; however, the molecules attached in the first step always dominated the mixed monolayer (data not shown).

As shown in Figure 4.3 (a), the CyV characteristics of a mixed SAM formed from a solution with a molar ratio of **Fc-BzOH**:**Por-BzOH** = 1:1.4 was examined at scan rates of 10, 50, and 100 V/s. As the scan rate increases, the separation increases between the oxidation and reduction voltages. The peak separations are 0.02, 0.02, and 0.04 V at a scan rate of 2 V/s, for F, P1, and P2 peaks, respectively, and 0.10 V, 0.05 V and 0.07 V at 100 V/s. The average value of the oxidation and reduction voltages remains the same (-0.35 V, -0.70 V and -1.05 V for F, P1, and P2 peaks, respectively) over the entire range of scan rates (2 to 100

V/s). The scan-rate dependence of the peak separation could arise from either an increasing resistive drop in the electrolyte or limitations imposed by the intrinsic electron-transfer rate of the redox centers on the Si substrate (or a combination of both factors) [10, 12]. Figure 4.3 (b) shows the dependence of peak current density (J_P) on the scan rates for the F and P1 peaks of the mixed monolayer. The J_P for each scan rate was calculated by subtracting the background current from the peak current value. The relationship was linear for both the F and P1 peaks, thus confirming that the electrode process is only due to the surface-bound species [25]. The CyV current density of surface-bound species is given by $J_P = n^2F^2v\Gamma / 4RT$ [26], where, n is the number of redox states, v is the CyV scan rate, and Γ is the surface concentration of the attached species. Using the above equation and the current density values from CyV scans, the surface molecular coverage is calculated to be 2.3×10^{13} molecules/cm^2 and 1.0×10^{13} molecules/cm^2 for **Fc-BzOH** and **Por-BzOH**, respectively. These estimated values match closely with the experimental data shown in Table 4.1.

The C-V and G-V characteristics of the SAMs were examined at 100 Hz, as shown in Figure 4.4. The SAMs examined include those prepared exclusively from **Fc-BzOH**, from **Por-BzOH**, and mixed SAMs of the two compounds formed with several different molar ratios (1:0.35, 1:1.4 and 1:3.5). Even at low frequency, the capacitance and conductance values are such that the quality factor of the whole system is large enough to provide reasonable accuracy in the measurements. The C-V/G-V curves can be divided into four regions: inversion, depletion, accumulation, and redox regions. The inversion, depletion, and accumulation phenomena are associated with the silicon substrate.

The C-V and G-V curves resemble those of the characteristic metal-oxide-semiconductor (MOS) capacitor except for the presence of additional peaks related to the redox charging and discharging of molecules in the region beyond accumulation of the Si substrate. Each of the mixed SAMs shows three peaks corresponding to the charging behavior of the two different redox species. The redox peaks are very high compared to the capacitance and conductance values in the accumulation and depletion region of the Si substrate, indicating very high charge levels during the redox process. As the ratio of **Fc-BzOH**:**Por-BzOH** decreases, the capacitance and conductance peaks due to **Por-BzOH**

increase whereas those for **Fc-BzOH** decrease, which is in agreement with the CyV measurements.

Our success in obtaining mixed SAMs with well-defined redox states on Si can be contrasted with our previous unsuccessful attempts to form such SAMs on Au surfaces [27]. These earlier studies, which relied on attachment via a thiol-terminated tether, used mixtures of ferrocenes and porphyrins, different types of porphyrins, and different types of triple-decker sandwich coordination complexes. While co-deposition of the thiol species could be achieved on Au, the redox waves were invariably extremely broadened and poorly defined. This characteristic is most likely due to the fact that the Au-S bond is relatively weak and its hybridization can be influenced by the packing of molecules on the surface [28], thereby resulting in very heterogeneous packing of the redox molecules in mixed SAMs. In contrast, the Si-O bond is very strong and the Si-O-C bond is not easily bent [29] resulting in much better organized mixed SAMs.

The reversible, stable and distinct charging and discharging peaks of the SAM in the EMS capacitor make this structure attractive as a multibit memory device. The presence of three distinct cationic redox states obtained with the mixed SAMs gives rise to four states of memory (00, 01, 10, and 11). The 00 memory state corresponds to the neutral state of both molecules (non-oxidized, at 0 V or above). Memory state 01 corresponds to oxidation of the **Fc-BzOH** molecules while the **Por-BzOH** molecules remain neutral (at –0.35 V). The 10 and 11 states of the memory device correspond to the first and second oxidation states of **Por-BzOH**, respectively, with **Fc-BzOH** in the oxidized state (at –0.70 V and ≤ –1.05 V, respectively). Four states (two bits) in one memory cell location are very attractive for increasing memory density without the need for reducing the cell size.

The fact that the EMS capacitor operates at low applied voltage is a further advantage of the device and suggests possible applications in both random access and FLASH memory. The relatively low write and erase voltages of the EMS devices are attractive compared to traditional FLASH devices wherein the operating gate voltages are much higher. The charge-retention time of the EMS capacitor can also be tuned by inserting a barrier between the redox center and the substrate electrode. Such a barrier can be constructed by building a thin oxide layer on silicon [9] and/or by increasing the length of the molecular tether. Furthermore, the **Fc-BzOH** SAMs on silicon exhibit similar electrical characteristics when

the device area is scaled down by more than six orders of magnitude, which confirms one of the key advantages predicted for scaling of molecular-based devices.

4.3 Stacked Molecular Multilayer Film for Multibit Memory

4.3.1 Experimental Details

A **Por-BzOH** SAM was formed on p-Si surface using the attachment procedure detailed previously. After a cleaning step discussed in Chapter 2 was performed, **P-Fc** was deposited on top of the **Por-BzOH** SAM via placing droplets of **P-Fc** solution for 5 minutes per drop. The thickness of **P-Fc** layer was controlled by the deposition time (i.e., the number of drops). Two different deposition times were investigated for stacked multilayer film ***1***: 30 minutes (6 drops of **P-Fc** solution) and ***2***: 15 minutes (3 drops of **P-Fc** solution). During the deposition of **P-Fc** layer, the samples were kept at 200^{o}C. After the attachment of **P-Fc** layer, the samples were cleaned thrice in THF and DC solvents with sonication. As control experiments, the samples have also been cleaned with other solvents including PC to make sure all the remaining **P-Fc** molecules are tightly bonded to the surface. Next, the samples were dried by flowing Argon. During the whole attachment process, the samples were kept in inert environment filled with pure, ambient argon gas. A solution of 1.0 M TBAH in PC was applied on the top of stacked multilayer film as the conducting electrolyte for electrical characterization.

4.3.2 Electrical Characterization and Discussion

The cyclic voltammetric curves of stacked multilayer films ***1*** and ***2*** are shown in Figure 4.5 (a) and (b), respectively. The y-axis *J/υ* represents the current density normalized to corresponding voltage scan rate. The redox peaks associated with **P-Fc** and **Por-BzOH** molecules in the stacked multilayer films are well separated. Both stacked multilayer films show three redox-current peaks at discrete applied potentials (applied to the gate) corresponding to the **P-Fc** peak, designated F (at –0.40 V), and the two **Por-BzOH** peaks, termed P1 (at –0.75 V) and P2 (at –1.15 V). Integrating the area under the peak and dividing the respective scan rate give the surface coverage of molecules. Stacked multilayer film ***1*** consists of monolayer of **Por-BzOH** and about 1 layer of **P-Fc**, with surface coverage of

3.5×10^{13} and 3.1×10^{13} molecules/cm^2, respectively. Stacked multilayer film ***2*** consists of monolayer of **Por-BzOH** and about 3 layers of **P-Fc**, with surface coverage of 3.2×10^{13} and 9.1×10^{13} molecules/cm^2, respectively. At low scan rates, the differences in oxidation and reduction peak voltages are minimized. As scan rate increases, the peak F becomes lower in magnitude and shifts to the left (more negative), and finally merges with peak P1. There was no such peak shifting and merging observed in the case of mixed monolayers. [30] This result indicates that **P-Fc** molecules have slower kinetic rates than the **Por-BzOH** molecules suggesting that **P-Fc** layer is indeed stacked on top of **Por-BzOH** layer, which increases its tunneling distance from the substrate.

In order to confirm that both molecular layers are surface bonded [26], F and P1 peaks were plotted against scan rate and are shown in Figure 4.6. It is found that the curves are very linear at low scan rate. It should be noted that the typical cyclic voltammetric curves of redox-active molecule in solution are linear with square-root of scan rate. [26] This result indicated that the **P-Fc** layer was attached tightly on the surface and not simply dissolved in the electrolyte solution during the measurement.

It can also be observed that the F peak shifts and finally merges with P1 peak. This is attributed to the fact that the separation of oxidation and reduction peaks for **P-Fc** molecules is much larger than that of **Por-BzOH** molecules in the stacked multilayer film. Figure 4.7 shows the dependence of peak separation of F and P1 redox states on scan rate. As scan rate increases, the peak separation of F increases dramatically compared to that of P1. This is because **P-Fc** layer has a layer of **Por-BzOH** between it and Si surface. The electrons tunneling from ferrocene molecules to Si surface face a longer distance and thicker barrier. The rate of electron transfer across a molecule bridge decreases exponentially with the distance of the bridge.

Capacitance-voltage and conductance-voltage characteristics of stacked multilayer film ***1*** have also been examined at 100 Hz (Figure 4.8) and show three peaks corresponding to the charging behaviors of two different redox molecules (**P-Fc** and **Por-BzOH**) in stacked multilayer film. The C-V and G-V resemble those of a MOS capacitor except for the presence of additional peaks related to redox processes. All the three peaks occur in the accumulation region of Si substrate. The first conductance peak at Vg of 0.40V is corresponding to the depletion of Si substrate. The other three conductance peaks at -0.4, -

0.75 and -1.15 are corresponding to peak F, P1 and P2. The ferrocene peak not showing up in C-V curve is associated with its slower kinetic rate even though the conductance shows a peak This similar result are observed in case of SAMs on oxide (T_{OX}>2.0 nm). [9]

4.4 Conclusions of Approach towards Multibit Memory

In summary, we have demonstrated that (1) mixed SAMs of redox-active molecules on Si, and (2) stacked multilayer films exhibit multiple well-defined redox states. The mixed-SAM and stacked multilayer approaches are very attractive owing to the fact that these approaches may be far simpler synthetically than preparing a single molecule that exhibits three (or more) redox states, however the disadvantage of this method is that the density of a given peak goes down. In addition, the two approaches should be amenable to extension to mixtures containing three (or more) components to further increase the number of stored bits.

4.5 References

[1] A. Aviram and M. Ratner, "*Molecular rectifiers*," CHEMICAL PHYSICS LETTERS, vol. 29, pp. 277-283, 1974.

[2] H. Kuhn and D. Mobius, "*Systems of monomolecular layers - assembling and physico-chemical behavior*," ANGEWANDTE CHEMIE-INTERNATIONAL EDITION, vol. 10, pp. 620-&, 1971.

[3] C. Collier, J. Jeppesen, Y. Luo, J. Perkins, E. Wong, J. Heath, and J. Stoddart, "*Molecular-based electronically switchable tunnel junction devices*," JOURNAL OF THE AMERICAN CHEMICAL SOCIETY, vol. 123, pp. 12632-12641, 2001.

[4] J. Heath and M. Ratner, "*Molecular electronics*," PHYSICS TODAY, vol. 56, pp. 43-49, 2003.

[5] J. Heath, P. Kuekes, G. Snider, and R. Williams, "*A defect-tolerant computer architecture: Opportunities for nanotechnology*," SCIENCE, vol. 280, pp. 1716-1721, 1998.

[6] J. Chen, W. Wang, M. Reed, A. Rawlett, D. Price, and J. Tour, "*Room-temperature negative differential resistance in nanoscale molecular junctions*," APPLIED PHYSICS LETTERS, vol. 77, pp. 1224-1226, 2000.

[7] K. Roth, J. Lindsey, D. Bocian, and W. Kuhr, "*Characterization of charge storage in redox-active self-assembled monolayers*," LANGMUIR, vol. 18, pp. 4030-4040, 2002.

[8] Y. Chen, G. Jung, D. Ohlberg, X. Li, D. Stewart, J. Jeppesen, K. Nielsen, J. Stoddart, and R. Williams, "*Nanoscale molecular-switch crossbar circuits*," NANOTECHNOLOGY, vol. 14, pp. 462-468, 2003.

[9] Q. Li, S. Surthi, G. Mathur, S. Gowda, V. Misra, T. Sorenson, R. Tenent, W. Kuhr, S. Tamaru, J. Lindsey, Z. Liu, and D. Bocian, "*Electrical characterization of redox-active molecular monolayers on sio2 for memory applications*," APPLIED PHYSICS LETTERS, vol. 83, pp. 198-200, 2003.

[10] Q. Li, G. Mathur, M. Homsi, S. Surthi, V. Misra, V. Malinovskii, K. Schweikart, L. Yu, J. Lindsey, Z. Liu, R. Dabke, A. Yasseri, D. Bocian, and W. Kuhr, "*Capacitance and conductance characterization of ferrocene-containing self-assembled monolayers*

on silicon surfaces for memory applications," APPLIED PHYSICS LETTERS, vol. 81, pp. 1494-1496, 2002.

[11] K. Roth, Z. Liu, D. Gryko, C. Clausen, J. Lindsey, D. Bocian, and W. Kuhr, "*Charge-retention characteristics of self-assembled monolayers of molecular-wire-linked porphyrins on gold*," MOLECULES AS COMPONENTS OF ELECTRONIC DEVICES, vol. 844, pp. 51-61, 2003.

[12] K. Roth, A. Yasseri, Z. Liu, R. Dabke, V. Malinovskii, K. Schweikart, L. Yu, H. Tiznado, F. Zaera, J. Lindsey, W. Kuhr, and D. Bocian, "*Measurements of electron-transfer rates of charge-storage molecular monolayers on si(100). Toward hybrid molecular/semiconductor information storage devices*," JOURNAL OF THE AMERICAN CHEMICAL SOCIETY, vol. 125, pp. 505-517, 2003.

[13] D. Gryko, C. Clausen, K. Roth, N. Dontha, D. Bocian, W. Kuhr, and J. Lindsey, "*Synthesis of "porphyrin-linker-thiol" molecules with diverse linkers for studies of molecular-based information storage*," JOURNAL OF ORGANIC CHEMISTRY, vol. 65, pp. 7345-7355, 2000.

[14] D. Gryko, F. Zhao, A. Yasseri, K. Roth, D. Bocian, W. Kuhr, and J. Lindsey, "*Synthesis of thiol-derivatized ferrocene-porphyrins for studies of multibit information storage*," JOURNAL OF ORGANIC CHEMISTRY, vol. 65, pp. 7356-7362, 2000.

[15] R. Loewe, A. Ambroise, K. Muthukumaran, K. Padmaja, A. Lysenko, G. Mathur, Q. Li, D. Bocian, V. Misra, and J. Lindsey, "*Porphyrins bearing mono or tripodal benzylphosphonic acid tethers for attachment to oxide surfaces*," JOURNAL OF ORGANIC CHEMISTRY, vol. 69, pp. 1453-1460, 2004.

[16] C. Clausen, D. Gryko, R. Dabke, N. Dontha, D. Bocian, W. Kuhr, and J. Lindsey, "*Synthesis of thiol-derivatized porphyrin dimers and trimers for studies of architectural effects on multibit information storage*," JOURNAL OF ORGANIC CHEMISTRY, vol. 65, pp. 7363-7370, 2000.

[17] C. Clausen, D. Gryko, A. Yasseri, J. Diers, D. Bocian, W. Kuhr, and J. Lindsey, "*Investigation of tightly coupled porphyrin arrays comprised of identical monomers for multibit information storage*," JOURNAL OF ORGANIC CHEMISTRY, vol. 65, pp. 7371-7378, 2000.

[18] A. Balakumar, A. Lysenko, C. Carcel, V. Malinovskii, D. Gryko, K. Schweikart, R. Loewe, A. Yasseri, Z. Liu, D. Bocian, and J. Lindsey, "*Diverse redox-active molecules bearing o-, s-, or se-terminated tethers for attachment to silicon in studies of molecular information storage*," JOURNAL OF ORGANIC CHEMISTRY, vol. 69, pp. 1435-1443, 2004.

[19] K. Schweikart, V. Malinovskii, J. Diers, A. Yasseri, D. Bocian, W. Kuhr, and J. Lindsey, "*Design, synthesis, and characterization of prototypical multistate counters in three distinct architectures*," JOURNAL OF MATERIALS CHEMISTRY, vol. 12, pp. 808-828, 2002.

[20] D. Collard and M. Fox, "*Use of electroactive thiols to study the formation and exchange of alkanethiol monolayers on gold*," LANGMUIR, vol. 7, pp. 1192-1197, 1991.

[21] A. El Kasmi, J. Wallace, E. Bowden, S. Binet, and R. Linderman, "*Controlling interfacial electron-transfer kinetics of cytochrome c with mixed self-assembled monolayers*," JOURNAL OF THE AMERICAN CHEMICAL SOCIETY, vol. 120, pp. 225-226, 1998.

[22] Y. Kashiwagi, K. Uchiyama, F. Kurashima, J. Anzai, and T. Osa, "*Enantioselective oxidation of amines on a gold electrode modified by a self-assembled monolayer of a chiral nitroxyl radical compound*," ANALYTICAL SCIENCES, vol. 15, pp. 907-909, 1999.

[23] I. Willner and B. Willner, "*Molecular and biomolecular optoelectronics*," PURE AND APPLIED CHEMISTRY, vol. 73, pp. 535-542, 2001.

[24] H. Imahori, H. Norieda, H. Yamada, Y. Nishimura, I. Yamazaki, Y. Sakata, and S. Fukuzumi, "*Light-harvesting and photocurrent generation by cold electrodes modified with mixed self-assembled monolayers of boron-dipyrrin and ferrocene-porphyrin-fullerene triad*," JOURNAL OF THE AMERICAN CHEMICAL SOCIETY, vol. 123, pp. 100-110, 2001.

[25] H. Kuramitz, K. Sugawara, M. Kawasaki, K. Hasebe, H. Nakamura, and S. Tanaka, "*Electrocatalytic reduction of hemoglobin at a self-assembled monolayer electrode containing redox dye, nile blue as an electron-transfer mediator*," ANALYTICAL SCIENCES, vol. 15, pp. 589-592, 1999.

[26] A. J. Bard and L. R. Faulkner, *Electrochemical methods: Fundamentals and applications*: John Wiley & Sons, New York 1980.

[27] D. Gryko, J. Li, J. Diers, K. Roth, D. Bocian, W. Kuhr, and J. Lindsey, "*Studies related to the design and synthesis of a molecular octal counter*," JOURNAL OF MATERIALS CHEMISTRY, vol. 11, pp. 1162-1180, 2001.

[28] L. Dubois and R. Nuzzo, "*Synthesis, structure, and properties of model organic-surfaces*," ANNUAL REVIEW OF PHYSICAL CHEMISTRY, vol. 43, pp. 437-463, 1992.

[29] C. Choi, D. Liu, J. Evans, and M. Gordon, "*Passive and active oxidation of si(100) by atomic oxygen: A theoretical study of possible reaction mechanisms*," JOURNAL OF THE AMERICAN CHEMICAL SOCIETY, vol. 124, pp. 8730-8740, 2002.

[30] Q. Li, G. Mathur, S. Gowda, S. Surthi, Q. Zhao, L. Yu, J. Lindsey, D. Bocian, and V. Misra, "*Multibit memory using self-assembly of mixed ferrocene/porphyrin monolayers on silicon*," ADVANCED MATERIALS, vol. 16, pp. 133-+, 2004.

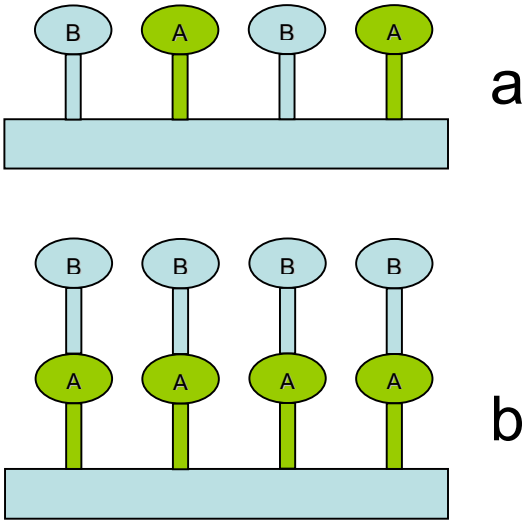

Figure 4.1 Schematic diagrams of mixed monolayer (a) and stacked multilayer (b) of two different redox-active molecules A and B.

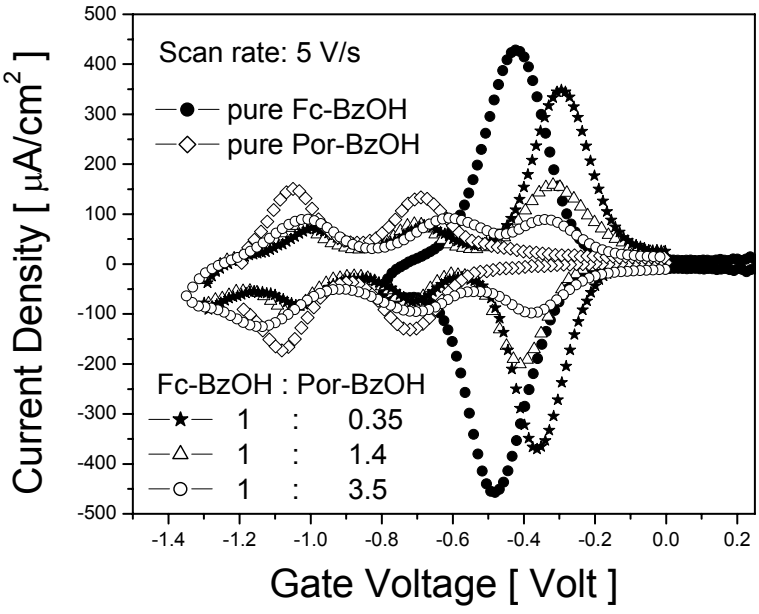

Figure 4.2 Cyclic voltammetry of SAMs of pure **Fc-BzOH**, pure **Por-BzOH**, or mixed SAMs of **Fc-BzOH**:**Por-BzOH** with molar ratios as shown.

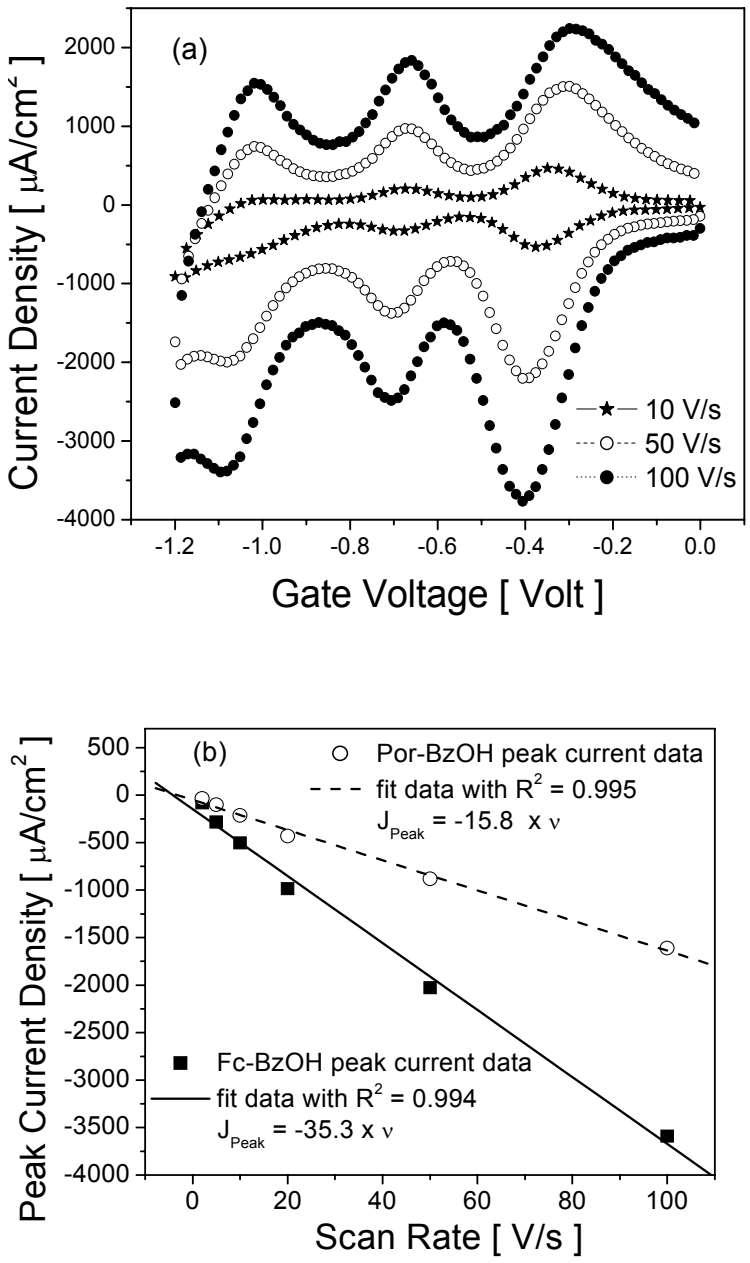

Figure 4.3 Data for a SAM prepared from a solution containing **Fc-BzOH**:**Por-BzOH** in a 1:1.4 molar ratio. (a) Cyclic voltammetry at scan rates of 10, 50 and 100 V/s. (b) Peak current density as a function of CyV scan rate of **Fc-BzOH** and **Por-BzOH** redox peaks. The R^2 values denote the correlation coefficient of the linear fit.

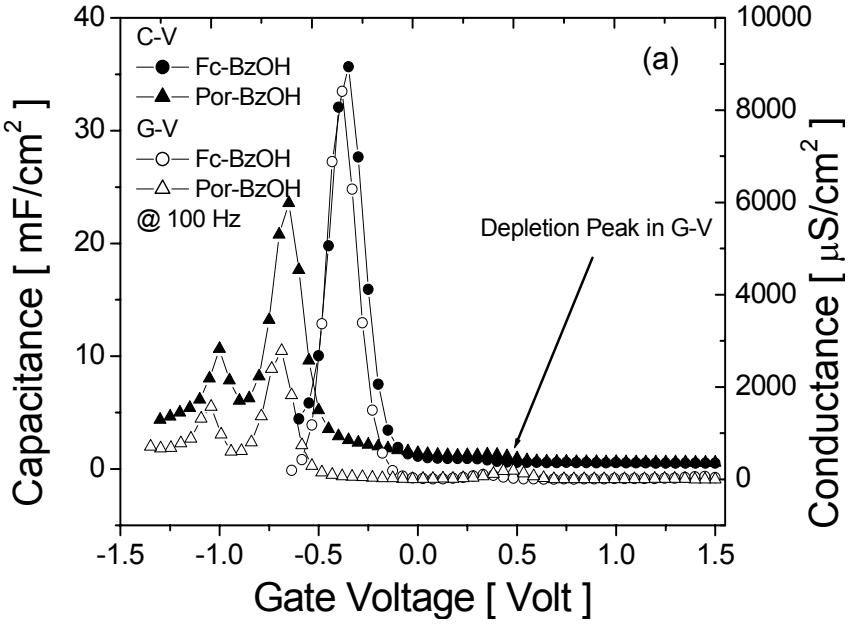
C-V
Fc-BzOH
Por-BzOH
G-V
Fc-BzOH
Por-BzOH
@ 100 Hz
(a)
Depletion Peak in G-V
Capacitance [mF/cm^2]
Conductance [μS/cm^2]
Gate Voltage [Volt]

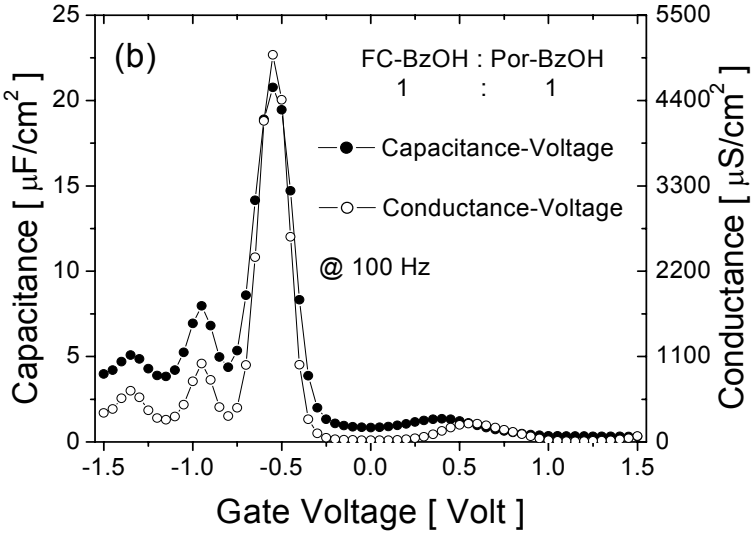
(b)
FC-BzOH : Por-BzOH
1 : 1
Capacitance-Voltage
Conductance-Voltage
@ 100 Hz
Capacitance [μF/cm^2]
Conductance [μS/cm^2]
Gate Voltage [Volt]

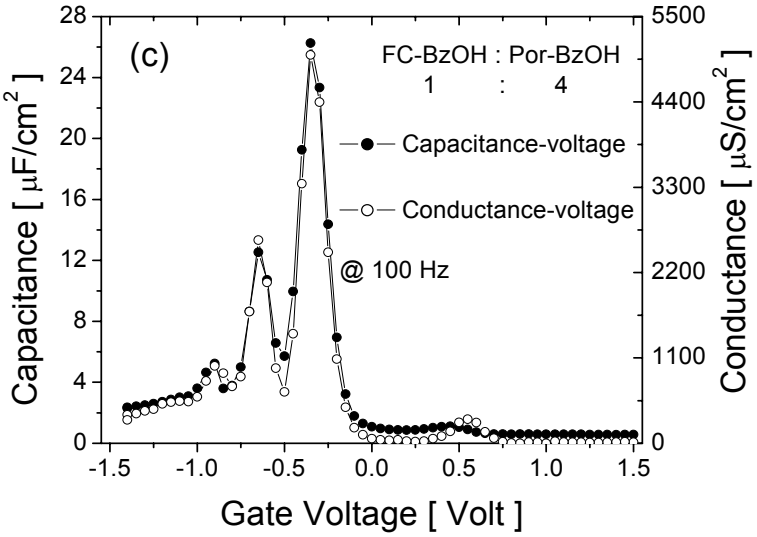

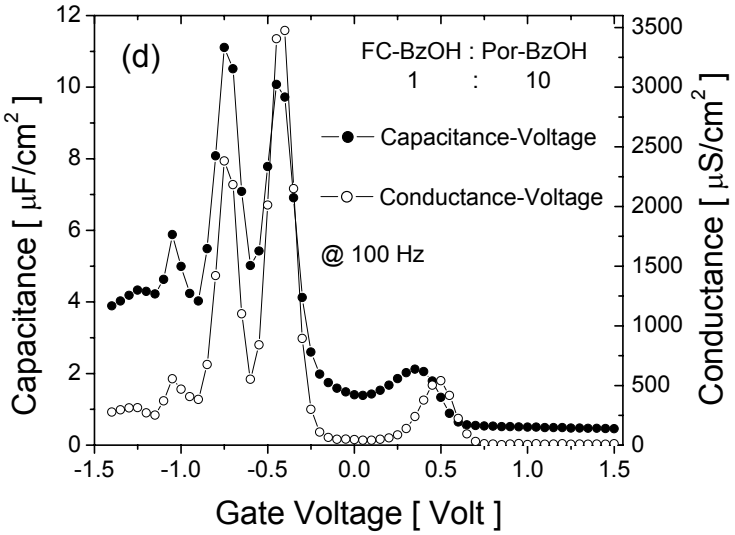

Figure 4.4 Capacitance-voltage and conductance-voltage characteristics with (a) SAMs of pure **Fc-BzOH** or pure **Por-BzOH**; and (b-d) mixed SAMs formed by solutions of **Fc-BzOH**:**Por-BzOH** in the molar ratios indicated.

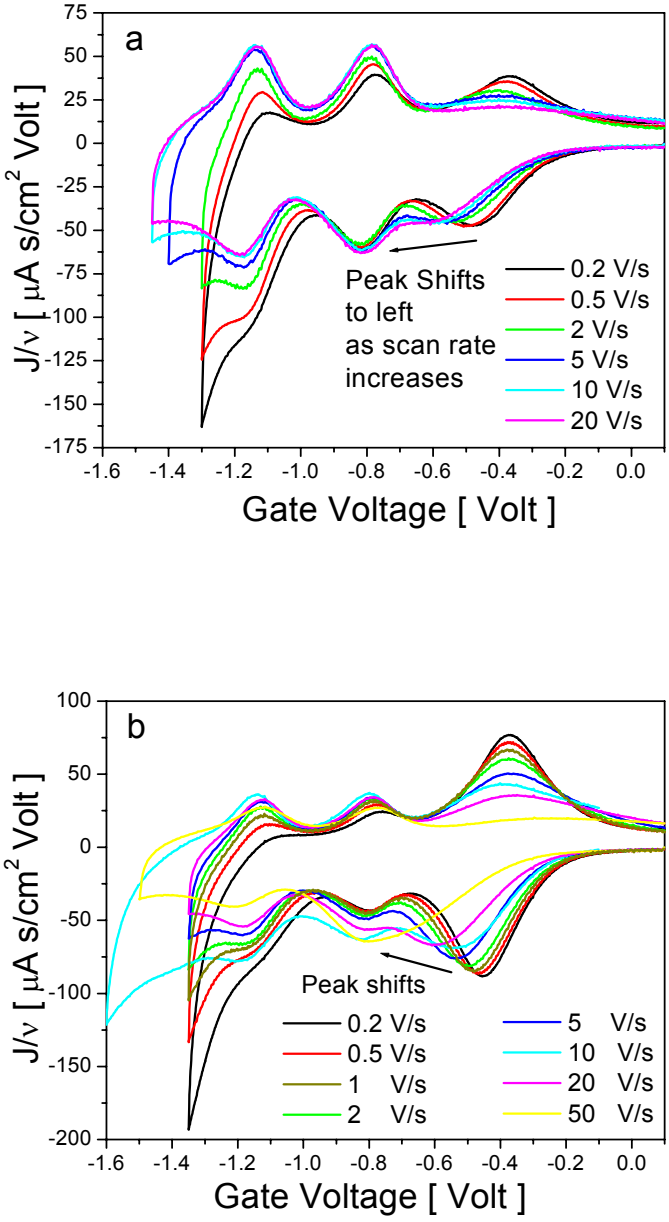

Figure 4.5 Cyclic voltammetry of two stacked multilayer film configurations consisting of monolayer of **Por-BzOH** and (a) monolayer of **P-Fc** or (b) triple layers of **P-Fc** on top of it. The y-axis is *J/υ* representing current density divided by corresponding scan rate.

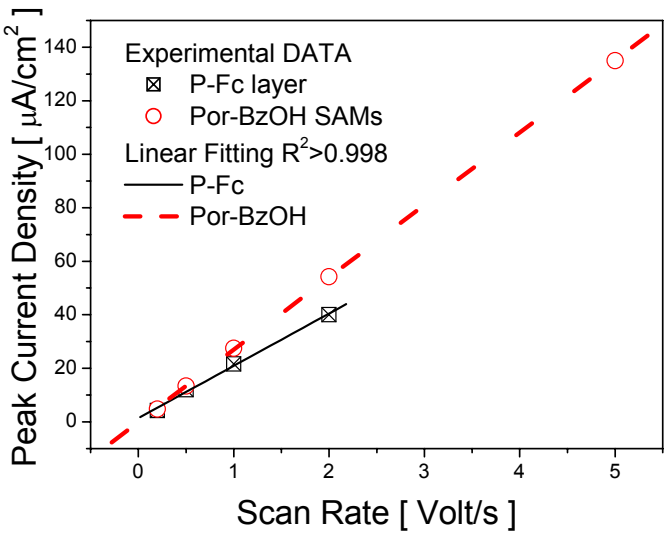

Figure 4.6 Peak current density as a function of CyV scan rate of **P-Fc** and **Por-BzOH** redox peaks. The R^2 values denote the correlation coefficient of the linear fit.

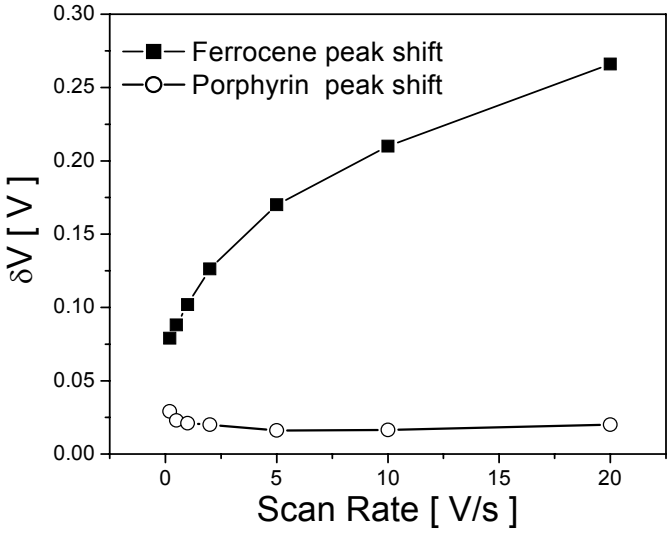

Figure 4.7 The dependence of peak separation between oxidation and reduction state of **P-Fc** and **Por-BzOH** molecules on scan rate.

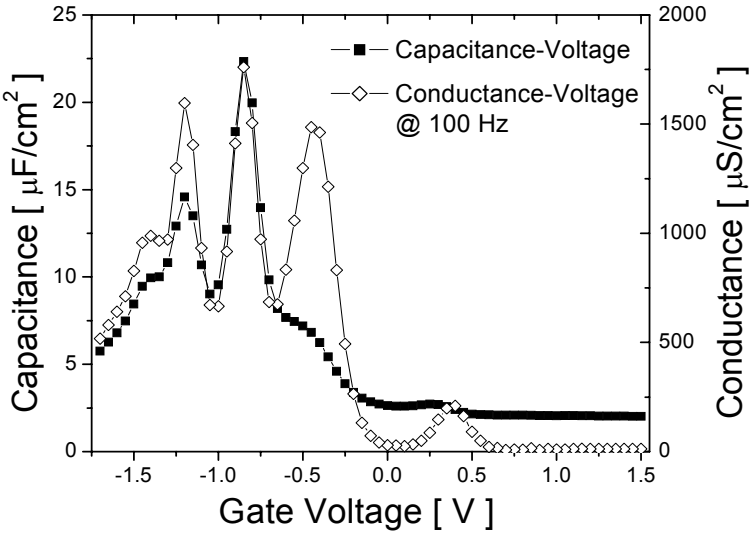

Figure 4.8 Capacitance-voltage and conductance-voltage characteristics of stacked multilayer film with about one layer of **P-Fc** stacked on top of a layer of **Por-BzOH**.

Table 4.1 Effect of variation in molar ratio of **Fc-BzOH** and **Por-BzOH** on molecular coverage: COV_{Fc} and COV_{Por} for **Fc-BzOH** and **Por-BzOH**, respectively.

Fc-BzOH: Por-BzOH Molar Ratio	**COV_{Fc} (Molecules/cm^2)**	**COV_{Por} (Molecules/cm^2)**
1 : 0	1.0×10^{14}	-
1 : 0.35	7.7×10^{13}	0.74×10^{13}
1 : 1.4	2.4×10^{13}	0.96×10^{13}
1 : 3.5	1.6×10^{13}	1.6×10^{13}
0 : 1	-	2.3×10^{13}

.

Chapter 5 Properties of Molecular Multilayer Film and Non-volatile Electrical Switching in Metal/Molecule/Silicon Devices

5.1 Introduction

For the past few decades, molecule-based electronic devices have been gaining more and more interest for molecule's inherent scalability and electronic properties [1-5]. The approach of our group is focused on hybrid CMOS/molecular devices which incorporate redox-active molecules for application in FLASH or dynamic random access memory (DRAM) [6-8]. This strategy utilizes charge storage through electrochemical redox processes which requires an ion-balancing double-layer interface between the electrolyte and molecule. An alternative and perhaps simpler strategy to incorporate molecules in a solid-state device is to use a metal/molecule/metal sandwich structure wherein the molecules are deposited between two metal electrodes by vaporization, self-assembly or Langmuir-Blodgett methods. This approach of using metals to contact molecules in two terminal solid-state devices has recently been reported by several groups, leading to a diverse set of voltage-current behaviors including current rectification [4, 9, 10], switching [5, 11-13], and negative differential resistance (NDR) [14-16].

Recently, non-volatile reversible-switching properties have been reported in a two terminal structure consisting of rotaxane molecules with Pt and Ti as top and bottom electrodes, respectively. [17] The authors have also reported that the molecular-mechanical redox process of rotaxane molecule was not solely responsible for the switching behavior. [18] Although molecules are expected to act as the active elements in these metal/molecule/metal devices, it is difficult to separate the effect of metal electrode from that of the molecule. [19] Utilizing a variety of molecules and electrodes is necessary to further understand this behavior. For example, it is still unknown what is expected to occur when one of the electrodes is a semiconductor. In addition, the difference between redox and non-redox active molecules will also shed light on this subject.

In this chapter, we research on (1) the properties of molecular multilayer film, and (2) the reversible electrical switching characteristics in metal/molecule-multilayer/silicon (MMS) devices. The molecules used in this study include electrochemically redox-active dihydroxyphosphorylmethylferrocene (**P-Fc**) which has oxidation and reduction states that consist of electron discharging and charging through the redox centers of the molecule, respectively. For comparison, nonredox-active molecule has also been used in the MMS sandwich structures. Molecular multilayer film instead of monolayer has been investigated for MMS sandwich structures to avoid shorts when metals are deposited directly on monolayers. Various control experiments were performed to further investigate the physical mechanism of this switching property.

5.2 Properties of Molecular Multilayer Film

5.2.1 Deposition of Molecular Multilayer Film on Si

The silicon substrates used were (100) p-Si (B-doped, $5x10^{18}/cm^3$) wafers. Active areas of $1x10^{-4}$ cm^2 and $4x10^{-4}$ cm^2 were defined through a 450-nm field oxide via photolithography. A 5-nm sacrificial thermal oxide was grown and then subjected to 1% Hydrofluoric acid in water solution to obtain a flat and hydrogenated silicon surface for attachment of molecules. The molecule solution for attachment was prepared by dissolving 0.5 mg of the **P-Fc** molecules in 2 ml benzonitrile (Aldrich, 99.8%). The molecule solution was deposited on the sample by the droplet method with an attachment time of 3 minutes per drop. The sample was kept in Ar at a set temperature during the attachment process. Various temperatures and various attachment times were examined to evaluate their effect on the formation of molecular multilayer films. The investigated attachment times were 6, 15, 30 and 60 minutes, corresponding to 2, 5, 10 and 20 drops of molecule solution for deposition, respectively. Each droplet contains about 3 μL of molecule solution. After deposition, the samples were cleaned with sonication in tetrahydrofuran (Aldrich, 99.8%) three times and then cleaned with sonication in dichloromethane (Aldrich, 99.8%) three times. A solution of 1.0 M tetrabutylammonium hexafluorophosphate (TBAH) (Aldrich) in propylene carbonate (PC) (Aldrich, 99.7%) was used as the supporting electrolyte. The counter electrode was prepared by with sonication the silver wire in 7.0 M NH_4OH and rinsing in deionized water

and ethanol. While the mechanisms responsible for the surface reaction of multilayer film are still unclear, electrochemical characterizations indicates that more than a monolayer of redox-active molecules tightly attach on silicon surface. Control experiments have shown that the multilayer films survive much longer sonication cleanning with different solvent including PC.

5.2.2 Electrochemical Characterization of Molecular Multilayer Films

Over 40 samples of self-assembled **P-Fc** multilayer film were fabricated at 200^{o}C for 4 different attachment times to obtain multilayer film of different thicknesses. Representative cyclic voltammetry for these multilayer films of 6 (film ***a***), 15 (film ***b***), 30 (film ***c***) and 60 (film ***d***) minutes are shown in Figure 5.1 (a), (b), (c) and (d), respectively. Distinct oxidation (bottom curves) and reduction (top curves) peaks were observed for **P-Fc** multilayer films at different scan rates representing oxidation and reduction processes, respectively. The redox potential which is the middle of oxidation and reduction waves is about 0.50 V for all the multilayer films. The surface coverage of the molecules was extracted by normalizing the area under the oxidation waves by the product of scan rate and electron charge. The surface coverage of these four multilayer films a, b, c, and d are 1.8, 3.6, 14.8, and 44.8 $\times 10^{14}$ molecules/cm^2, corresponding to about 1.5, 3, 12, 36 layers of **P-Fc** molecules, respectively, if we are using 1.25×10^{14} molecules/cm^2 as the monolayer coverage. [7] As the number of layers increases the separation ($\Delta \boldsymbol{V}$) between oxidation and reduction peaks increases. The $\Delta \boldsymbol{V}$ is about 0.4 V for multilayer film ***d*** at 1 V/s.

Since the multilayer films have significant thickness, both electron tunneling and diffusion mechanisms affect the total current. The current peak is more nonlinear with voltage scan rate as the thickness increases. [20] As shown in Figure 2 (a), the peak current density ($\boldsymbol{J_P}$) is relatively linear with scan rate when the thickness is smaller than 3 layers but is getting more nonlinear for thicker multilayer films (12 and 36 layers). If we roughly describe the current density as a function of scan rate $\boldsymbol{\upsilon}$ as $J_P = C_1 \upsilon^{\alpha}$, coefficient $\boldsymbol{\alpha}$ is 1 for linear and less than 1 for nonlinear relationship. As shown in Figure 2 (b), coefficient α is the slope of curves Log($\boldsymbol{J_P}$)~Log($\boldsymbol{\upsilon}$). Coefficient $\boldsymbol{\alpha}$ is close to 1 for thin multilayer films and getting smaller for thicker multilayer film (up to 0.919 for multilayer film ***d***). This result

indicates that for thicker multilayer film, electron diffusion becomes more important factor for the total current. In addition, the peak current-scan rate dependence of multilayer film is different than a molecular solution. Typically, for the cyclic voltammetry of redox-active molecular solution, the peak current of oxidation/reduction current is linear with the square-root of scan rate, i.e., coefficient α is 0.5. [20] Thereby, the above measurements indicate that the multilayer films are bonded on the surface and the charge transfer inside the film through two paths includes both tunneling and diffusion.

Figure 5.3 shows that for a thick multilayer film, fewer molecules are oxidized at higher scan rates. This is because the diffusion inside the film is time limited. The thicker the multilayer film is, the slower the kinetic rate is. At a low voltage scan rates, the charges in the redox centers located on the upper part of the multilayer film need more time to move to Si substrate. Therefore, at high scan rates, the charges in the upper part of the multilayer film will not have enough time to completely move to Si substrate, and therefore do not contribute to the measured charge once the scan is finished.

At potentials where no redox reaction can occur, the current obtained from the sample is due to charging and discharging current of a parallel-plate capacitor, i.e. background current (J_B) which is simply described as $J_B = C_0 v$, where C_0 is unit background capacitance of multilayer: $C_0 = \varepsilon\varepsilon_0 / l$ (**ε** is the dielectric constant and ***l*** is the thickness of multilayer). Therefore, J_B is inversely proportional to ***l***. ***l*** is the product of the number of layers and the thickness of each monolayer, which is assumed to be ~1 nm. Figure 5.4 shows that at scan rates of 1 V/s, peak current density increases with increasing thickness of multilayer films, while the background current decreases. The same behavior was observed for all scan rates. Taking into account the effect of noise level and the capacitance of overlap field oxide (designated as coefficient ***A*****,** which is relatively constant with thickness of multilayer film), an equation $J_B = A + B / l$ was used to fit the experimental data, where $B = \varepsilon\varepsilon_0 \upsilon$. As shown in Figure 5.4, the fits have R^2>0.98 and yields ***A***=1.98×10-11 A/cm2 and ***B***=7.22×10-17 A/cm. This result indicates the multilayer is more insulating as it is thicker and has higher redox current. It also justifies that thicker multilayer could be obtained by increasing the deposition time.

These results are all in agreement with that of Figure 5.2 and also indicate that multilayer film of various thicknesses can be obtained through this attachment method.

5.2.3 The Effect of Attachment Temperature

The attachment temperature was found to have a strong effect on multilayer film formation. Five deposition temperatures: 80^{o}C, 100 ^{o}C, 150 ^{o}C, 170 ^{o}C and 200 ^{o}C were investigated for a constant deposition time of 30 minutes to form the multilayer film. More than twenty samples were prepared for each temperature. The maximum, average and minimum thickness of the samples attached at each temperature were obtained. As shown in Figure 5.5, the upper, middle and bottom line represent the maximum, average and minimum values of the surface coverage and thickness for multilayer films, respectively. There is a "jump" between 150^{o}C and 170^{o}C showing that multilayer films can be formed at a temperature over 150^{o}C. This result indicates that the reaction mechanism for multilayer film is activated by higher temperature (>150^{o}C). This result also shows that the formation and thickness of multilayer film can also be controlled by attachment temperature.

5.2.4 The Effect of Deposition Time

As shown in Figure 5.6, the coverage and thickness (the number of layers) of the multilayer films increase as the deposition time increases. The upper, mid and bottom line represent the maximum, average and minimum values of coverage and thickness of the multilayer films attached at the same temperature (200^{o}C) for various deposition times, respectively. About 36 layers can be obtained by 60-minutes deposition of molecule solution. By using 1 nm as the approximate value of thickness of a monolayer of ferrocene, the thickness of 36-layer multilayer film is about 36 nm. This result indicates that the thickness of multilayer film can be controlled by deposition time.

5.3 Non-volatile Electrical Switching in Metal/Molecule/Silicon Devices

5.3.1 Metal/Molecule/Si Structure and Experimental Detail

The fabricated metal/molecular-multilayer/Si sandwich structure is shown in Figure 5.7. After the attachment molecular multilayer film, a eutectic metal Gallium Indium (GaIn) (99.99%, Ga : In = 75.5 : 24.5 wt %) was placed on the top of the multilayer film as the gate electrode by a Dip-Pen like technique. This GaIn metal is in liquid phase in room temperature and will become solid when temperature is lower than 273 K. The eutectic metal GaIn was selected instead of deposited metal as the top contact electrode for molecules to minimize the process damage of metal deposition to molecule multilayer films and allow the investigation of the intrinsic MMS structures. Deposited or vaporized metals such as Au, Ti, Al, W and Ni have been tried as top contacts on the molecular multilayer film. The MMS sandwich devices using these kind of metal as gate electrode always show shorted current after several cycles of electrical characterization. For the purpose of comparison, nonredox-active molecule 4-(dihydroxyphosphorylmethyl)biphenyl (**P-B**) were also investigated for MMS structure. Both **P-Fc** and P-B have been shown in Figure 1 (b) and (c), respectively.

The current-voltage (I-V) characteristics of MMS devices were obtained using a HP 4155B. The samples were measured using a cascade probe station which provides good contact to the Si substrate and is capable to increase the temperature up to 400^{o}C. The devices were electrically characterized at various temperatures. The measurement at temperature lower than room temperature was done using a MMR system.

5.3.2 Nonvolatile Switching Current-Voltage Characterization

Figure 5.8 displays the typical CyV curves of redox active **P-Fc** and non-redox active **P-B** multilayer film control samples measured using electrolyte solution (1.0-M TBAH+PC) as the conducting contact. Oxidation (bottom curves) and reduction (top curves) peaks were observed for **P-Fc** multilayer film at different scan rates representing oxidation and reduction processes, respectively. As expected, the CyV curves of **P-B** nonredox-active multilayer

film didn't show any current peaks. The oxidation and reduction peaks for **P-Fc** were observed at a gate voltage of ~ -0.50 V. The surface coverage of **P-Fc** molecule was calculated as 3.58×10^{15} molecules/cm^2 by integrating the area under the CV peak and dividing by the scan rate. This total charge corresponded to ~ 28 layers of **P-Fc** on the silicon surface. (The number of layers was obtained by dividing multilayer coverage by the typical monolayer coverage: 1.25×10^{14} cm^{-2}. [7])

Figure 5.9 (a) shows the asymmetric I-V hysteresis loop of the GaIn/**P-Fc** multilayer/Si sandwich device (**#1**). The gate voltage was swept from –2.8 V to 3.5 V and then back to –2.8 V. After the gate voltage was swept to 3.5 V, the return I-V sweep was shifted to the left compared to the forward sweep. This resulted in a hysteresis shift such that the device had a higher current value at the same gate voltage after switching back from 3.5 V than before. The device retains this "high-current state" until it is swept to a negative gate voltage of ~-2.8V. In this range, a distinct current peak was observed at -1.45 V. Therefore, in this MMS device, a high positive voltage (~ +3.5 V) switches the device to high-current state and a negative voltage (~ -2.8 V) erases and switches the device back to its low-current state. Furthermore, these switching characteristics are reversible and stable. Also, as shown in Fig. 5.9 (a), no scan rate dependence on the I-V characteristics was observed. This suggests that the I-V characteristics are not generated by charge storage through the molecules since any charging current in the system would have a direct correlation with scan rate.

Several control experiments were conducted to understand the MMS system. As shown in Figure 5.9 (b), the GaIn/**P-B** multilayer/Si sandwiched device (**#2**) displayed very similar I-V characteristics to device **#1**. Even though the **P-B** molecule is nonredox-active, device **#2** still switched reversibly and repeatedly between high-current and low-current states and exhibited distinct current peaks at approximately –0.90 V. The difference in the peak potentials between the two molecules may be related to the difference in their thickness. These results suggest that the switching characteristics are independent of the molecular species since both non-redox and redox molecules exhibit almost identical results.

In addition, as the GaIn metal was replaced by metal Au and Ti via e-beam evaporation and then Au/Ti/molecular multilayer/Si structure was formed, the devices displayed similar but unstable I-V characteristics. The current values were significantly higher (~30×) than with GaIn eutectic and the devices became shorted after several voltage sweeps. This unstable behavior may be a result of the damage caused to the molecules by the relatively high-energy metal particles during the E-beam evaporation. To further understand the system, molecular multilayer film were substituted by a single monolayer. [21] These devices displayed the same type of switching characteristics as the MMS devices but were very unstable and became shorted after a few cycles. This may be due to the fact that the monolayer is more vulnerable to damage/diffusion from the gate contact. Finally, placing a metal eutectic GaIn contact pad on the silicon surface without molecule multilayer or monolayer only resulted in shorts without any switching behavior. This result indicates that the presence of molecules is necessary to observe the switching characteristics.

These results obtained in this work have similarities to I-V characteristics obtained with percolation NDR [22], phase-change non-volatile memory [23] and current filaments [24-26]. Even though experimental results indicated that these switching characteristics and distinct current peaks are independent of the molecular species and not related to redox-charge storage, the mechanism and physics involved in asymmetry switching behaviors are still unclear. We believe that these characteristics are dominated by the interaction of the interface between metal electrode and molecules. Since the coverage of the molecules is accompanied by defects and pores, filaments can form through these pores. For example, metal deposited on porous dielectrics have reported to give similar IV characteristics to those observed in this work [26]. In such structures, conductivity is dominated by a matrix of conductivity filaments. The conduction through these filaments is ohmic at low voltages, but at higher voltages Joule heating starts rupturing the filaments which cause the current to decrease resulting in a negative differential peak [26]. The mechanisms observed in our work may be related to these filaments or metal percolation however, further studies are in progress to uncover the physics of the interactions.

To shed more insight into the modulation of the I-V characteristics, the effect of the varying positive switching voltages (V_{SW}) was investigated. As shown in Figure 5.10 (a),

device **#1** the peaks in the negative gate voltage region (0 → -2.8V) showed a direct correlation to the positive switching gate voltage (V_{SW}=2.0, 2.5, 3.0 and 3.5 V). As shown in Figure 5.10 (b), higher V_{SW} voltages induce a higher current peak at negative gate voltage (-1.45 V). The peak current is close to zero when V_{SW} is lower than 1.0 V and saturated when V_{SW} is higher than 4.0 V. Thus, the peak current of these devices can be controlled by the value of V_{SW}. In addition, increasing the hold time of the V_{SW} also increased the peak indicating a voltage-time enhanced mechanism. Furthermore, the observed switching behaviors are non-volatile. Between "writing at positive V_G" and "reading at negative V_G", no significant degradation of both states was measured after waiting for more than 72 hours. However, reading the device at a negative gate voltage actually erases the high-current state. An alternate method is to read the state at small positive gate voltages where $V_{READ} << V_{SW}$. As shown in Figure 5.11, the high/low-current states can be read at V_G <0.5 V without switching the devices. The current ratio of high-current and low-current states at V_G of 0.04 and 0.5 V is about 1500 and 600, respectively. Although increasing the V_{READ} to 1V improves the ratio of the high-current to low-current, it can also slowly erase the low current state. The I-V characteristics observed here are very stable and no significant degradation was observed for both the two states after more than 3 days in ambient air conditions. In summary, the low operating voltage, good stability and long retention time observed in these MMS devices are attractive for application in non-volatile memory device.

5.3.3 C-V and G-V Characterization

As shown in Figure 5.12, the C-V&G-V characteristics at 1 MHz have been obtained for MMS devices. Same capacitance and conductance were observed at various frequencies from 5 to 1000 kHz. After the MMS device has been set to high-current state at positive gate voltage, G-V curves show a peak at negative voltage and C-V curves show reverse wave with a minimum. The conductance peak is corresponding to the current peak in I-V characteristics. Then the device has been set back to low-current state. The conductance of this device is very high so it dominates the whole impedance. In the low-current state where conductance is low, the quality factor Q is still reasonable high (>6) so that the impedance results can be measured. While in the high-current state (high conductance), Q is so small (<0.1) that the impedance of MMS can not be precisely measured.

5.3.4 The Effect of Multilayer Film Thickness

As shown in Figure 5.13, The I-V hysteresis for MMS sandwiched devices with various thickness of multilayer films have been obtained at room temperature. The thicknesses investigated in the figure are 6, 15 and 28 layers. Figure 5.14 shows the peaks of Fig. 5.13 in more detail and larger scale. The thinnest multilayer film (6 layers) has the highest hysteresis current in the positive-potential side and highest peak in the negative-potential side. On the other hand, the thickest multilayer film (28 layers) has the lowest current and peak. The position of current peak also shifts more negative as the thickness increases. These results indicate that (1) current decreases as thickness increases; (2) higher gate voltage is needed to reduce high-current state to low-current state.

5.3.5 The Effect of Characterization Temperature

As shown in Figure 5.15, the same MMS device with 15 layers of **P-Fc** multilayer film was characterized at various temperatures: room temperature (about 20^{o}C), 80^{o}C and -30^{o}C. It should be noted that the GaIn was in solid state at -30^{o}C. The highest hysteresis current and peak were observed when the sample was measured at room temperature. The observed current levels did not showing a clear trend (increase/decrease) with changes in temperature. As shown Figure 5.16, the peak position shifts to more negative voltages as the temperature decreases. We believe that at lower temperature, more energy from the applied voltage is needed to activate and reduce the interface reaction, thereby resulting in an increase of the peak voltage.

5.4 Conclusions of Molecular Multilayer Film and Nonvolatile Electrical Switching

In summary, the findings in this chapter include: (1) various thickness of molecular multilayer films can be obtained; (2) nonvolatile electrical switching characteristics have been observed for metal/molecule/Si sandwiched devices; (3) current through MMS device decreases as thickness increase and peak position shifts to more negative as temperature decreases or thickness increases.

5.5 References

[1] A. Aviram and M. Ratner, "*Molecular rectifiers*," CHEMICAL PHYSICS LETTERS, vol. 29, pp. 277-283, 1974.

[2] J. Heath and M. Ratner, "*Molecular electronics*," PHYSICS TODAY, vol. 56, pp. 43-49, 2003.

[3] H. Kuhn and D. Mobius, "*Systems of monomolecular layers - assembling and physico-chemical behavior*," ANGEWANDTE CHEMIE-INTERNATIONAL EDITION, vol. 10, pp. 620-&, 1971.

[4] M. Ratner and A. Aviram, "*Molecular rectifiers - model calculations*," BULLETIN OF THE AMERICAN PHYSICAL SOCIETY, vol. 19, pp. 341-341, 1974.

[5] C. Collier, J. Jeppesen, Y. Luo, J. Perkins, E. Wong, J. Heath, and J. Stoddart, "*Molecular-based electronically switchable tunnel junction devices*," JOURNAL OF THE AMERICAN CHEMICAL SOCIETY, vol. 123, pp. 12632-12641, 2001.

[6] Q. Li, G. Mathur, S. Gowda, S. Surthi, Q. Zhao, L. Yu, J. Lindsey, D. Bocian, and V. Misra, "*Multibit memory using self-assembly of mixed ferrocene/porphyrin monolayers on silicon*," ADVANCED MATERIALS, vol. 16, pp. 133-+, 2004.

[7] Q. Li, S. Surthi, G. Mathur, S. Gowda, V. Misra, T. Sorenson, R. Tenent, W. Kuhr, S. Tamaru, J. Lindsey, Z. Liu, and D. Bocian, "*Electrical characterization of redox-active molecular monolayers on sio2 for memory applications*," APPLIED PHYSICS LETTERS, vol. 83, pp. 198-200, 2003.

[8] K. Roth, N. Dontha, R. Dabke, D. Gryko, C. Clausen, J. Lindsey, D. Bocian, and W. Kuhr, "*Molecular approach toward information storage based on the redox properties of porphyrins in self-assembled monolayers*," JOURNAL OF VACUUM SCIENCE & TECHNOLOGY B, vol. 18, pp. 2359-2364, 2000.

[9] A. Martin and J. Sambles, "*Molecular rectification, photodiodes and symmetry*," NANOTECHNOLOGY, vol. 7, pp. 401-405, 1996.

[10] R. Metzger, "*Unimolecular rectification down to 105 k and spectroscopy of hexadecylquinolinium tricyanoquinodimethanide*," SYNTHETIC METALS, vol. 109, pp. 23-28, 2000.

[11] Z. Donhauser, B. Mantooth, K. Kelly, L. Bumm, J. Monnell, J. Stapleton, D. Price, A. Rawlett, D. Allara, J. Tour, and P. Weiss, "*Conductance switching in single*

molecules through conformational changes," SCIENCE, vol. 292, pp. 2303-2307, 2001.

[12] G. Ramachandran, T. Hopson, A. Rawlett, L. Nagahara, A. Primak, and S. Lindsay, "*A bond-fluctuation mechanism for stochastic switching in wired molecules*," SCIENCE, vol. 300, pp. 1413-1416, 2003.

[13] J. Chen, W. Wang, J. Klemic, M. Reed, B. Axelrod, D. Kaschak, A. Rawlett, D. Price, S. Dirk, J. Tour, D. Grubisha, and D. Bennett, "*Molecular wires, switches, and memories*," MOLECULAR ELECTRONICS II, vol. 960, pp. 69-99, 2002.

[14] J. Chen, M. Reed, A. Rawlett, and J. Tour, "*Large on-off ratios and negative differential resistance in a molecular electronic device*," SCIENCE, vol. 286, pp. 1550-1552, 1999.

[15] N. Guisinger, R. Basu, M. Greene, A. Baluch, and M. Hersam, "*Observed suppression of room temperature negative differential resistance in organic monolayers on si(100)*," NANOTECHNOLOGY, vol. 15, pp. S452-S458, 2004.

[16] N. Guisinger, M. Greene, R. Basu, A. Baluch, and M. Hersam, "*Room temperature negative differential resistance through individual organic molecules on silicon surfaces*," NANO LETTERS, vol. 4, pp. 55-59, 2004.

[17] Y. Chen, D. Ohlberg, X. Li, D. Stewart, R. Williams, J. Jeppesen, K. Nielsen, J. Stoddart, D. Olynick, and E. Anderson, "*Nanoscale molecular-switch devices fabricated by imprint lithography*," APPLIED PHYSICS LETTERS, vol. 82, pp. 1610-1612, 2003.

[18] D. Stewart, D. Ohlberg, P. Beck, Y. Chen, R. Williams, J. Jeppesen, K. Nielsen, and J. Stoddart, "*Molecule-independent electrical switching in pt/organic monolayer/ti devices*," NANO LETTERS, vol. 4, pp. 133-136, 2004.

[19] J. Hsu, Y. Loo, D. Lang, and J. Rogers, "*Nature of electrical contacts in a metal-molecule-semiconductor system*," JOURNAL OF VACUUM SCIENCE & TECHNOLOGY B, vol. 21, pp. 1928-1935, 2003.

[20] A. J. Bard and L. R. Faulkner, *Electrochemical methods: Fundamentals and applications*: John Wiley & Sons, New York 1980.

[21] Q. Li, G. Mathur, M. Homsi, S. Surthi, V. Misra, V. Malinovskii, K. Schweikart, L. Yu, J. Lindsey, Z. Liu, R. Dabke, A. Yasseri, D. Bocian, and W. Kuhr, "*Capacitance*

and conductance characterization of ferrocene-containing self-assembled monolayers on silicon surfaces for memory applications," APPLIED PHYSICS LETTERS, vol. 81, pp. 1494-1496, 2002.

[22] B. Ridley, "*Hot-electron percolation*," SOLID-STATE ELECTRONICS, vol. 33, pp. 859-861, 1990.

[23] S. K. Lai, presented at IEDM, 2003.

[24] A. Chesnys, S. Karpinskas, and A. Urbelis, "*Current-voltage characteristic and parameters of the current filament region of an amorphous gallium telluride-crystalline silicon barrier negistor structure*," TECHNICAL PHYSICS, vol. 47, pp. 1263-1267, 2002.

[25] R. Sharpe and R. Palmer, "*"concerted" regeneration of electroformed metal-insulator-metal devices*," JOURNAL OF APPLIED PHYSICS, vol. 79, pp. 8565-8570, 1996.

[26] R. Thurstans and D. Oxley, "*The electroformed metal-insulator-metal structure: A comprehensive model*," JOURNAL OF PHYSICS D-APPLIED PHYSICS, vol. 35, pp. 802-809, 2002.

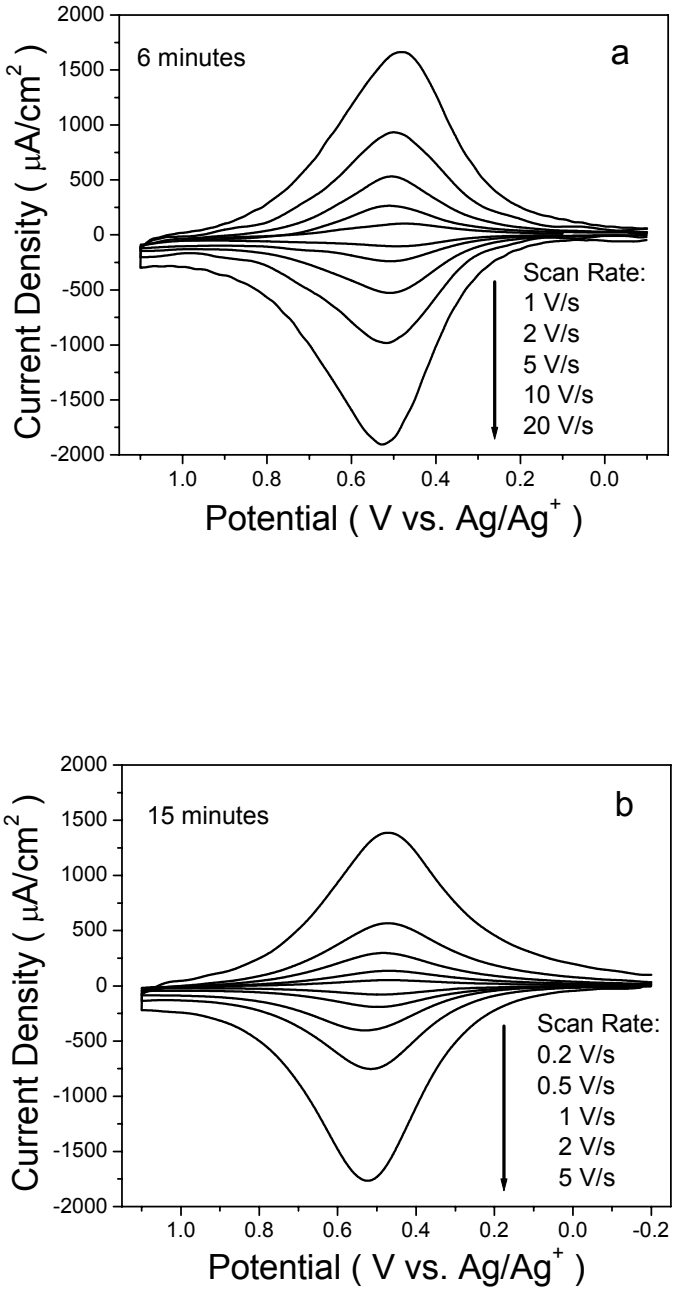

Figure 5.1

Representative cyclic voltammograms of **P-Fc** multilayer films on Si microelectrodes at different potential scan rates. The multilayer films were deposited for various attachment times: 6 minutes (a), 15 minutes (b), 30 minutes (c) and 60 minutes (d).

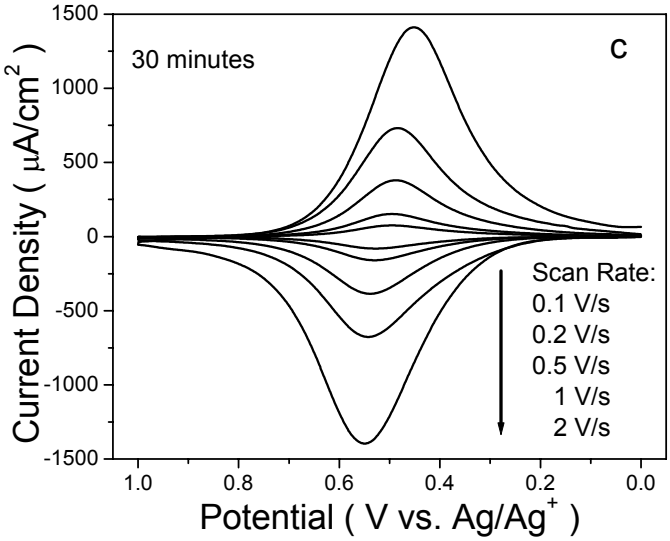

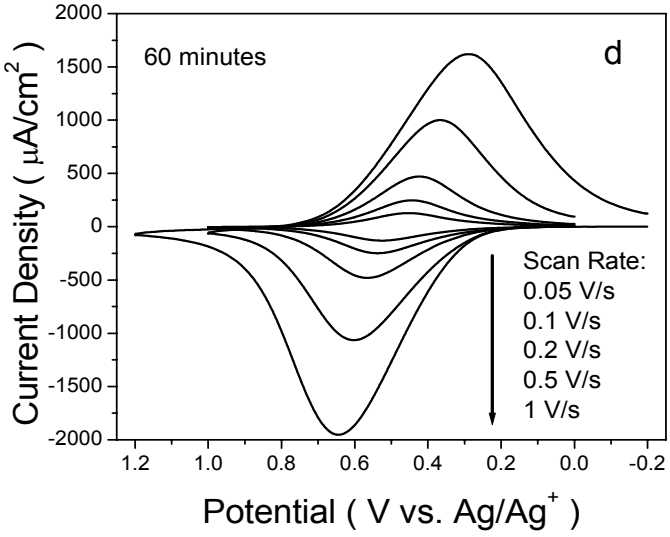

Figure 5.1 Representative cyclic voltammograms of **P-Fc** multilayer films on Si microelectrodes at different potential scan rates. The multilayer films were deposited for various attachment times: 6 minutes (a), 15 minutes (b), 30 minutes (c) and 60 minutes (d).

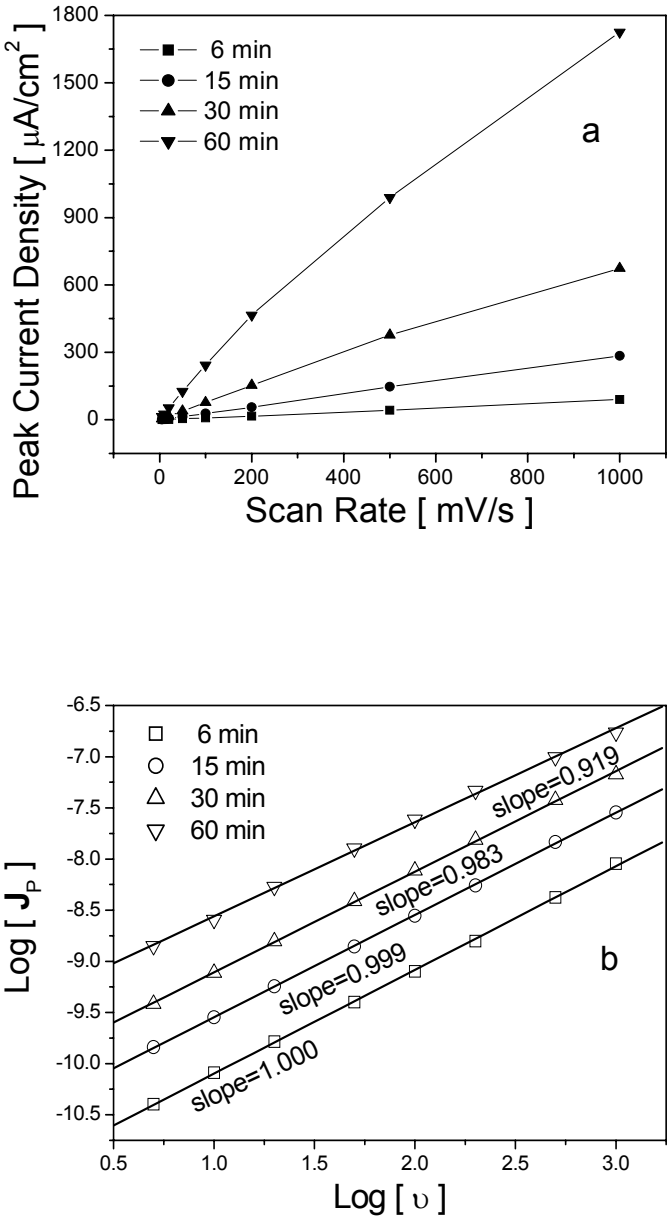

Figure 5.2 (a) Peak current density of multilayer films deposited for 6, 15, 30 and 60 minutes as a functions of potential scan rate. (b) Peak current and scan rate in log-scale and the linear fitting of $Log(J_P) \sim Log(v)$.

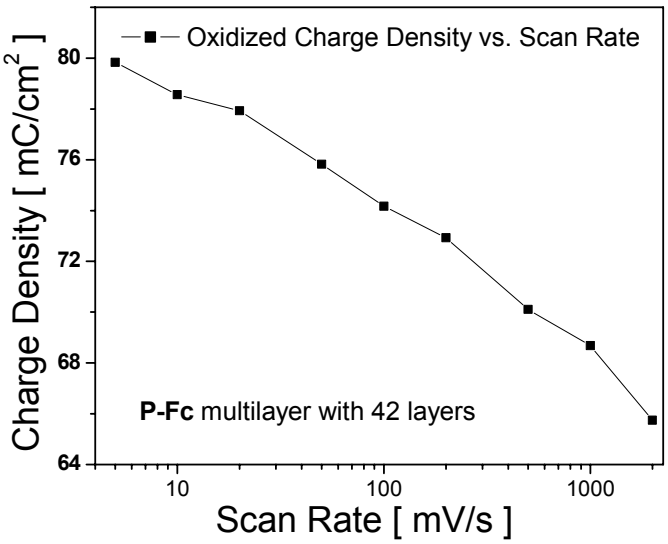

Figure 5.3 Charge density of **P-Fc** multilayer film with 42 layers in oxidation decreases as the scan rate increases. Lower scan rate provides longer time to oxidize more redox centers.

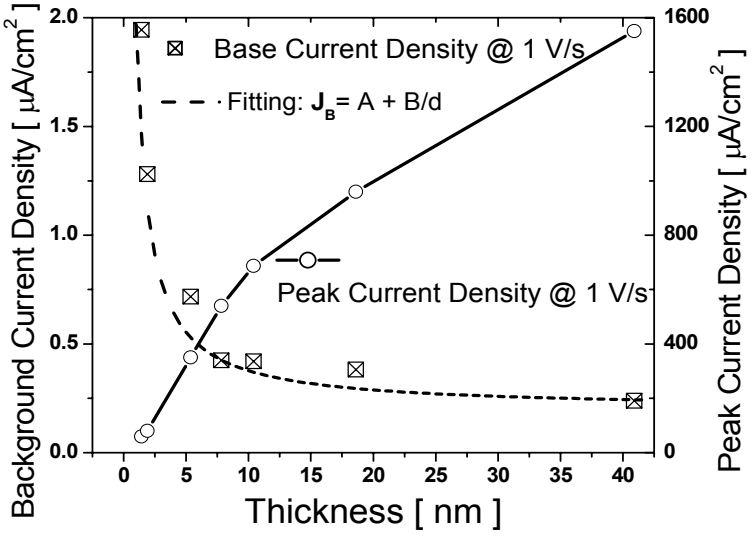

Figure 5.4 At 1 V/s, peak current density increases with increasing thickness of multilayer films, while background current decreases. Equation J_B=A+B/d was used to fit the experimental data very well when A=1.98×10^{-11} A/cm^2 and B=7.22×10^{-17} A/cm.

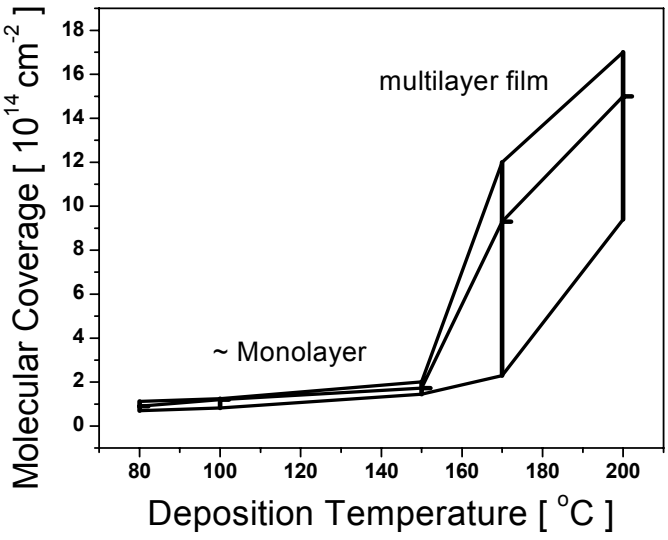

Figure 5.5 Molecular coverage as a function of deposition temperature (for 30 minutes) indicates that multilayer could be formed when temperature is over 150°C.

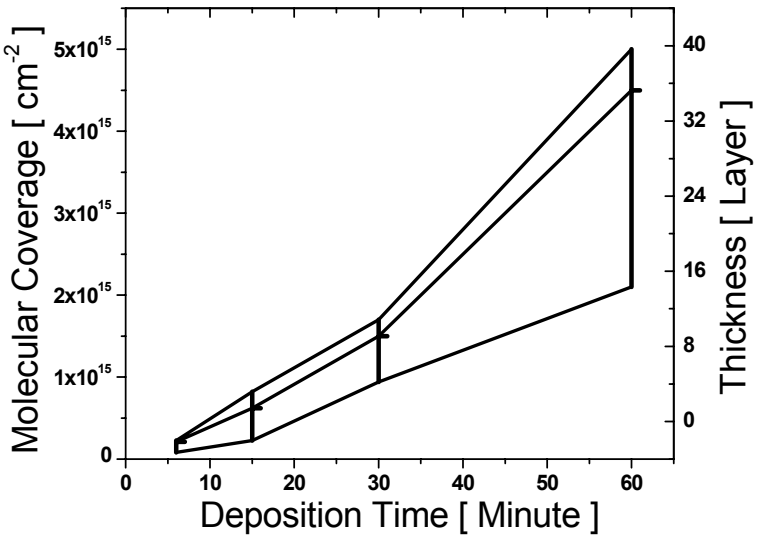

Figure 5.6 Surface coverage and thickness (the number of layers) of multilayer film increases as deposition time increases.

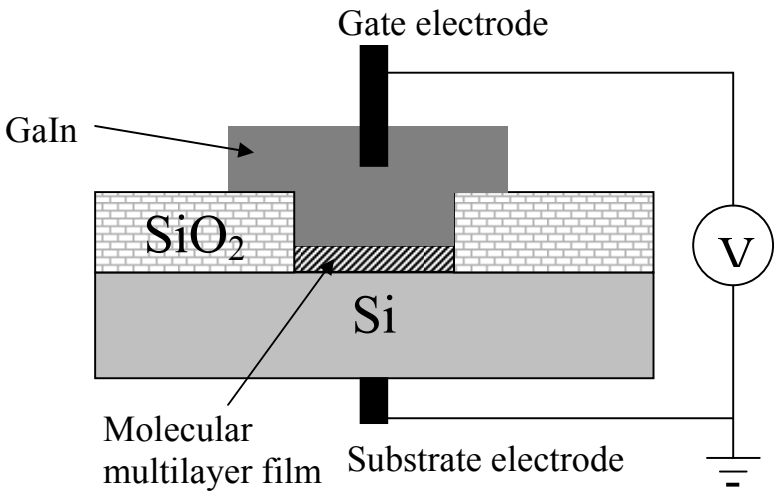

(a)

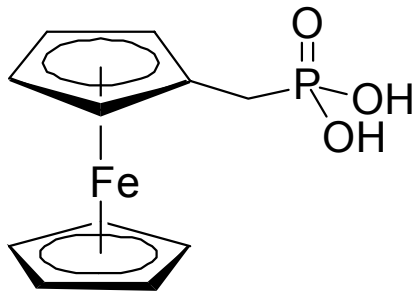

(b)

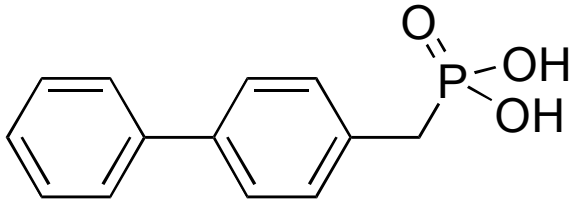

(c)

Figure 5.7 (a) The schematic diagram of GaIn metal/molecule/Si sandwiched device; (b) and (c) the structure of dihydroxyphosphorylmethylferrocene (**P-Fc**) and 4-(dihydroxyphosphorylmethyl)biphenyl (**P-B**), respectively.

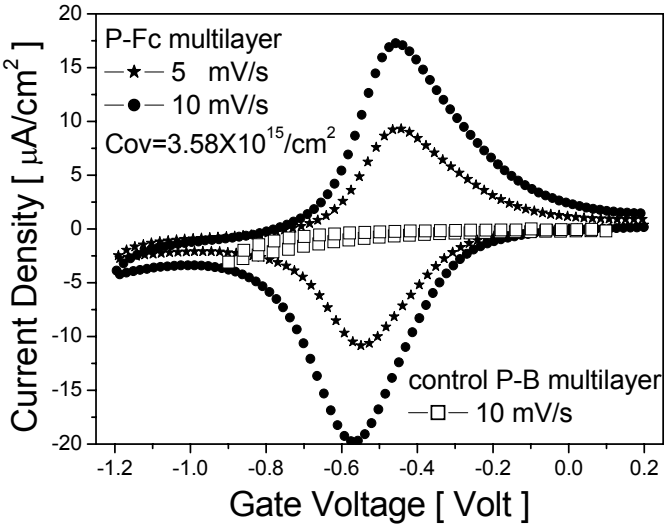

Figure 5.8 Representative cyclic voltammetry of **P-Fc** multilayer on Si is measured with top electrolyte at potential scan rates: 5 and 10 mV/s show oxidation-reduction reaction peaks. The surface coverage is about 3.58×10^{15} molecules/cm^2. Cyclic voltammetry of nonredox- active P-B multilayer on Si at 10 mV/s does not show redox peaks.

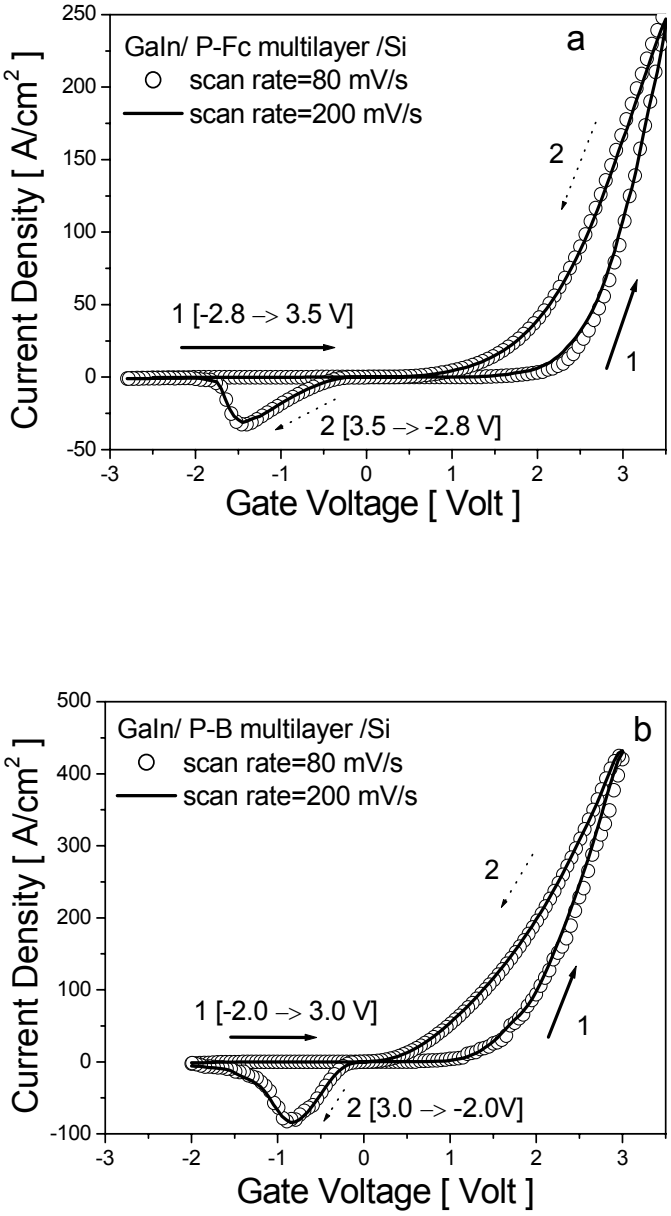

Figure 5.9 I-V hysteresis loops of GaIn/**P-Fc** multilayer/Si (a) and GaIn/**P-B** multilayer/Si (b) devices at potential scan rates: 80 mV/s and 200 mV/s. The scan-rate independence indicated the hysteresis and current peaks were not due to charge storage and redox processes.

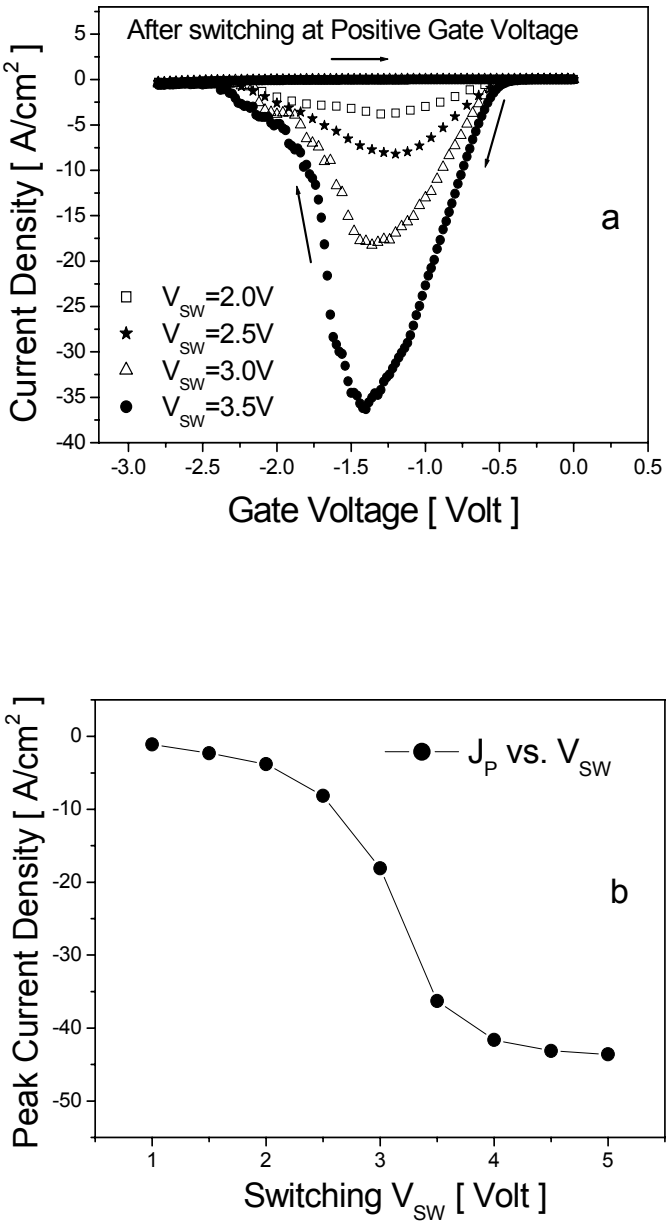

Figure 5.10 (a) The I-V sweeps after the devices being switched at increasing switching voltages (V_{SW}): 2.0, 2.5, 3.0 and 3.5 V show increasing current peak at -1.45 V; (b) shows the peak current density increases from zero as V_{SW} increases and saturates under $V_{SW} > 4.5$ V.

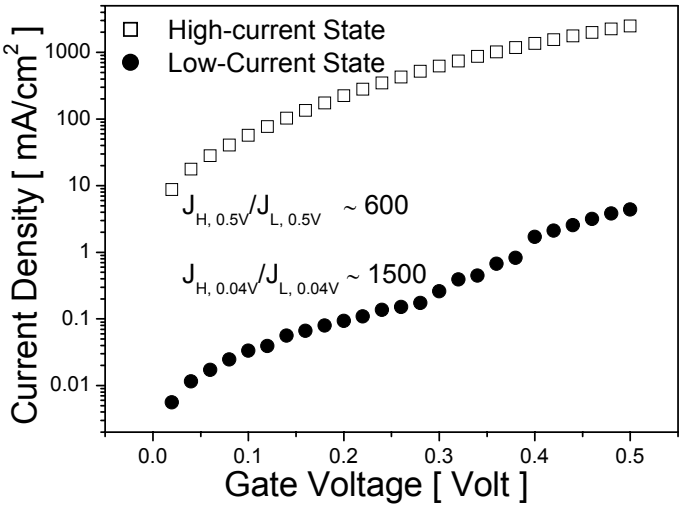

Figure 5.11 The high-current and low-current states of the device can be read at positive low V_G (<0.5 V) without being switched; the current ratio between these two states at 0.04 and 0.5 V are about 1500 and 600, respectively.

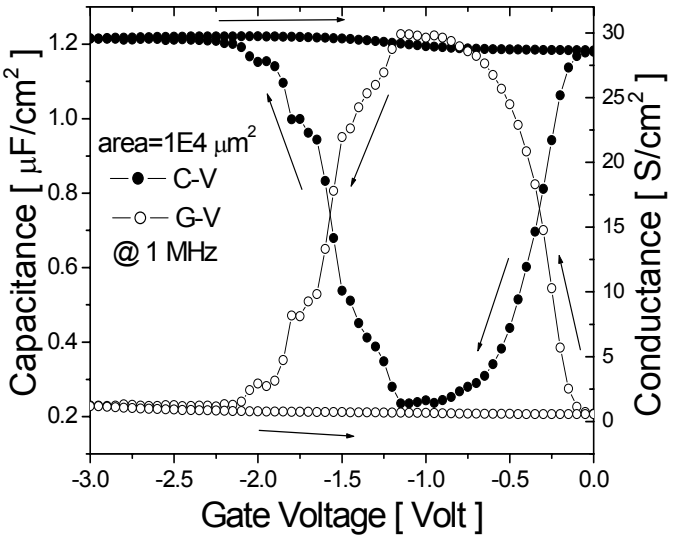

Figure 5.12 C-V&G-V characteristics of MMS device was obtained at 1 MHz.

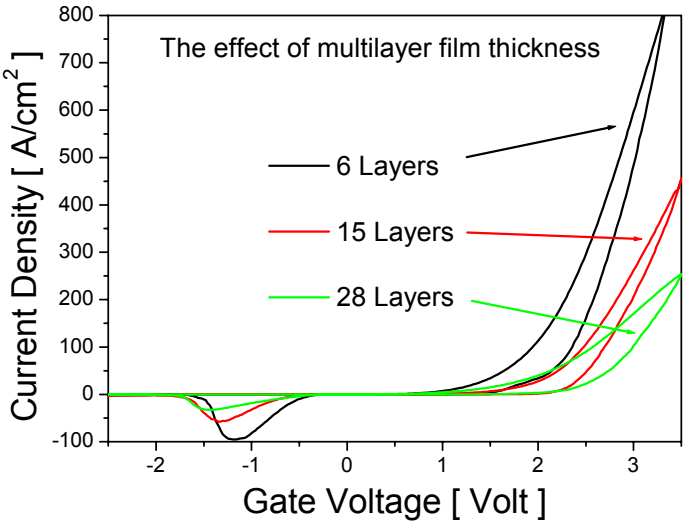

Figure 5.13 The thickness of multilayer film has an effect on I-V characteristics of MMS sandwiched devices.

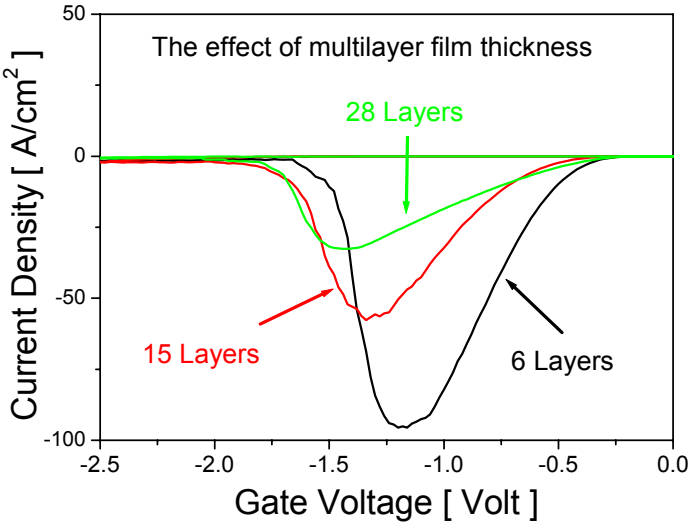

Figure 5.14 More details of Fig. 5.12 in left part show that the thicker the multilayer film, the lower current peak. The peak position shifts left as the thickness increase.

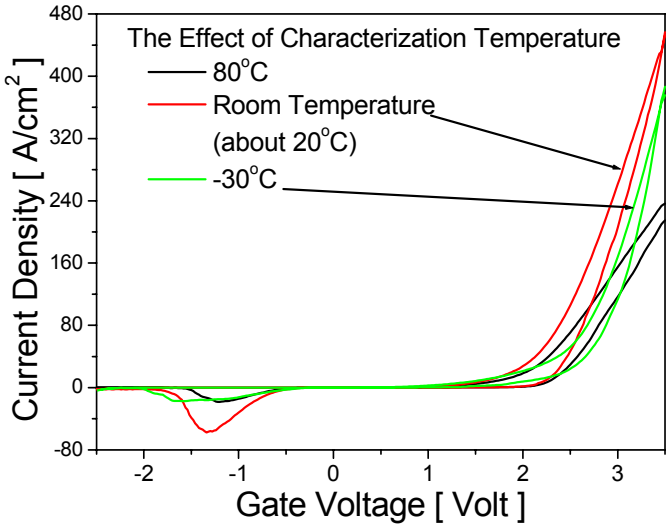

Figure 5.15 The I-V characteristics have been obtained for MMS device at various characterization temperatures.

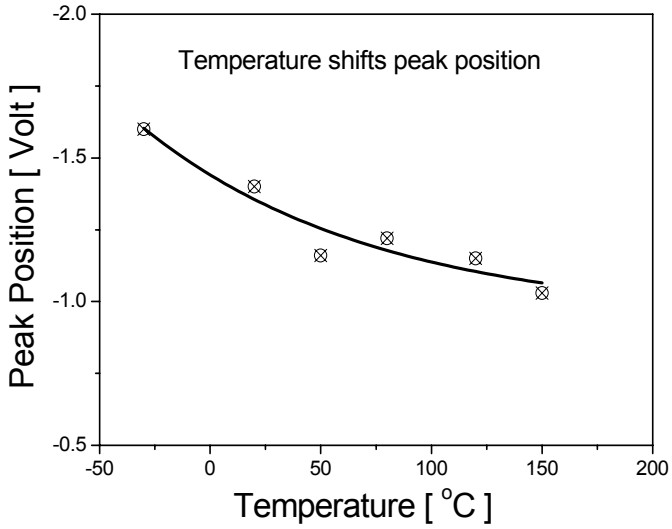

Figure 5.16 The position of current peak (V_p) at negative potential shifts more negative as temperature (T) decreases. V_P tends to decreases exponentially as temperature increases.

Chapter 6 Summary and Future Research Directions

6.1 Summary of Approach towards Hybrid CMOS/Molecular Electronics

The focus of our research has been on integrating redox-active molecules into Si-based structures to (1) understand the properties of molecules; (2) generate a new class of hybrid CMOS/molecular devices for memory applications; and (3) open new routes for developing molecular-only devices. This dissertation has concentrated on the fabrication, characterization and modeling of hybrid silicon-molecular devices. The major findings of this work are summarized in the following section:

A. Specific procedures have been developed for the attachment of molecules on Si and SiO_2 surfaces including solution-phase and vapor-phase deposition. Attachment conditions have been optimized for tightly-bonded, well-packed molecular layers including attachment time, number of drops of molecule solution, attachment temperature, and inert environment.

B. Hybrid silicon-molecular devices have been characterized using traditional cyclic voltammetry, capacitance-voltage/conductance-voltage measurements, impedance spectroscopy and DC small-signal current-voltage measurement. The redox properties of molecule have been well studied through these characterization techniques. A simplified energy band diagram has also been provided for the

electrolyte/molecule/Si structure. The stability of molecule has been investigated in controlled environment and unprotected environment.

C. A current-voltage model has been developed for electrolyte/molecule/Si structure using Maxwell's equations combining the approximation of kinetic rates and non-ideal factor. Equivalent RC circuits have been developed, and a set of corresponding RC coefficients have been extracted for this EMS structure.

D. A possible way to utilize redox-active molecule for application in DRAM has been studied by using 1T-1C structure with a regular transistor and a silicon-molecular capacitor. Single and multiple discrete redox states have been written or erased through control of the transistor.

E. Multibit memory has been achieved through two ways via attachment engineering: (1) mixing two different redox molecules with well-separated redox potential and (2) stacking two different redox molecules by attaching one on the top of another. These two ways have the advantages of process simplicity.

F. Redox multilayer films have been attached on Si with various thicknesses controlled by deposition time and temperature. Very high molecular coverage has been obtained by optimizing deposition time and temperature. Furthermore, nonvolatile electrical switching has been found in metal/molecule/Si structure using these multilayer film and Gallium/Indium metal. The switching properties are very stable, the retention of

this switching is very long, and the ratio of high/low current is very high for memory application. A set of reference experiments indicated that these switching properties are not due to redox process.

6.2 Future Research Directions

There are several areas that need further investigation to continue the research in this approach. First, the attachment of molecules on Si-based structure, including vapor phase deposition and attachment on various surfaces, needs to be further optimized for memory application. Second, the packaging technology of molecular devices needs to be developed to protect molecule from environmental and electrical stress. Third, the application of molecule in DRAM structure needs further investigation including device structure, write/read operation of multiple bits, and memory retention. Fourth, the application molecular field effect transistor based on the knowledge of electrolyte/molecule/Si capacitor need to be explored. We need to study the effect of charging/discharging of molecule to the Si channel and its possible application in FLASH memory. Fifth, we need to examine the mechanism and physics of nonvolatile electrical switching of metal/molecule/Si sandwiched junction. In addition, more specific models and equivalent circuit need to be developed for various molecules and EMS structures.

Appendix

Appendix A Electrical Characterization of Redox-Active Molecular Monolayers on SiO_2 for Memory Applications

Electrical Characterization of Redox-Active Molecular Monolayers on SiO_2 for Memory Applications

Qiliang Li, Shyam Surthi, Guru Mathur, and Srivardhan Gowda
Department of Electrical and Computer Engineering, North Carolina State University, Raleigh, North Carolina 27695

Thomas A. Sorenson and Robert C. Tenent
ZettaCore, Inc., 920 Main Campus Drive, Raleigh, North Carolina 27606

Muthukumaran Kannan, Shun-ichi Tamaru, and Jonathan S. Lindsey
Department of Chemistry, North Carolina State University, Raleigh, North Carolina 27695

Zhiming Liu, Rajeev B. Dabke, Amir Yasseri, David F. Bocian, and Werner G. Kuhr
Department of Chemistry, University of California, Riverside, California 92521

Veena Misra*
Department of Electrical and Computer Engineering, North Carolina State University, Raleigh, North Carolina 27695

Published in Appl. Phys. Lett., vol. 83, pp. 198-201, 2003.

*Corresponding Author: vmisra@eos.ncsu.edu

Electrical Characterization of Redox-Active Molecular Monolayers on SiO_2 for Memory Applications

Qiliang Li, Shyam Surthi, Guru Mathur, and Srivardhan Gowda
Department of Electrical and Computer Engineering, North Carolina State University, Raleigh, North Carolina 27695

Thomas A. Sorenson and Robert C. Tenent
ZettaCore, Inc., 920 Main Campus Drive, Raleigh, North Carolina 27606

Muthukumaran Kannan, Shun-ichi Tamaru, and Jonathan S. Lindsey
Department of Chemistry, North Carolina State University, Raleigh, North Carolina 27695

Zhiming Liu, Rajeev B. Dabke, Amir Yasseri, David F. Bocian, and Werner G. Kuhr
Department of Chemistry, University of California, Riverside, California 92521

Veena Misra*
Department of Electrical and Computer Engineering, North Carolina State University, Raleigh, North Carolina 27695

ABSTRACT

Hybrid silicon capacitors have been successfully fabricated by attaching monolayers of redox-active molecules via self-assembly to ultra thin silicon dioxide layers. Capacitance, conductance, and cyclic voltammetric measurements have been used to characterize these capacitors. The presence of distinct capacitance and conductance peaks associated with oxidation and reduction of the monolayers at low gate voltages indicates discrete electron storage states for these capacitors, suggesting their feasibility in memory devices. The inherent molecular scalability and low-power operation coupled with existing silicon technology support the approach of hybrid molecule-silicon devices as a strong candidate for next generation electronic devices.

*Corresponding Author: vmisra@eos.ncsu.edu

1. INTRODUCTION

Molecules are increasingly playing a key role in the field of nanoscale electronic devices due to their intrinsic scalability and electronic properties [1-4]. The approach in this work is focused on hybrid silicon-molecular devices wherein redox-active charge storage molecules are incorporated into silicon structures to generate a new class of nanoscale electronic devices. These redox-active molecules, which can be designed to self-assemble on surfaces as monolayers, exhibit charge states at distinct voltages. Application of an oxidizing voltage causes the redox-active monolayers to lose electrons, resulting in a positively charged monolayer (write state). When a reducing voltage is applied, electrons are transferred to the molecules to the neutral state (erase state). We have previously reported on redox-active self-assembled monolayers (SAMs) attached to silicon surfaces characterized via impedance methods [5]. In the present work, we have studied the properties of redox-active monolayers that are attached to ultra-thin SiO_2 layers via synthetically designed linker functional groups. In this case, the linker and silicon dioxide lie between the redox-active molecular component and the bottom electrode (Si substrate) and act as tunneling barriers. Both the linker and the SiO_2 layers can be synthetically tailored to obtain desired redox potentials, tunneling probability, and retention times [6]. Barrier tuning via SiO_2 layers and appropriate linker lengths is very attractive for memory applications such as FLASH or DRAM, provided that the write (oxidation) and erase (reduction) voltages are not significantly increased. In this letter, we report the behavior of redox-active molecules that are attached to varying thicknesses of SiO_2 layers to form molecule/SiO_2/Si capacitor structures.

2. EXPERIMENTAL

The structure of an Electrolyte-Molecule-SiO_2-Si (EMOS) capacitor is shown in Figure 1, where the SiO_2 layer lies between the molecule and the Si substrate. The substrates used were (100) p-Si (B, $5x10^{18}/cm^3$) wafers. Active areas of $1x10^{-4}$ cm^2 and $4x10^{-4}$ cm^2 were defined through a 380-nm field oxide using photolithography. A 5-nm thermal oxide was grown and then subjected to 1% HF solution to obtain thinner SiO_2 layers that ranged from 1.2 nm to 3 nm. The oxide thickness (T_{OX}) of the etched samples was measured by ellipsometry. Figure 1 also shows the structure of the molecule used in this work,

dihydroxyphosphorylmethylferrocene (**1**) [7]. The attachment of **1** to SiO_2 layers was achieved via the phosphonate group. The attachment solution was prepared by dissolving 1 mg of the **1** in 1 ml tetrahydrofuran. The temperature of the sample was kept at 60 °C during the attachment process. The attachment using the phosphonate-terminated linkers results in P-O-Si linkages. The electrical characterization utilized a silver gate electrode and a solution of 1.0 M tetrabutylammonium hexafluorophosphate in propylene carbonate as the conducting gate electrolyte. The simplified equivalent circuit of the capacitor is also shown in Figure 1 and indicates the contribution of electrolyte, thin oxide, overlap silicon oxide, molecular SAM, and the silicon substrate capacitances: C_E, C_O, C_{OL}, C_M and C_S, respectively. The capacitance-voltage (*C-V*) and conductance-voltage (*G-V*) characteristics were measured using an HP 4284A LCR meter. Traditional cyclic voltammetry measurements were obtained using a custom LabVIEW program.

3. RESULTS AND DISCUSSION

As shown in Figure 2, oxidation and reduction peaks were observed in cyclic voltammetry measurement for the EMOS capacitors with oxide thickness (T_{OX}): 1.25 nm at different scanning rates from 2 V/s to 20 V/s. Also shown is a CyV scan for an electrolyte-oxide-semiconductor (EOS) capacitor with the same T_{OX} at 5 V/s, which showed no peaks. The gate voltages are referenced to the top silver electrode/electrolyte contact. The bottom curves represent the oxidation processes whereas the top curves represent the reduction processes. Positive charge is stored by removing an electron from the molecule, leaving behind a hole. The current peaks observed at oxidizing and reducing voltages (V_{PO} and V_{PR}) are due to the charging and discharging transient currents associated with oxidation and reduction of the molecules. As the CyV scan rate is increased, the oxidation voltages shift to left while the reduction voltages shift to right. Hence the peak separation ($\Delta V_P = V_{PR} - V_{PO}$) increases from 0.18 V to 0.38 V as the scanning rate increases from 2 to 20 V/s, though the average redox voltage $\{V_O = (V_{PR} + V_{PO})/2\}$ remains constant at –0.19 V. The increasing peak separation could be attributed to increasingly large resistive drop in the electrolyte and also could also indicate that the scan rates are faster than the overall rate of electron transfer between the redox center in **1** and the Si substrate [8, 9]. The overall electron transfer rate in this case is determined by the slower of the processes in series: the redox reaction rate and

electron tunneling through the oxide. From our earlier work on attachment of 4-ferrocenylbenzyl alcohol on Si, we find that the ΔV_P is only 0.07 V in the case of Si compared to 0.38 V for SiO_2 at a scan rate of 20 V/s. This leads us to believe that the electron tunneling through oxide (T_{OX}=1.25 nm) is slower compared to the redox kinetics and hence the rate determining step. Another difference between the attachment to Si and SiO_2 is the dependence of peak CyV current on scan rate, which is expected to be linear for surface bound redox-active species. The dependence in the case of Si is close to linear for scan rates of up to 100 V/s, whereas the peak current variation can be approximated with square root of scan rate for attachment to SiO_2. This again implies slower effective rate of electron transfer kinetics through the SiO_2 layer.

The cyclic voltammetry of the ferrocene-EMOS (F-EMOS) capacitor structures with varying oxide thickness is shown in Figure 3. The bottom curve represents oxidation cycle and the top curve represents reduction cycle. Positive charge is stored by removing an electron from the molecule, leaving behind a hole. As shown, the oxidation potential increases as T_{ox} increases from 1.25 nm to 2.36 nm. With thicker oxide (e.g. T_{OX}=2.85 nm) EMOS, the redox peaks are not observed. As the oxide thickness increases, a larger potential is dropped across the oxide thereby increasing the total applied potential needed to oxidize the molecules. In addition, with increasing oxide thickness, the tunneling rate through the oxide decreases exponentially, slowing down the effective rate of electron transfer from the redox center to Si. This acts as a kinetic barrier and introduces larger separation between the oxidation and reduction peaks, which increases from 0.22 V (at 2V/s) to 1.80 V (at 20V/s). This indicates that, at these scan rates, changing the oxide thickness can tune the redox voltages of the EMOS capacitor system and introduce hysteresis due to additional voltage drops across the oxide. The molecule coverage over SiO_2 was calculated by integrating the oxidation peak and was found to be in the range of $0.9\text{x}10^{14}$ to 1.1×10^{14} cm^{-2} for all four T_{ox} Values. This coverage density is comparable with the coverage density obtained of ferrocene molecules on Si surface [5]. These values indicate that the SAMs are very dense and comparable to the surface density of silicon atoms ($\sim10^{14}$ cm^{-2}).

The C-V and G-V characteristics of these EMOS capacitors are presented in Figures 4(a) and 4(b). The peaks observed in capacitance and conductance measurements (near –0.1 to –0.2V) are attributed to the movement of charge to or from trapped state in the redox

active molecule. This mechanism is similar to the dependence of interface states on frequency in a metal-SiO_2-Si capacitor [10]. It should be noted that no such peak was observed with SiO_2 layers that did not contain any redox-active monolayers. Another peak was observed between 0.5V and 1V for all samples including controls and was attributed to the depletion in the semiconductor. The occurrence of the redox peaks depended both on the measurement frequency and the oxide thickness. The measurement frequency affects the measurements in two ways. Firstly, at low frequencies such as 100Hz, the charge movement to/from the molecule can occur at a rate commensurate with the measurement signal and therefore, contributes to a net capacitance change as reflected by the peak in C-V. As the frequency is increased, the electron transfer process becomes rate limiting, which consequently reduces amplitude of the peaks [5]. Therefore, no peak is observed in C-V and G-V at these frequencies. Secondly, at higher frequencies the limited ionic movement associated with the electrolyte prevents accurate measurements [11, 12]. The effective capacitance of the electrolyte decreases dramatically and begins to dominate the total capacitance in a series circuit. Hence, all the measurements reported here were performed at 100 Hz.

As shown in Figure 4(a), the capacitance values near accumulation for the EMOS structures scale in accordance with the SiO_2 thickness. The capacitance and conductance peaks with ferrocene monolayers are especially pronounced for thinnest oxide (1.25 nm), but reduce in amplitude as the oxide thickness increases to 1.49 nm. For SiO_2 thickness greater than 1.8 nm, no redox related peaks were observed in the *C-V* and *G-V* data. As the oxide thickness is increased, the tunneling rate (and hence the overall electron transfer rate) decreases exponentially and very low frequencies are needed to measure the redox peaks. Although such low frequencies cannot be generated through an HP4284A (C-V and G-V were also measured at 20 Hz and did not show peak for thicker oxides), they can be achieved via quasi-static measurements, such as cyclic voltammetry, which as shown in Figure 3, does indicate the presence of peaks at low scan rates for thicker SiO_2 layers. To ascertain the dependence of properties on the tunneling rate through oxide, we also prepared an EMOS structure with T_{OX}=1.4 nm, where the thin oxide was grown by rapid thermal annealing (RTA) in 10% O_2/Ar mixture at 600 ^oC for 1 minute (data not shown). For same thickness, the electron-tunneling rate through RTA oxide is expected to be much smaller than the

etchback oxide. As expected, we observed a much larger peak separation of 0.60 V in this EMOS at a lower scan rate of only 0.1 V/s. Also, no redox-related peaks were observed in the C-V and G-V scans for this sample.

4. CONCLUSIONS

In this paper, we have reported conventional C-V, G-V, and cyclic voltammetric measurements on redox-active molecular SAMs attached to thin silicon oxide. We have shown that (1) the EMOS capacitor exhibits distinct capacitance and conductance peaks associated with trapping and detrapping of the charge in the molecules, and (2) the EMOS capacitors exhibit voltage shifts and hysteresis that can be tuned by increasing the tunnel barrier. These results verify the presence of reversible charge trapping, a key requirement for memory applications. This work has also demonstrated that EMOS structures are very useful tools for characterizing charge-storage molecular monolayers. Due to the molecular scalability and low-power operation, hybrid molecular-silicon structures may be strong candidates for the next generation of electronic devices.

This work was supported by the DARPA Moletronics Program (MDA972-01-C-0072) and ZettaCore, Inc.

REFERENCES

[1] M. Reed, C. Zhou, C. Muller, T. Burgin, and J. Tour, "*Conductance of a molecular junction*," SCIENCE, vol. 278, pp. 252-254, 1997.

[2] C. Collier, E. Wong, M. Belohradsky, F. Raymo, J. Stoddart, P. Kuekes, R. Williams, and J. Heath, "*Electronically configurable molecular-based logic gates*," SCIENCE, vol. 285, pp. 391-394, 1999.

[3] S. Coulter, J. Hovis, M. Ellison, and R. Hamers, "*Reactions of substituted aromatic hydrocarbons with the si(001) surface*," JOURNAL OF VACUUM SCIENCE & TECHNOLOGY A-VACUUM SURFACES AND FILMS, vol. 18, pp. 1965-1970, 2000.

[4] C. Engtrakul and L. Sita, "*Ferrocene-based nanoelectronics: 2,5-diethynylpyridine as a reversible switching element*," NANO LETTERS, vol. 1, pp. 541-549, 2001.

[5] Q. Li, G. Mathur, M. Homsi, S. Surthi, V. Misra, V. Malinovskii, K. Schweikart, L. Yu, J. Lindsey, Z. Liu, R. Dabke, A. Yasseri, D. Bocian, and W. Kuhr, "*Capacitance and conductance characterization of ferrocene-containing self-assembled monolayers on silicon surfaces for memory applications*," APPLIED PHYSICS LETTERS, vol. 81, pp. 1494-1496, 2002.

[6] K. Roth, J. Lindsey, D. Bocian, and W. Kuhr, "*Characterization of charge storage in redox-active self-assembled monolayers*," LANGMUIR, vol. 18, pp. 4030-4040, 2002.

[7] S. Alley and W. Henderson, "*Synthesis and characterisation of ferrocenyl-phosphonic and -arsonic acids*," JOURNAL OF ORGANOMETALLIC CHEMISTRY, vol. 637, pp. 216-229, 2001.

[8] K. Roth, A. Yasseri, Z. Liu, R. Dabke, V. Malinovskii, K. Schweikart, L. Yu, H. Tiznado, F. Zaera, J. Lindsey, W. Kuhr, and D. Bocian, "*Measurements of electron-transfer rates of charge-storage molecular monolayers on si(100). Toward hybrid molecular/semiconductor information storage devices*," JOURNAL OF THE AMERICAN CHEMICAL SOCIETY, vol. 125, pp. 505-517, 2003.

[9] S. O'connor, G. Olsen, and S. Creager, "*A nernstian electron source model for the ac voltammetric response of a reversible surface redox reaction using large-amplitude ac voltages*," JOURNAL OF ELECTROANALYTICAL CHEMISTRY, vol. 466, pp. 197-202, 1999.

[10] S. Kar, C. Miramond, and D. Vuillaume, "*Properties of electronic traps at silicon/1-octadecene interfaces*," APPLIED PHYSICS LETTERS, vol. 78, pp. 1288-1290, 2001.

[11] A. Chandra and B. Bagchi, "*Frequency dependence of ionic conductivity of electrolyte solutions*," JOURNAL OF CHEMICAL PHYSICS, vol. 112, pp. 1876-1886, 2000.

[12] V. Gaiduk, B. Tseitlin, and D. Crothers, "*Calculation of the microwave and far-infrared spectra of aqueous electrolyte solutions from a molecular model. On the ionic-conductivity dispersion sigma(omega)*," JOURNAL OF MOLECULAR LIQUIDS, vol. 89, pp. 81-109, 2000.

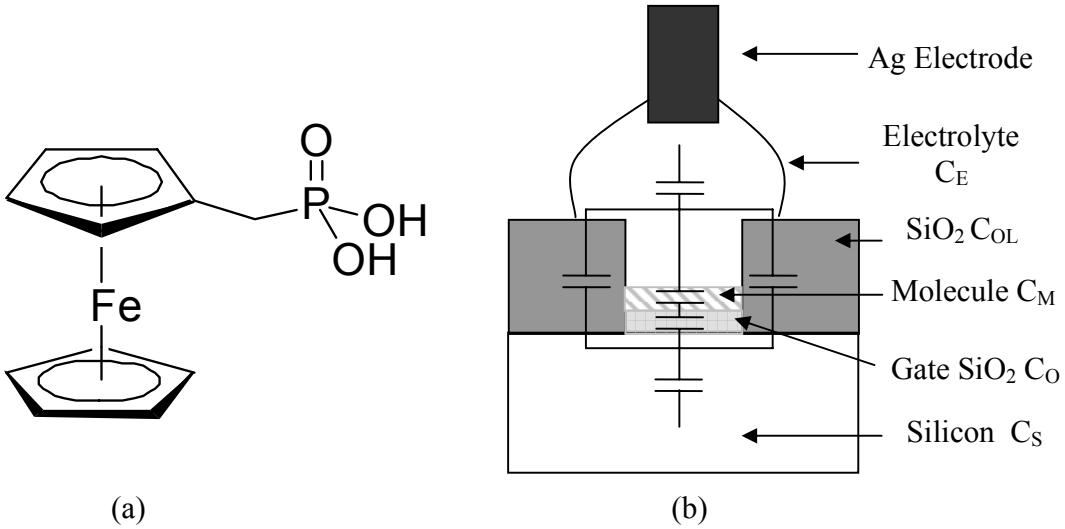

(a) (b)

Figure 1. (a) The structure of dihydroxyphosphorylmethylferrocene (**1**). (b) Schematic of the electrolyte-molecule-oxide-silicon (EMOS) capacitor with a simplified equivalent circuit. The attachment on SiO_2 surface is achieved by a covalent bond of carbon-oxygen-silicon.

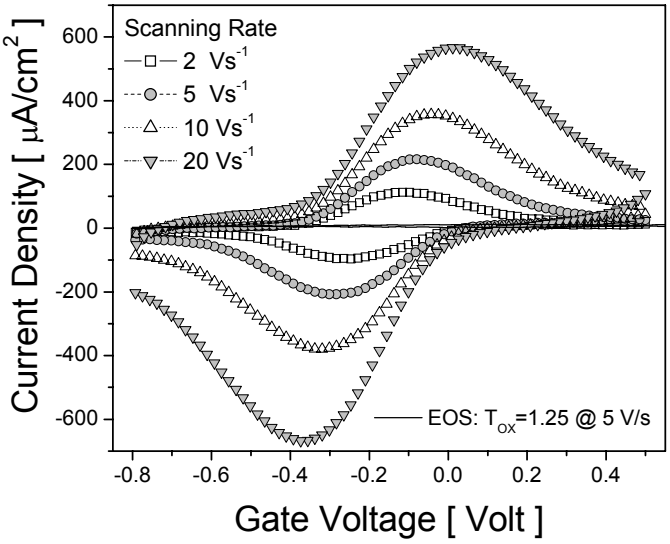

Figure 2 Cyclic voltammetry of the electrolyte-molecule-oxide-silicon (T_{OX}=1.25 nm) capacitor with voltage scanning rates: 2 V/s, 5 V/s, 10 V/s and 20 V/s. Cyclic voltammetry of electrolyte-oxide-silicon (T_{OX}=1.25 nm) capacitor at 5 V/s does not show redox peaks. Gate Voltage refers to the potential applied to the Ag wire counter electrode.

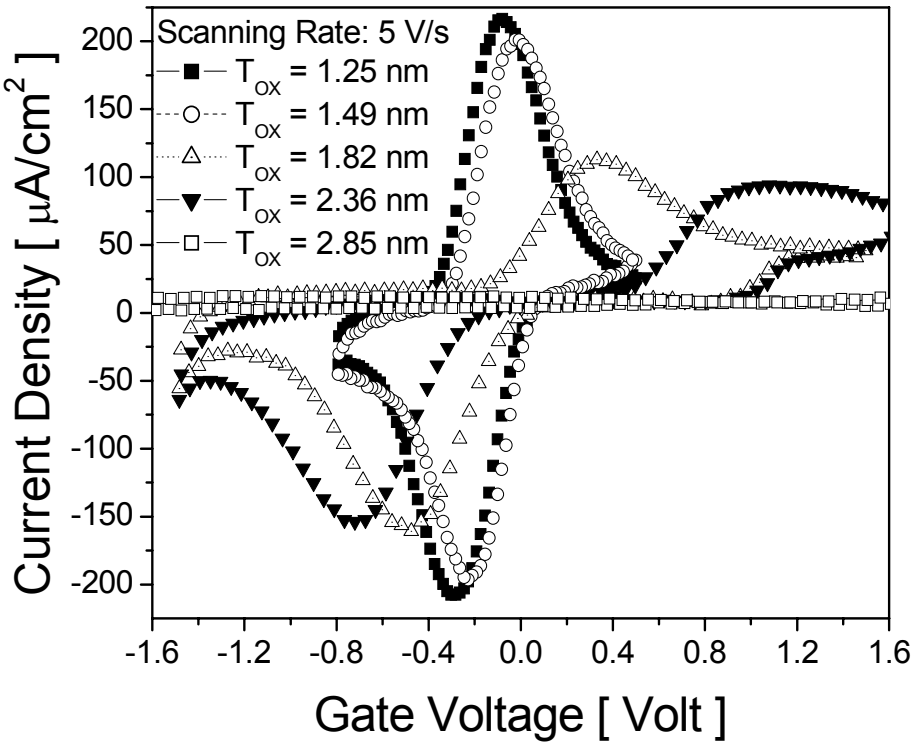

Figure 3. Cyclic voltammetry of the electrolyte-molecule-oxide-silicon (T_{OX}=1.25 – 2.85 nm) capacitor at scanning rates 5 V/s. No peaks are observed for the capacitor with T_{OX}=2.85 nm. Gate Voltage refers to the potential applied to the Ag wire counter electrode.

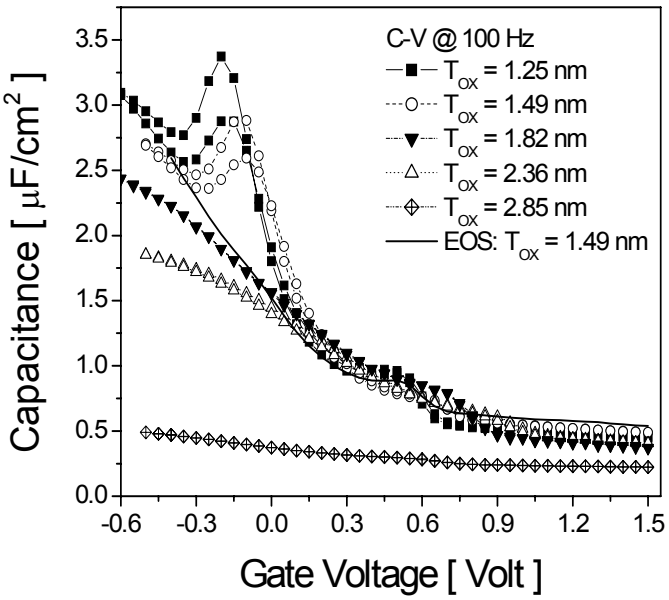

(a)

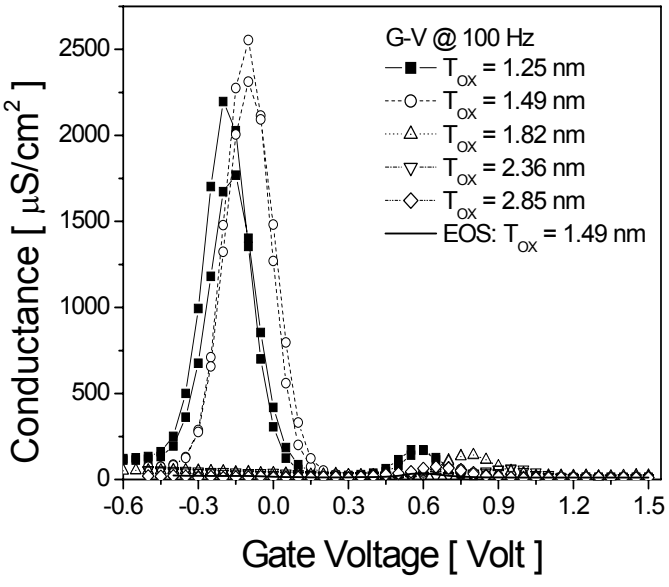

(b)

Figure 4. (a) Capacitance voltage and (b) Conductance voltage hysteresis of the electrolyte-molecule-oxide-silicon (T_{OX}=1.25 – 2.85 nm) capacitor and electrolyte-oxide-silicon (T_{OX}=1.49 nm) capacitance at 100 Hz. All the curves show depletion peaks but only the EMOS capacitors with $T_{OX} < 1.8$ nm show oxidation and reduction peaks.

Table I

Experimental result for ferrocene-EMOS capacitors with different T_{OX} including redox voltage and molecule coverage density. T_{OX} = 1.25, 1.49, 1.82 and 2.36 nm.

T_{OX} (nm)	V_{PO} (V)	V_{PR} (V)	V_{OX} (V)	Coverage ($\times 10^{13}$ cm^{-2}) By CyV @5Vs
1.25	-0.30	-0.08	-0.2	10.5
1.49	-0.23	-0.02	-0.1	11.1
1.82	-0.48	0.35	No peak	11.1
2.36	-0.72	1.08	No peak	9.1

Appendix B Multiple-bit Storage Properties of Porphyrin Monolayers on SiO_2

Multiple-bit Storage Properties of porphyrin monolayers on SiO_2

Qiliang Li, Shyam Surthi, Guru Mathur, Srivardhan Gowda, Qian Zhao
Department of Electrical and Computer Engineering, North Carolina State University, Raleigh, North Carolina 27695

Thomas A. Sorenson and Robert C. Tenent
ZettaCore, Inc., 920 Main Campus Drive, Raleigh, North Carolina 27606

Kannan Muthukumaran and Jonathan S. Lindsey
Department of Chemistry, North Carolina State University, Raleigh, North Carolina 27695

Veena Misra
Department of Electrical and Computer Engineering, North Carolina State University, Raleigh, North Carolina 27695

Published in Appl. Phys. Lett., vol. 85, pp. 1829-1831, 2004.

* Corresponding Author: vmisra@eos.ncsu.edu

Multiple-bit Storage Properties of porphyrin monolayers on SiO_2

Qiliang Li, Shyam Surthi, Guru Mathur, Srivardhan Gowda, Qian Zhao
Department of Electrical and Computer Engineering, North Carolina State University, Raleigh, North Carolina 27695

Thomas A. Sorenson and Robert C. Tenent
ZettaCore, Inc., 920 Main Campus Drive, Raleigh, North Carolina 27606

Kannan Muthukumaran and Jonathan S. Lindsey
Department of Chemistry, North Carolina State University, Raleigh, North Carolina 27695

Veena Misra
Department of Electrical and Computer Engineering, North Carolina State University, Raleigh, North Carolina 27695

ABSTRACT

Hybrid molecule-silicon capacitors have been fabricated by the self-assembly of a monolayer of porphyrin molecules on a silicon oxide surface. The porphyrin employed [5-(4-dihydroxyphosphorylphenyl)-10,15,20-trimesitylporphinatozinc(II)] attaches to silicon oxide via a phosphonate linkage. Cyclic voltammetry current and capacitance/conductance measurements have been used to characterize the capacitors. The presence of multiple distinct peaks in current density and capacitance/conductance measurements are associated with oxidation and reduction of the molecular monolayer. The charge-storage states of the capacitor indicate applicability for use in multiple-bit memory devices. The inherent molecular scalability and multibit features in conjunction with existing silicon technology makes hybrid molecule-silicon devices strong candidates for use as future electronic devices.

* Corresponding Author: vmisra@eos.ncsu.edu

INTRODUCTION

As silicon technology scales into the nanoregime, questions concerning the scalability of devices that rely on the bulk properties of silicon have prompted exploration of alternate technologies such as molecular electronics [1-4]. One of the long-term objectives of molecular electronics is to learn to construct circuitry using molecular components in a bottom-up approach. A more near-term strategy entails the development of hybrid molecule-silicon devices where molecules are used to augment the features of traditional, silicon-based, photolithographically constructed circuitry. The use of molecules in electronic devices is very attractive owing to the intrinsic scalability of molecular properties and the ability to tune electronic properties over a broad range through molecular design and chemical synthesis [5].

We have recently investigated hybrid silicon-molecular capacitors wherein redox-active monolayers are incorporated into silicon devices to generate nanoscale memory devices. The redox-active molecules can be tailored to give self-assembled monolayers (SAMs) on various surfaces and exhibit charged states at distinct voltages. Our initial studies of hybrid silicon-molecular capacitors employed a ferrocene derivative attached to a silicon surface [6]. We subsequently examined a ferrocene derivative (**1**) attached to SiO_2 (Fig. 1(a)) [7]. Fabricating SAMs on a SiO_2 surface rather than silicon offers distinct advantages: (i) SiO_2 provides a more stable surface for molecular attachment; and (ii) both the molecular linker and SiO_2 layer can be synthetically tailored to obtain the desired redox potential, electron-transfer rate, and charge-retention time [8].

The density of memory storage can in principle be increased through the use of molecules that exhibit multiple charged states at distinct voltages. Ferrocene molecules such as **1** exhibit two stable states, the neutral state and the mono-positively charged state. Zinc-porphyrins such as **2** (Fig. 1(b)) exhibit three stable states: neutral, mono-positively charged, and di-positively charged. Fabricating SAMs of porphyrin molecules rather than ferrocene molecules on a SiO_2 surface offers the advantage of multiple-bit memory storage. In this letter, we report on the formation of SAMs of porphyrin **2** on SiO_2. Comparisons are made with an analogous capacitor that contains ferrocene **1** and a control structure that lacks redox-active molecules altogether. The test structures have been characterized by impedance spectroscopy (capacitance and conductance) and cyclic voltammetry. Such analysis is essential for understanding the behavior of hybrid molecule-silicon devices.

EXPERIMENTAL

Hybrid molecule-silicon capacitors composed of an electrolyte-molecule-SiO_2-Si (EMOS) structure were fabricated by forming SAMs on a SiO_2 surface followed by deposition of an electrolyte as the conducting medium for attachment of the gate electrode. A schematic of the EMOS structure is shown in Fig. 2. The substrates used were (100) p-Si (B, 5×10^{18} cm^{-3}) wafers. Active areas of 1×10^{-4} cm^2 and 4×10^{-4} cm^2 were defined through a 450-nm field oxide using photolithography. A 10-nm sacrificial oxide was grown thermally and removed by treatment with a 1% HF solution. Then a 4.5-nm thermal oxide was grown and then subjected to a controlled etch in 1% HF solution to obtain 1.3-nm SiO_2 layers. The oxide thickness (T_{ox}) of the samples was measured by ellipsometry. The synthesis of 5-(4-dihydroxyphosphorylphenyl)-10,15,20-trimesitylporphinatozinc(II) (**2**) was recently reported [9]. The SAM was prepared by applying a solution of **2** (0.8 mg) in *N,N*-dimethylformamide (0.5 mL) to the test sample, which was held at 80 °C during the attachment process. Each porphyrin molecule is tethered to the SiO_2 surface via a phosphonate linkage (entailing one or two P–O–Si bonds at each phosphorus atom) to the SiO_2 surface. For electrical characterization, a solution of 1.0 M tetrabutylammonium hexafluorophosphate in propylene carbonate was used as the conducting gate electrolyte with a silver gate electrode. The simplified equivalent circuit of the capacitor (shown in Fig. 2) indicates the contribution of electrolyte, thin oxide, overlap silicon oxide, molecular SAM, and silicon substrate capacitances C_E, C_O, C_{OL}, C_M, and C_S, respectively. The cyclic voltammetry (CyV) current-voltage characteristics were measured on a CHI600A Electrochemical Analyzer, whereas the capacitance-voltage (*C-V*) and conductance-voltage (*G-V*) measurements were performed on a HP 4284A LCR meter. The electrical behavior of an EMOS capacitor containing dihydroxyphosphorylmethylferrocene (**1**) on SiO_2 has been reported [7].

RESULTS AND DISCUSSION

The current-voltage CyV characteristics of the EMOS capacitor incorporating **2** at various voltage scan rates (2 to 50 V/s) are shown in Fig. 3. Two distinct current peaks are observed in each oxidation scan and in each reduction scan. The first oxidation peak occurs at a gate voltage (V_G) of -0.7 V and the second at -1.1 V (for the scan at the lowest scan rate). The V_G value in all measurements is referenced to the top silver electrode/electrolyte contact.

The measurements for an electrolyte-oxide-silicon (EOS) capacitor (lacking molecules) with the same oxide thickness are also shown, where no peaks were observed. The lower curves for the EMOS capacitor represent oxidation processes whereas the upper curves represent reduction processes. During oxidation, positive charges are stored by removing electrons from the molecules, leaving behind holes in the molecular SAM. During reduction, electrons transfer back to the molecules from the substrate, thereby neutralizing the molecular SAM. The two redox waves observed at different potentials are associated with the two discrete redox states of the porphyrin molecule. At a given scan rate, the amplitude of the respective oxidation and reduction waves for each charged state were equal to each other (with respect to the background current). This equivalence indicates an equivalent amount of charge is being transferred in and out of the SAMs in the oxidation/reduction steps. Integration of the area under any of the peaks and dividing by voltage scan rate and electron charge provides a measure of the coverage of porphyrin molecules on the SiO_2 surface, which was calculated to be ~2×10^{13}/cm^2.

The peak current density (J_P) for each scan rate was calculated by averaging the four redox peak currents with respect to the background current (J_B). The currents J_P and J_B increased linearly with increasing voltage scan rate ($v = dV/dt$), as shown in Fig. 4. A linear fit obtained for the data, with zero intercept, showed an excellent fit for both J_P and J_B ($R^2 > 0.99$). To explain the linear relation, the total current (i) can be expressed as the rate of the flow of charge (Q) with time (t) through the SAMs:

$$i = \frac{\partial Q}{\partial t} = \left(C + V \times \frac{\partial C}{\partial V} \right) \times \nu$$

Here, C represents the total capacitance of the EMOS gatestack (a combination of the capacitive components shown in Fig. 2) and V is the potential applied. The term $(C + V \times \partial C/\partial V)$ in this equation is found to be 15.74 μF/cm^2, obtained by adding the slopes of J_P vs. v and J_B vs. v, as the total current is made up of the background and redox-related current. When the capacitor is in the initial neutral state, i.e. at V_G = -0.10 V, the EMOS capacitor behaves like a parallel-plate capacitor without the redox functionality. The capacitance is constant in this region, which implies that the term $\partial C/\partial V$ is zero. Under these conditions, the above equation becomes $i = C \times v$. Here, i represents the background current and the constant C is1.56 μF/cm^2, obtained from the slope of J_B vs. v in Fig. 4. This value of

background capacitance is very close to that obtained from the *C-V* measurement at a V_G of -0.10 V (Fig. 5(a)), suggesting the similarity between these two measurement techniques.

The *C-V* and *G-V* measurements at 100 Hz are shown in Figs. 5(a) and 5(b), respectively. The measurements reported here are limited at low frequencies, because at higher frequencies (>10 kHz) the limited ionic movement associated with the electrolyte prevents accurate measurements [10-11]. At higher frequencies, the effective capacitance of the electrolyte decreases dramatically and begins to dominate the total capacitance in a series circuit, whereupon the redox peaks are not observed. The curves in Fig. 5 show the depletion and accumulation of the silicon substrate. The curves resemble typical *C-V* and *G-V* curves obtained on metal-SiO_2-Si structures on p-type silicon except that two distinct peaks occur in the accumulation region. This is due to the fact that the redox potentials occur at negative gate biases which place the Si in accumulation. Because the EMOS structure has a large capacitance, the quality factor is still reasonably large at lower frequencies (Q_f > 10 at 100 Hz), thereby allowing robust measurements. The two redox peaks in *C-V*/*G-V* are observed at V_G of -0.6 V and -1.0 V, which are slightly different from the peak voltages obtained with current-voltage CyV measurements. This difference may be due to the different measurement techniques with different equipment and connector/cable assemblies. As shown in Fig. 5, peaks related to the redox processes are not observed for the EOS capacitor (which lacks molecules). It should also be noted, however, that conduction peaks due to the depletion of the silicon substrate are observed for both EMOS and EOS capacitors.

The EMOS capacitor containing **2** shows a hysteresis shift (ΔV) of -0.2 V in both *C-V* and *G-V*, whereas no such shift is observed for either the EOS capacitor or an EMOS capacitor constructed using a ferrocene compound (**1**) [7]. Figure 5(c) shows the *C-V* curves of the EOS capacitor and the EMOS capacitors (with **2** or **1**) at 10 kHz. This hysteresis may be due to the lower reduction peak values in *C-V* and *G-V* measurements compared to the corresponding oxidation peak values. This result suggests that not all of the molecules in the SAM are reduced in *C-V* hysteresis measurements, giving rise to a partially positively charged molecular monolayer. Such incomplete reduction of the monolayer may be due to a combination of two factors. First, there may be an insufficient number of electrons in the p-type substrate. The p-Si is in accumulation at these voltages, and the inherently slow process of thermal generation (as compared to the frequency of the measurements) limits the

availability of electrons. Secondly, the porphyrin molecules have a long linker (a phenyl-CH_2- unit) connecting the redox center to the SiO_2 surface, which can present an additional barrier to electron transfer. Even though all molecules are not reduced at the redox voltage, complete reduction will occur as V_G becomes more positive, thus causing the molecules to be reduced over a large range of V_G. Also, for positive values of V_G, the depletion capacitance of Si is very small and thus dominates the overall capacitance, possibly overshadowing the capacitance change due to redox activity. By contrast, the ferrocene molecules (**1**) have a short linker (a -CH_2- unit) connecting the redox center to the SiO_2 surface. Therefore, the EMOS capacitor with porphyrins (**2**) exhibits a larger hysteresis shift than that with ferrocenes (**1**).

The shift of the *C-V* characteristics as well as hysteretic behavior is attributed to the partially positively charged molecular monolayer in the porphyrin-based EMOS capacitor (containing **2**). For this EMOS capacitor, the flat-band voltage (V_{FB}) of the structure may be approximated as $V_{FB}= \phi_{ms}-Q_o/C_{M-E}$, (where ϕ_{ms} is the metal-semiconductor work function difference and Q_o is the remaining charge density of the monolayer). Thus, a positively charged layer can result in a negative shift of the flat-band voltage, as seen in the experimental data. As described above, the peaks associated with the redox activity of the SAMs are only observed at relatively low frequencies (<10 kHz); however, the hysteresis shift is observed at all frequencies studied here.

The reversible charging-discharging peaks, flat-band shift, and low voltage operation of the capacitor indicates possible applications for information-storage devices including nonvolatile random access memory devices. Similar results have also been obtained for porphyrin-based EMOS capacitors (containing **2**) on 0.7-nm and on 2.0-nm oxide, both of which showed a hysteresis shift of about -0.2 V. The flat-band voltage shift can be tuned by varying the length of linker between the redox center and the gate electrode. Moreover, the charge-retention time can be increased substantially by increasing both the oxide thickness and the molecular linker between the redox center and the substrate electrode. The relatively low write and erase voltages for this EMOS device are attractive compared with devices such as FLASH wherein the operating voltages are much higher. The multiple storage states of this EMOS capacitor make this hybrid molecule-silicon structure especially promising for multi-bit memory applications. Support for the hybrid molecule-silicon approach is

augmented by the availability of a variety of phosphonate-tethered porphyrins [12]. Other strategies for achieving multibit capabilities, such as constructing elaborate molecular architectures [13] or using mixed monolayers of different types of redox-active molecules [14], are also compatible with the hybrid molecule-silicon approach.

CONCLUSIONS

In this article, we have reported current-voltage and conventional *C-V* and *G-V* measurements on multiple-state redox-active molecular SAMs attached to thin silicon oxide. The EMOS capacitor exhibits distinct and multiple capacitance and conductance peaks associated with the two charged states of the porphyrin molecules (**2**). The EMOS capacitor exhibits voltage-shift behaviors that correspond to the charge in the molecules. No such flat-band voltage shifts are observed in a control EOS capacitor or in an EMOS capacitor that incorporates ferrocene molecules (**1**) as the redox-active element. These results indicate that porphyrin molecules are well suited for applications in hybrid memory devices. This work has also demonstrated that EMOS structures are very useful tools for characterizing charge-storage behavior of molecular monolayers. The hybrid approach provides an opportunity to meld the attractive features of molecules (multibit capabilities, low-voltage operation, intrinsic scalability, tunability of electronic properties and ease of integration with silicon) with semiconductor devices. Taken together, the results reported herein indicate that hybrid molecule-silicon structures are strong candidates for use in the next generation of memory devices.

This work was supported by the DARPA Moletronics Program (MDA972-01-C-0072) and ZettaCore, Inc.

REFERENCES

1. M. A. Reed, C. Zhou, and C. J. Muller, Science **278**, 252 (1997).
2. C. P. Collier, E. W. Wong, M. Belohradsky, F. M. Raymo, J. F. Stoddart, P. J. Kuekes, R. S. Williams, and J. R. Heath, Science **285**, 391 (1999).
3. S. K. Coulter, J. S. Hovis, M. D. Ellison, and R. J. Hamers, J. Vac. Sci. Technol. A **18**, 1965 (2000).
4. C. Engtrakul and L. R. Sita, Nano Lett. **1**, 541 (2001).
5. K. M. Roth, A. A. Yasseri, Z. Liu, R. B. Dabke, V. Malinovskii, K. Schweikart, L. Yu, H. Tiznado, F. Zaera, J. S. Lindsey, W. G. Kuhr, and D. F. Bocian, J. Am. Chem. Soc. **125**, 505 (2003).
6. Q. Li, G. Mathur, M. Homsi, S. Surthi, V. Misra, V. Malinovskii, K.-H. Schweikart, L. Yu, J. S. Lindsey, Z. Liu, R. B. Dabke, A. Yasseri, D. F. Bocian, and W. G. Kuhr, Appl. Phys. Lett. **81**, 1494 (2002).
7. Q. Li, S. Surthi, G. Mathur, S. Gowda, V. Misra, T. A. Sorenson, R. C. Tenent, W. G. Kuhr, S.-I. Tamaru, J. S. Lindsey, Z. Liu, and D. F. Bocian, Appl. Phys. Lett. **83**, 198 (2003).
8. S. Gowda, G. Mathur, Q. Li, S. Surthi, Q. Zhao, J. S. Lindsey, K. Mobley, D. F. Bocian, and V. Misra, Technical Digest-IEEE Meeting on Electron Devices 537–540 (2003).
9. K. Muthukumaran, R. S. Loewe, A. Ambroise, S.-I. Tamaru, Q. Li, G. Mathur, D. F. Bocian, V. Misra, and J. S. Lindsey J. Org. Chem. **69**, 1444-1452 (2004).
10. A. Chandra and B. Bagchi, J. Chem. Phys. **112**, 1876 (2000).
11. V. I. Gaiduk, B. M. Tseitlin, and D. S. F. Crothers, J. Mol. Liq. **89**, 81 (2000).
12. R. S. Loewe, A. Ambroise, K. Muthukumaran, K. Padmaja, A. B. Lysenko, G. Mathur, Q. Li, D. F. Bocian, V. Misra, and J. S. Lindsey, J. Org. Chem. **69**, 1453-1460 (2004).
13. K.-H. Schweikart, V. L. Malinovskii, J. R. Diers, A. A. Yasseri, D. F. Bocian, W. G. Kuhr, and J. S. Lindsey, J. Mater. Chem. **12**, 808 (2002).
14. Q. Li, G. Mathur, S. Gowda, S. Surthi, Q. Zhao, L. Yu, J. S. Lindsey, D. F. Bocian, and V. Misra, Adv. Mater. **16**, 133 (2004).

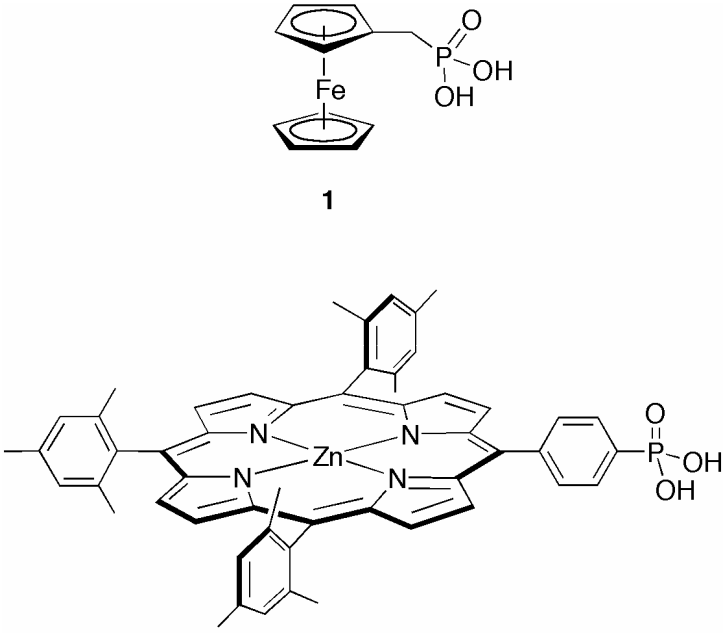

Figure 1 (a) The structure of dihydroxyphosphorylmethylferrocene (**1**). (b) The structure of 5-(4-dihydroxyphosphorylphenyl)-10,15,20 trimesitylporphinatozinc(II) (**2**). In both cases, molecular attachment to the SiO_2 surface is achieved by covalent P–O–Si bonds.

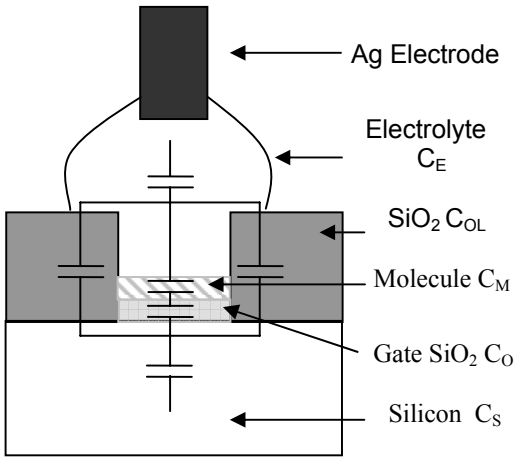

FIGURE 2

Figure 2. Schematic of the EMOS capacitor with a simplified equivalent circuit.

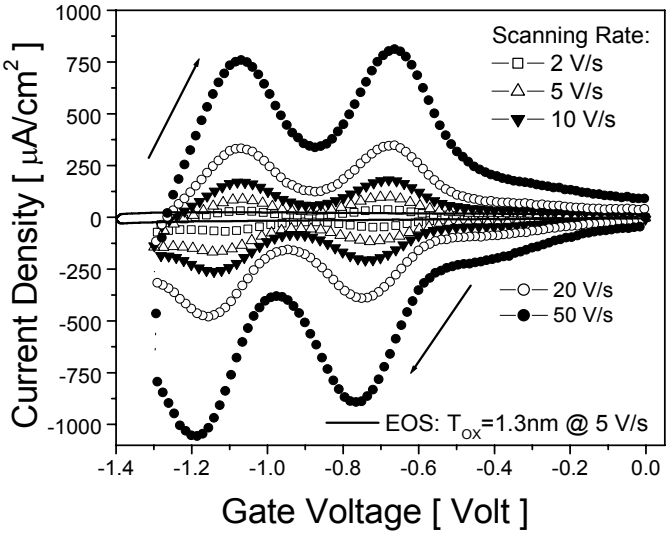

Figure 3. Current-voltage CyV characteristics of the EMOS capacitor (T_{ox} = 1.3 nm) containing **2** with voltage scan rates of 2, 5, 10, and 20 V/s. Cyclic voltammetry of the EOS capacitor (T_{ox} = 1.3 nm) at 5 V/s does not show redox peaks. Gate voltage is referenced to the potential applied to the Ag-wire top electrode.

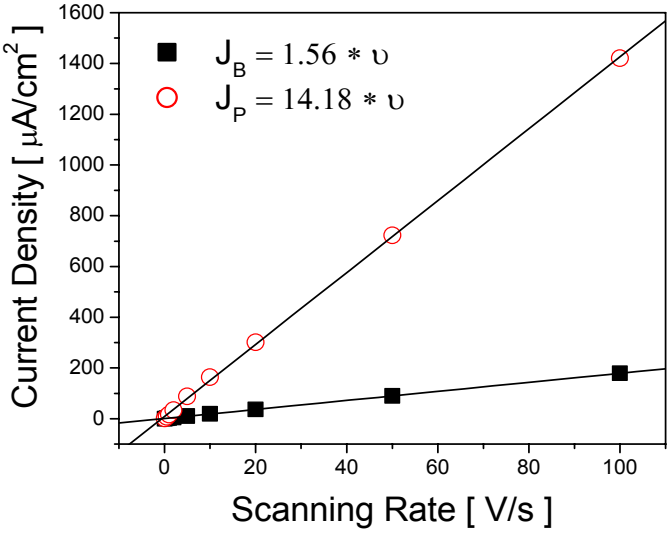

Figure 4. Background current (J_B) and peak current (J_P) versus voltage scanning rates (v) showing the linear dependence. Data were obtained for the EMOS capacitor (T_{ox} = 1.3 nm) containing **2**.

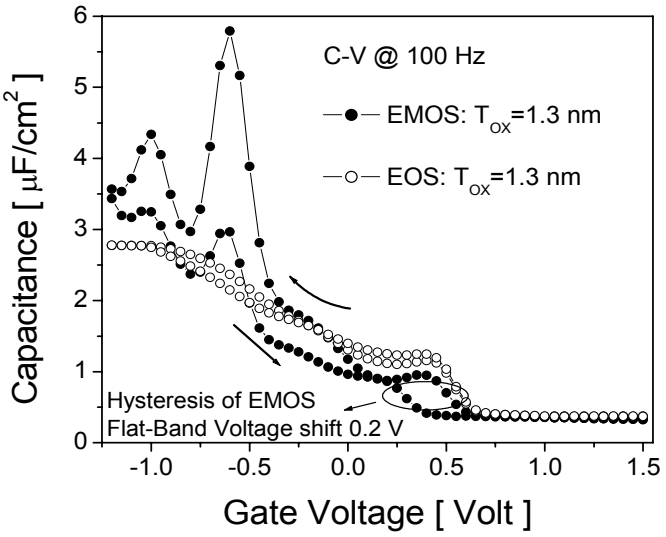

Figure 5(a)

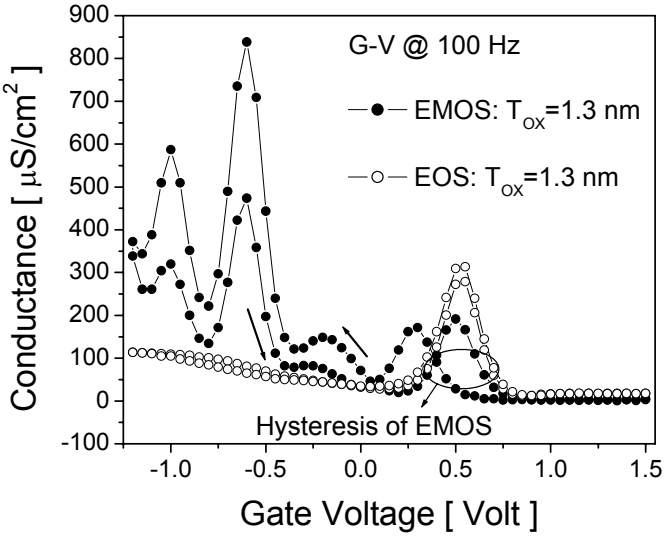

Figure 5(b)

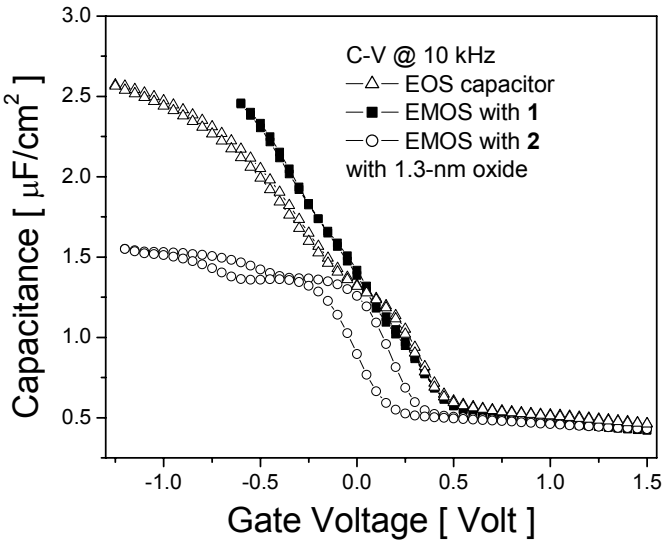

Figure 5(c)

Figure 5. (a) C-V and (b) G-V hysteresis of the EMOS capacitor containing **2** and the EOS capacitor (T_{ox} =1.3 nm) at 100 Hz. Both capacitors show a conductance peak around 0.5 V due to depletion of the silicon substrate. The EMOS capacitor shows two redox peaks and a hysteresis shift of -0.20 V while the EOS capacitor does not show any peak or hysteresis related to redox processes. (c) C-V hysteresis of an EOS capacitor and the EMOS capacitors containing ferrocene **1** or porphyrin **2** on oxide.